Development of Shear Plastic Hinge Models for Analysis of Reinforced Concrete Members

by

Amir Reza Tabkhi Wayghan

A thesis submitted to the Faculty of Graduate and Postdoctoral Affairs in partial fulfillment of the requirements for the degree of

Master of Applied Science

in

Civil Engineering

Carleton University
Ottawa, Ontario

Abstract

The lumped plasticity analysis approach is one of the most efficient methods to calculate the nonlinear behavior of reinforced concrete (RC) structures. However, the number of models that can capture shear effects using this approach are limited, and the existing models mostly require iterations or calibration. This study presents three shear hinge models developed based on the Modified Compression Field Theory, applicable to RC beams and columns with various shear span-to-depth ratios. A set of closed-form equations is developed for each model to calculate the shear force and shear deformation of the member at key points of the structural response. The proposed plastic hinge models are verified against various experimental results and finite element models. Moreover, parametric studies are conducted to assess the application range of the models. It is shown that the proposed models can accurately capture the nonlinear response of shear-critical RC structures in a computationally efficient manner.

Acknowledgements

I would like to express my deepest gratitude to my supervisor, Dr. Vahid Sadeghian, who always advised me throughout my research with his thoughtful comments and recommendations, helping me to improve in academic and personal aspects.

I would also like to thank my mother, father, and sister for their support and spiritual enlightenment in the moments where I felt exhausted. We were far apart but our hearts were close.

I should also thank Carleton University and the Civil Engineering Department who provided me with financial support.

Above all I would like to thank my wife Roshanak for her love and endless support, for tremendous understanding and encouragement, and for keeping me sane over the past two years. But most of all, thank you for being my best friend.

Table of Contents

List of Tables

List of Figures

List of Appendices

Chapter 1: Introduction

Despite significant research over the last few decades, computing the shear behavior of reinforced concrete (RC) structures still remains a challenging task. Major changes that occurred in shear design provisions of the latest revision of the ACI 318 code (ACI, 2019) show that there are still many aspects of the shear behavior that have not been fully solved yet. The shear response of concrete structures is not only dependent on complex material mechanisms, but also can be highly influenced by flexural and axial forces in a section. Besides, shear failure is inherently a brittle type of failure that could occur almost without warning making it extremely dangerous. The failure of warehouse roofs at US Air Force Bases in 1956 in Georgia, the collapse of the Sleipner A offshore platform in 1991 in the Norwegian sector of the North Sea with a total economic loss of about $700 million, the collapse of columns of the Hanshin Expressway during the 1995 Kobe earthquake in Japan, and the De la Concorde overpass bridge collapse in 2006 in Quebec, Canada are examples of shear failures in concrete structures. These shear failures and many others necessitate engineers and researchers to develop reliable analytical models capable of accurately predicting the shear behavior.

1.1 Nonlinear analytical approaches

Existing nonlinear analysis methods for RC structures can be broadly classified into three main groups: detailed finite element (FE) modeling, fiber-based analysis method, and lumped plasticity analysis method. Among these methods, detailed FE modeling with powerful 2D and 3D elements is perhaps the most accurate one. However, because of the high computational demand and modeling effort, application of this method is mostly limited to analysis of RC structures at the component-level (beams, columns, etc.). For

analysis of the entire structure (i.e., system-level analysis), engineers typically use frame-type analysis methods because of their computational efficiency and simplicity in modeling. Nonlinearity effects in frame-type analysis are taken into account using 1D elements based on either a distributed plasticity method or a lumped plasticity approach. The distributed plasticity approach (also known as fiber-based approach) calculates the nonlinear stresses and strains over the entire length of members typically based on the assumption of plane sections remain plane, while the lumped plasticity approach assumes nonlinearity is concentrated at predefined critical locations (i.e., plastic hinges) with the remaining part of members having a linear elastic behavior. The lumped plasticity approach is highly efficient and convenient to use making it an ideal analysis method for safety and performance assessment of RC structures at the system-level. However, it requires development of plastic hinges that are capable of accurately capturing nonlinearity effects in structures in a concentrated manner. The three analysis approaches described above are shown in Figure 1-1.

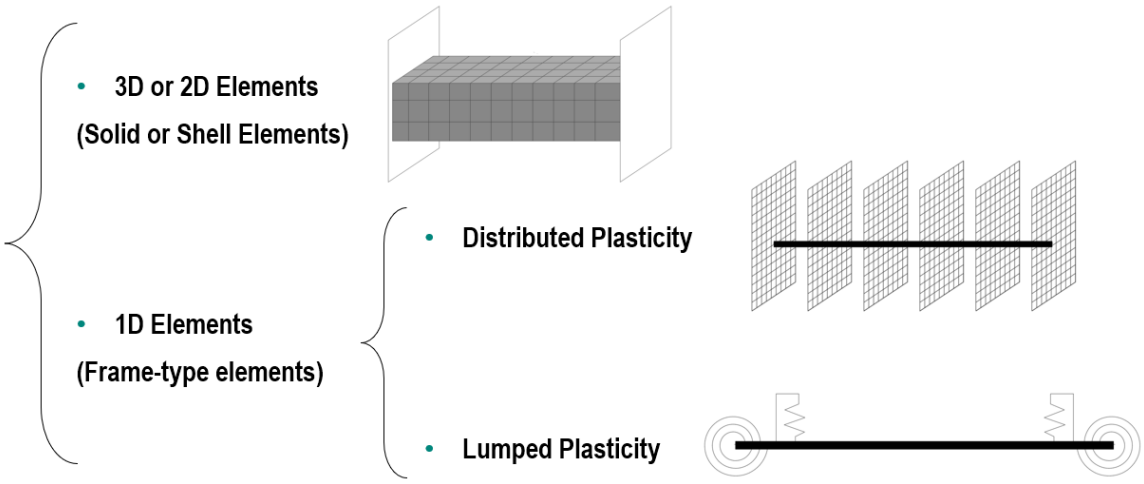

Figure 1-1 Different approaches for nonlinear analysis of RC members

1.2 Research objectives

The accuracy of the lumped plasticity analysis method is directly related to the ability of plastic hinges to capture nonlinearity effects. Most plastic hinges are developed for computing the flexural response of RC structures, and the number of shear plastic hinges available in the literature is limited mainly due to the complexity of shear behavior. This study aims to develop a series of rational plastic hinge models for nonlinear analysis of shear-critical RC structures that are applicable to beams and columns with various shear span to effective depth ratios (a/d). The models developed in this study are:

1. A shear plastic hinge model for slender beams ($a/d > 2$) capable of capturing advanced mechanisms such as interactions between shear force and bending moment, effects of nonlinear stress and strain distributions through the section, and compression softening effect in concrete.

2. A shear plastic hinge model for slender columns ($a/d > 2$) developed by extending the formulation of the previous model to account for the effect of axial load on the shear response.

3. A shear plastic hinge model for deep members ($a/d < 2$) developed by taking into account the effect of arch action on the shear behavior.

The accuracy and application range of the proposed models are assessed by analyzing a large number of shear-critical test specimens and comparing the results against experimental data and other analytical methods. Also, the effectiveness of the proposed models for nonlinear analysis of RC structures at the system-level is demonstrated through

analysis of three structural systems with shear-critical members using the lumped plasticity approach.

1.3 Thesis layout

This thesis comprises seven chapters described as follows:

Chapter 1 is a brief introduction on the importance of shear behavior in RC members, and different types of nonlinear analysis approaches to account for this effect. The research objectives and the layout of the thesis are also described in this chapter.

Chapter 2 describes a literature review on the existing shear hinge models proposed by other researchers.

Chapter 3 presents the shear hinge model developed for slender RC beams. It includes the model development, verifications at the component- and system-level, and a summary and conclusion. This chapter was written based on a journal paper titled *"A Shear Hinge Model for Analysis of Reinforced Concrete Beams"* that was recently published in the ACI Structural Journal (Tabkhi and Sadeghian, 2021a).

Chapter 4 presents an extension of the model developed in Chapter 3 for analysis of slender RC columns. It includes a discussion on the differences between the shear response of beams and columns, changes made to the model formulation to consider the effect of axial load, and a series of verification and parametric studies on RC columns at the component-level and RC frames with critical columns at the system-level. This chapter was also written based on a journal paper titled "*A Shear Hinge Model for Analysis of Reinforced Concrete Columns"* that was prepared by the author and recently was considered as accepted for

publication with only minor revisions in the ACI Structural Journal (Tabkhi and Sadeghian, 2021b).

Chapter 5 extends the model developed for slender columns in Chapter 4 to deep RC members ($a/d \leq 2.0$) by considering the arch action mechanism. Similar to the previous two chapters, the model formulation as well as verification and application studies are included. The verification and parametric studies were conducted on short columns and deep coupling beams at the component-level, and the application study was performed on a multi-storey RC coupled shear wall structure at the system-level. A journal paper titled *"Consideration of Shear Behavior in Macro-Modeling of Deep Reinforced Concrete Members"* is under preparation by the author that will reflect the results of this chapter.

Chapter 6 provides a summary and conclusion on the models developed in this thesis, and Chapter 7 states recommendations for future research on this topic.

Figure 1-2 shows the application of different shear hinge models developed in this study for analysis of a multi-story RC structure. Using the flowchart shown in Figure 1-3 the proper shear hinge model based on the formulation presented in Chapters 3 to 5 can be selected.

All papers used in this thesis were prepared by the author and his supervisor (Dr. Vahid Sadeghian).

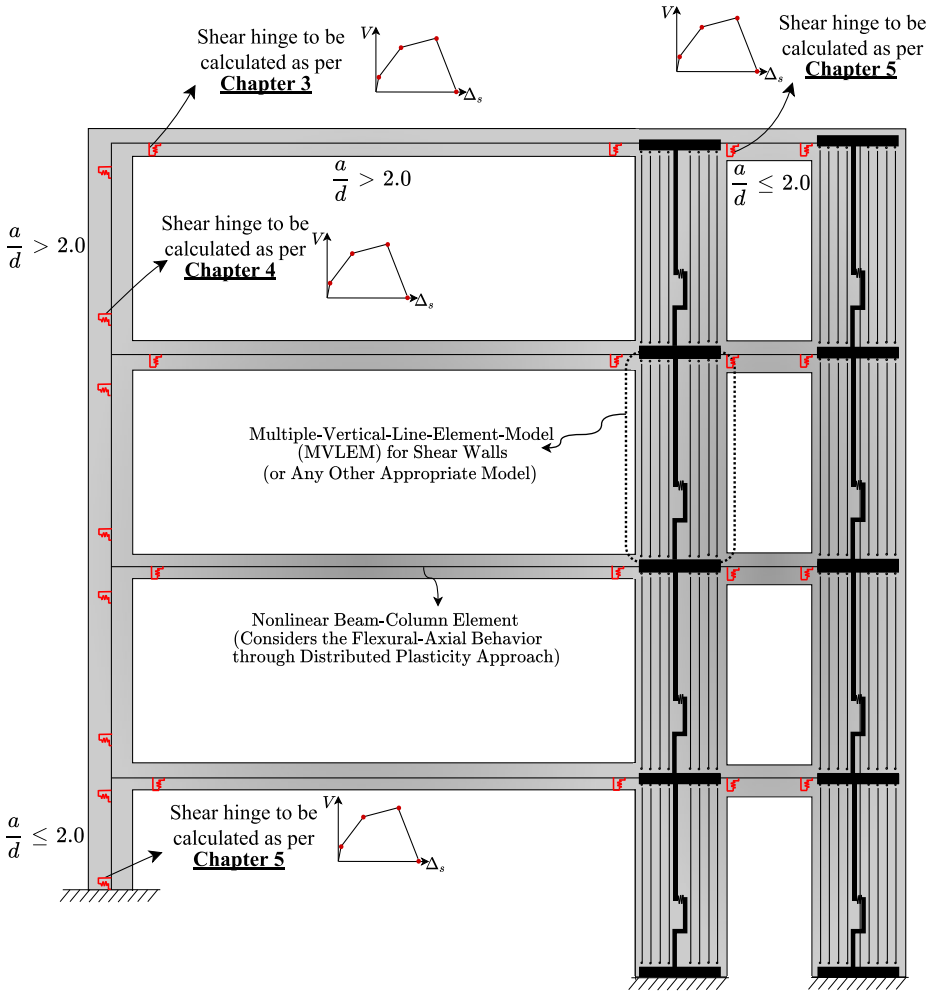

Figure 1-2 Application of the proposed models to various member types of an RC structure

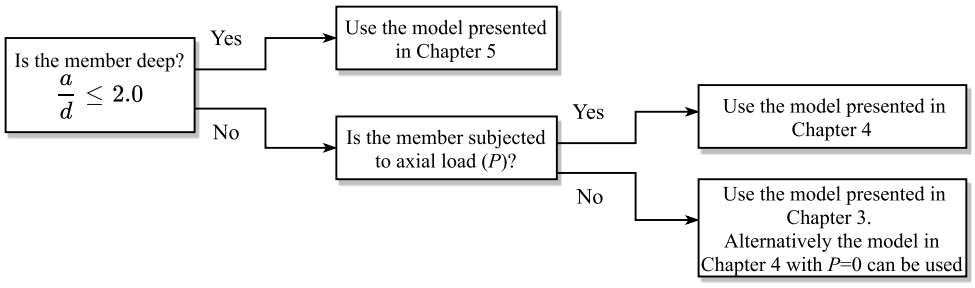

Figure 1-3 Flowchart for selecting the appropriate plastic hinge model based on this study

Chapter 2: Literature Review

The number of studies conducted on the performance assessment of shear-critical RC members using the lumped plasticity approach are limited, compared to the studies on the flexural and axial behavior or the studies that use other analysis approaches such as FE. In this chapter, the lumped plasticity models that are available in the research literature for computing the shear behavior of slender and deep members are presented and discussed. For deep members, other analytical methods such as the FE modeling and strut-and-tie methods are also reviewed in order to provide more insight into the effect of arch action.

2.1 Studies on slender members

Pincheira et al. (1999) presented a lumped plastic model for concrete columns that accounted for shear and flexural responses separately. Neglecting the flexural-shear interaction effects, however, influenced the accuracy of the model in predicting the shear behavior. The analytical model was compared with the experimental results of two rectangular RC columns that showed a shear dominated behavior with almost no flexural ductility. Since the influence of flexural-shear behavior was negligible in these specimens, the analytical and experimental results agreed well. The shear response curve of the model is shown in Figure 2-1.

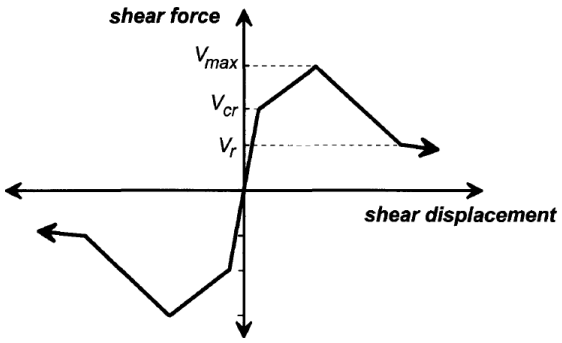

Figure 2-1 The shear response curve proposed by Pincheira et al. (1999)

Elwood (2004) presented a shear hinge model, as shown in Figure 2-2, with a trilinear response that incorporated a shear failure surface to determine the peak strength. The model was capable of capturing the response of RC columns under shear and axial loads and could account for strength degradation due to shear. However, it neglected the interaction effects between shear and bending moment.

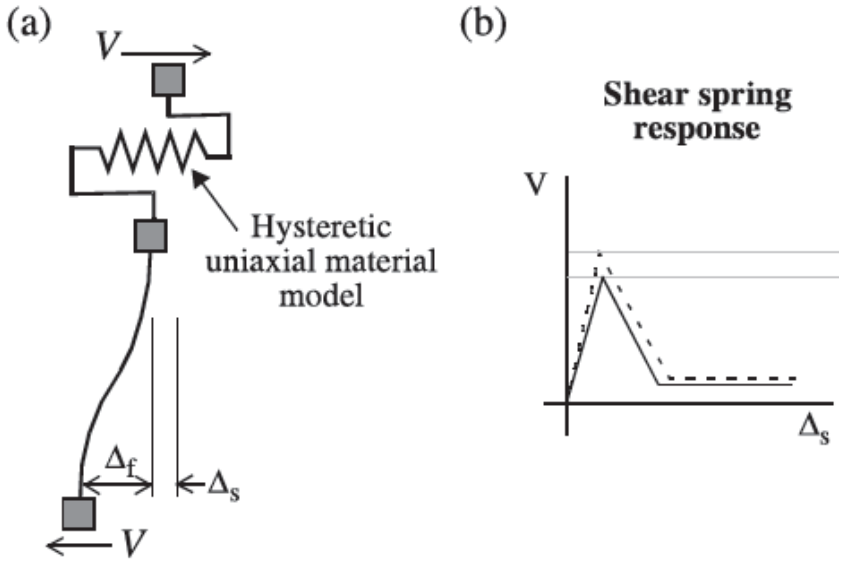

Figure 2-2 The shear spring model presented by Elwood (2004)

LeBorgne and Ghannoum (2014) proposed an analytical model based on the Elwood's (2004) study that consisted of a zero-length shear spring element placed in series with flexural elements (see Figure 2-3). The model could account for the lateral strength degradation of members subjected to seismic loading. Although the model was capable of capturing nonlinearity effects and strength degradation due to shear, it required calibration of strength and stiffness parameters prior to the analysis.

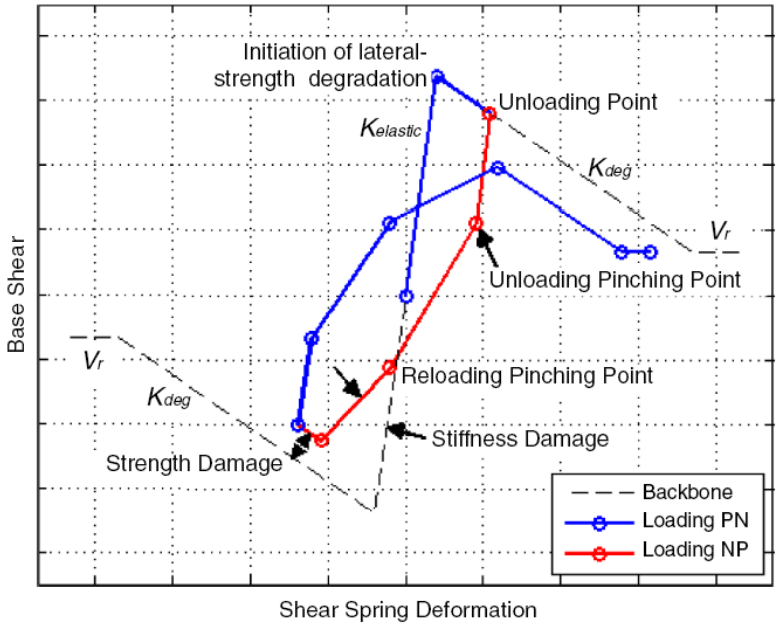

Figure 2-3 The load-deflection response of shear hinge model proposed by LeBorgne and Ghannoum (2014)

Sae-Long et al. (2019) presented a nonlinear fiber frame element that can be used for RC columns prone to shear or flexure-shear failure. As shown in Figure 2-4, they proposed a trilinear shear force versus shear strain response with closed-form equations to account for the shear behavior. The shear hinge model considered degradation in the shear strength through a reduction factor that was a function of the curvature ductility of columns.

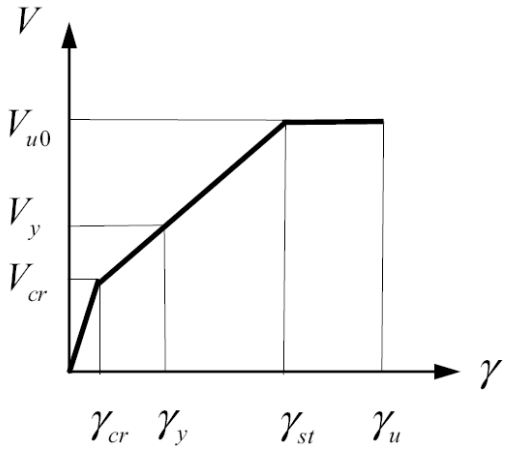

Figure 2-4 The trilinear shear hinge model proposed by Sae-Long et al. (2019)

ASCE/SEI 41 (2017) recommends a generalized load-displacement backbone curve for displacement-controlled RC elements, as shown in Figure 2-5, that can be utilized to define the response of shear plastic hinges. The backbone curve is presented in a normalized form to generalize its application. Thus, it requires defining the shear strength and deformation at the yielding point by the user. The model assumes a linear response up to the yielding point, which then followed by another line representing plastic deformations prior to reaching the peak shear strength. After the peak point, a sudden drop in the shear strength is assumed to represent the failure of the element due to shear. A small residual strength is considered in the model after reaching the failure point to avoid numerical instability in the analysis of the rest of the structural elements.

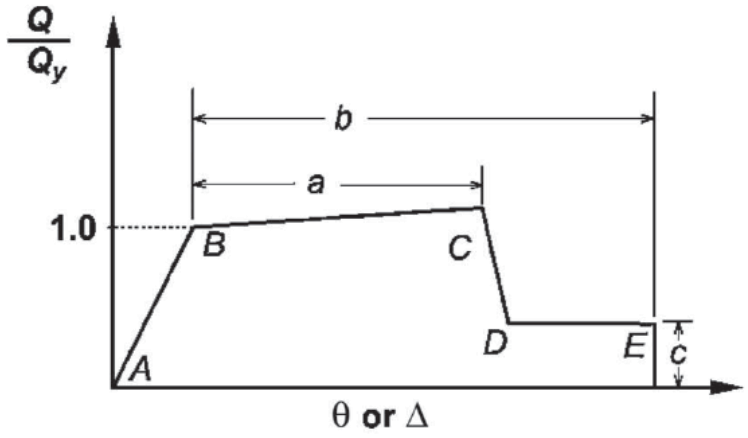

Figure 2-5 ASCE/SEI 41 (2017) generalized backbone curve

2.2 Studies on non-slender (deep) members

Over the last few decades, great efforts have been made to calculate the shear response of RC deep members. These efforts have resulted in three types of analysis methods: 1) FE method, 2) strut-and-tie model (STM), and 3) beam-arch action model. A review of the analytical studies conducted on shear-critical deep members is presented in the following.

2.2.1 Finite element method

FE method is able to consider a wide range of complex material and geometrical details making it one of the most accurate and powerful methods for analysis of deep members. However, this method is not suitable for analysis of large structural systems or daily design applications in engineering offices as it is computationally expensive and requires excessive modeling effort. Several researchers used FE tools to assess the component-level behavior of deep members. For example, Mohr (2007) analyzed a series of short RC coupling beams tested under monotonic and cyclic loading conditions using the VecTor2 FE software (Wong et al., 2013) in order to assess the confinement effect of the reinforcement. As shown in Figure 2-6, the analytical and experimental results correlated well in terms of the yield strength, ultimate strength, and displacement at the yielding point. However, the ultimate displacement of the coupling beams was slightly underestimated in some cases.

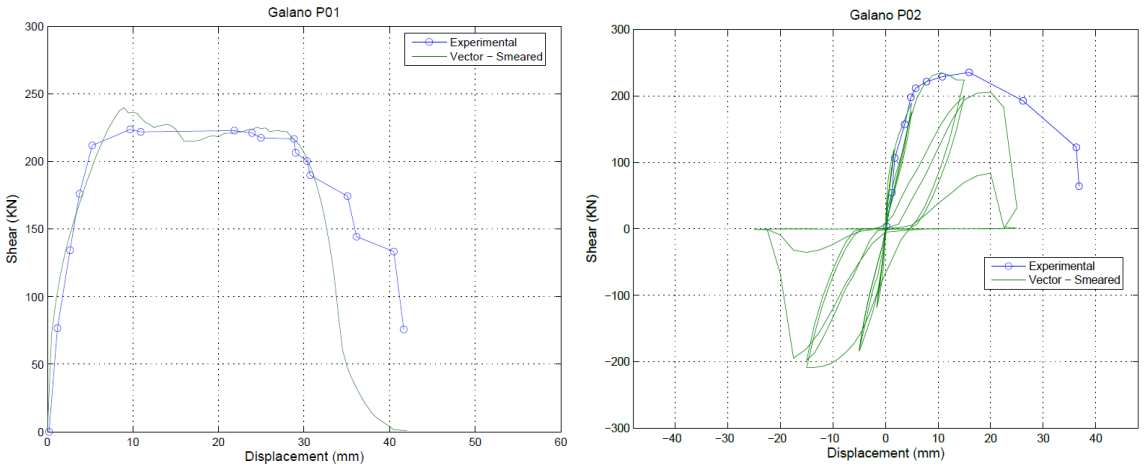

Figure 2-6 Verification of VecTor2 results for two short coupling beams by Mohr (2007)

Nguyen (2013) used another FE analysis software, ATENA (Červenka, 2020), to study the effect of various design parameters on the behavior of RC deep beams. He found that the

concrete compressive strength and loading configuration can have a substantial influence on the shear strength of deep beams. Figure 2-7 shows the observed and calculated crack patterns for a deep beam investigated in this study.

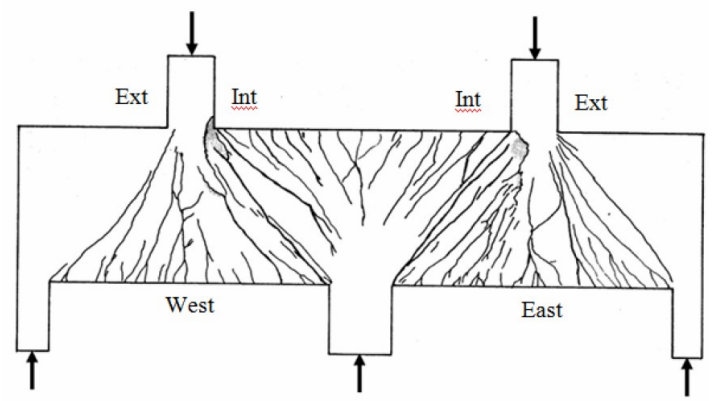

(a)

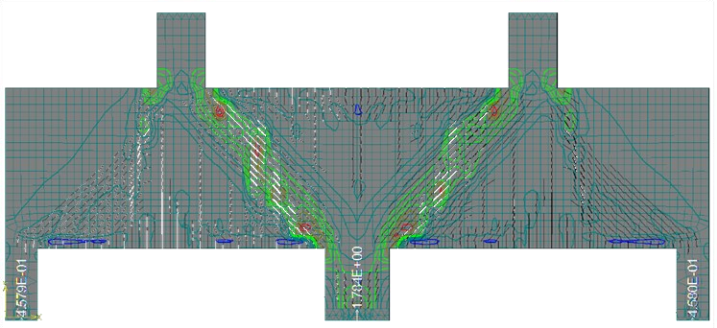

(b)

Figure 2-7 Comparison of crack patterns between a) experiment and b) ATENA program for a deep beam (Nguyen, 2013)

2.2.2 Strut-and-tie model

Another powerful method for estimating the capacity of deep RC members is STM, which is based on truss analogy and is widely accepted by many design codes, including ACI-318 (2019). This method requires having a strong knowledge and experience in structural analysis and design to understand and visualize the stress flow in structural members. STM has been a popular method for analysis of deep members as it can account for the complex stress flow in the disturbed region with reasonable accuracy.

Despite the abovementioned advantages, creating a proper STM model can be complicated and time-consuming. Any change to the loading condition or the geometry and reinforcement detailing of the member, may require substantial modifications to the model. Furthermore, a single solution may not exist for this method, and one can use any rational truss geometry. Thus, it is recommended to use more than one STM model, if possible, to ensure the safety of the design.

Ismail et al. (2018) provided a review of existing STM models for design of RC deep beams and proposed new formulation to calculate the effectiveness factor, a factor that accounts for the biaxial state of stress in the concrete strut in STM models. Through an extensive verification study, they demonstrated that choosing an appropriate geometry for the STM model is crucial for accurate calculation of the shear strength. Figure 2-8 shows the shear strength prediction of the STM model using various effectiveness factors for 224 RC deep beams with transverse reinforcement.

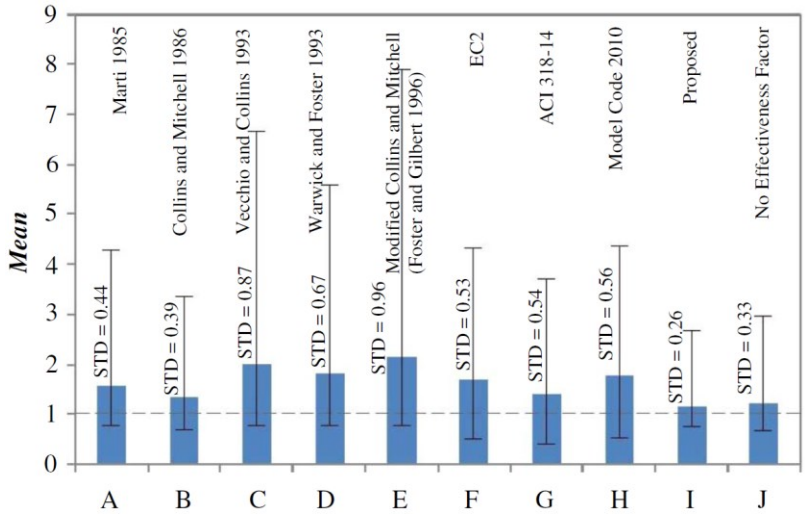

Figure 2-8 Shear strength prediction of 224 RC deep beams using STM with various effectiveness factors (Ismail et al., 2018)

Nabilah et al. (2020) proposed a nonlinear STM model to compute the deformation capacity of short conventionally reinforced coupling beams, as shown in Figure 2-9. In addition to truss elements representing stresses in the reinforcement and concrete, they used zero length elements to model slippage of the longitudinal reinforcement. The model was able to predict the response of coupling beams with good accuracy compared to the experimental results. However, for every beam, an exclusive model with unique geometry had to be created which made the modeling process tedious.

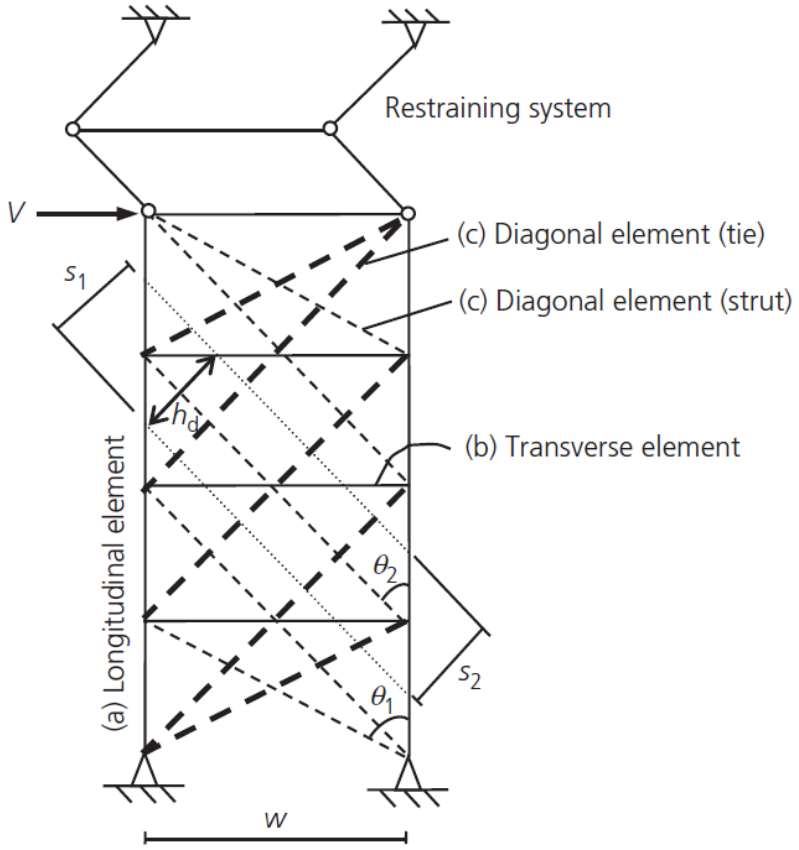

Figure 2-9 STM model by Nabilah et al. (2020) for beams under equal moments at their ends

2.2.3 Beam-arch action model

Calculating the shear behavior of deep RC members through the beam-arch action model is generally simpler and more practical than the FEM and STM methods. This method decouples the shear behavior of RC members into two separate actions: 1) the conventional

beam action resulted from flexural bending and 2) the arch action that forms due to direct transfer of the load to the support through an inclined compression chord. The shear response of slender members is governed by the beam action, while the behavior of deep members is highly affected by the arch action. Decoupling the beam action from the arch action enables explicit consideration of important mechanisms (e.g., dowel action, aggregate interlock) in the model which is not possible with the STM method. Also, since the contribution of the reinforcement to the shear strength is considered through the beam action, the variation in the model configuration is much less compared to the STM method.

Leondardt (1965) conducted a series of experimental tests on short beams and observed that a substantial portion of the shear force was resisted through an inclined compression chord. He concluded that due to the arch action the amount of shear reinforcement can be reduced in short beams compared to slender beams.

Kim et al. (1999) presented a shear strength equation for RC deep members calibrated against experimental data and derived based on an empirical relationship between the shear and the variation rate of bending moment along the beam span. Their equation predicted the shear strength of deep beams with decent accuracy for most cases, especially for models having low shear stress capacity. However, their study was focused only on the shear strength and no investigation was conducted on other important parameters of the shear response, such as shear deformation at the peak stress or ultimate shear deformation. The beam and arch action mechanisms contributing to the shear capacity of RC members in their model are shown in Figure 2-10.

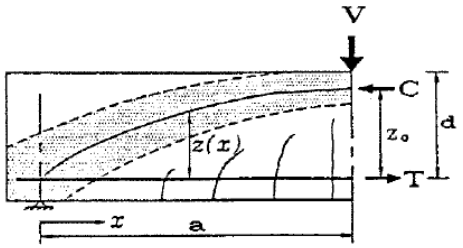

(a) Equilibrium in the shear span of a R/C Beam

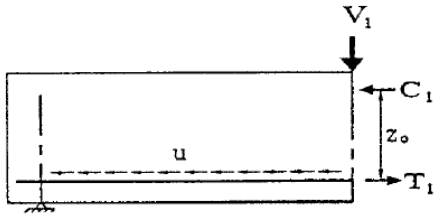

(b) Beam action contribution to shear

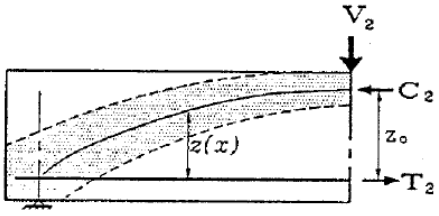

(c) Arch action contribution to shear

Figure 2-10 Mechanisms contributing to shear resistance (Kim et al., 1999)

Kim and Jeong (2011) proposed an iterative procedure to quantify the contribution of the arch action to the total shear strength of RC beams. The procedure was developed by investigating the deformation compatibility condition between the beam action and the arch action using the truss analogy and the Modified Compression Field Theory (MCFT) (Vecchio and Collins, 1986). The beam and arch action mechanisms considered by the model for RC beams are shown in Figure 2-11. While a good agreement was seen in the results when verified against experimental tests, a downside to this method was that it required several iterations to find the contribution factor for the arch action, as shown in Figure 2-12.

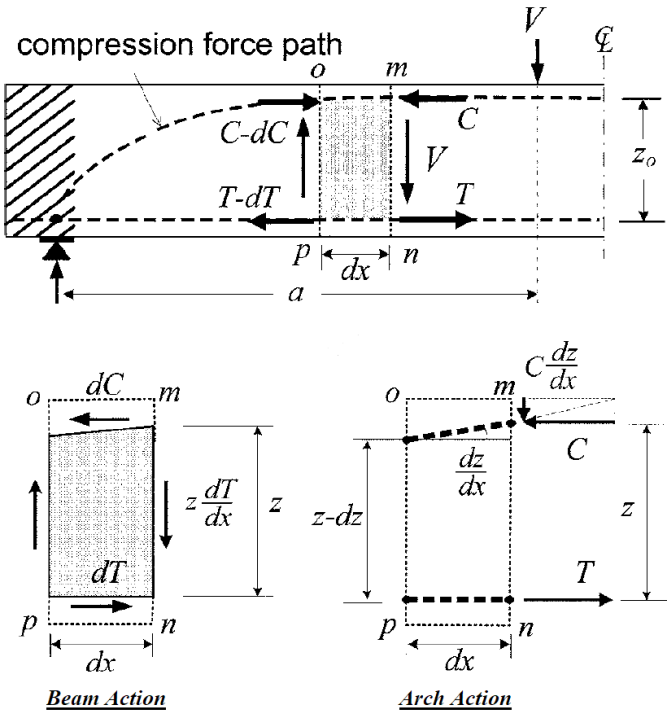

Figure 2-11 Beam and arch action mechanisms to resist shear force in RC beams (Kim and Jeong, 2011)

Pan and Li (2013) developed a model to calculate the shear strength of RC columns with a small span-to-depth ratio based on the beam-arch action mechanism. In their model, the shear strength was decomposed into three parts, contributions from the concrete web, the transverse reinforcement, and the inclined concrete compression chord (i.e., arch action). The two former ones were calculated using a procedure similar to that presented in the Canadian Concrete Design Code, CSA A23.3 (CSA, 2004). While the latter one was computed using the deformation compatibility condition between the beam action and the arch action, with consideration of the axial load effect. The arch action mechanism considered in the model is shown in Figure 2-13. Through a verification study, the authors demonstrated that their model was able to calculate the shear force capacity of deep RC columns with better accuracy than the previous beam-arch action models.

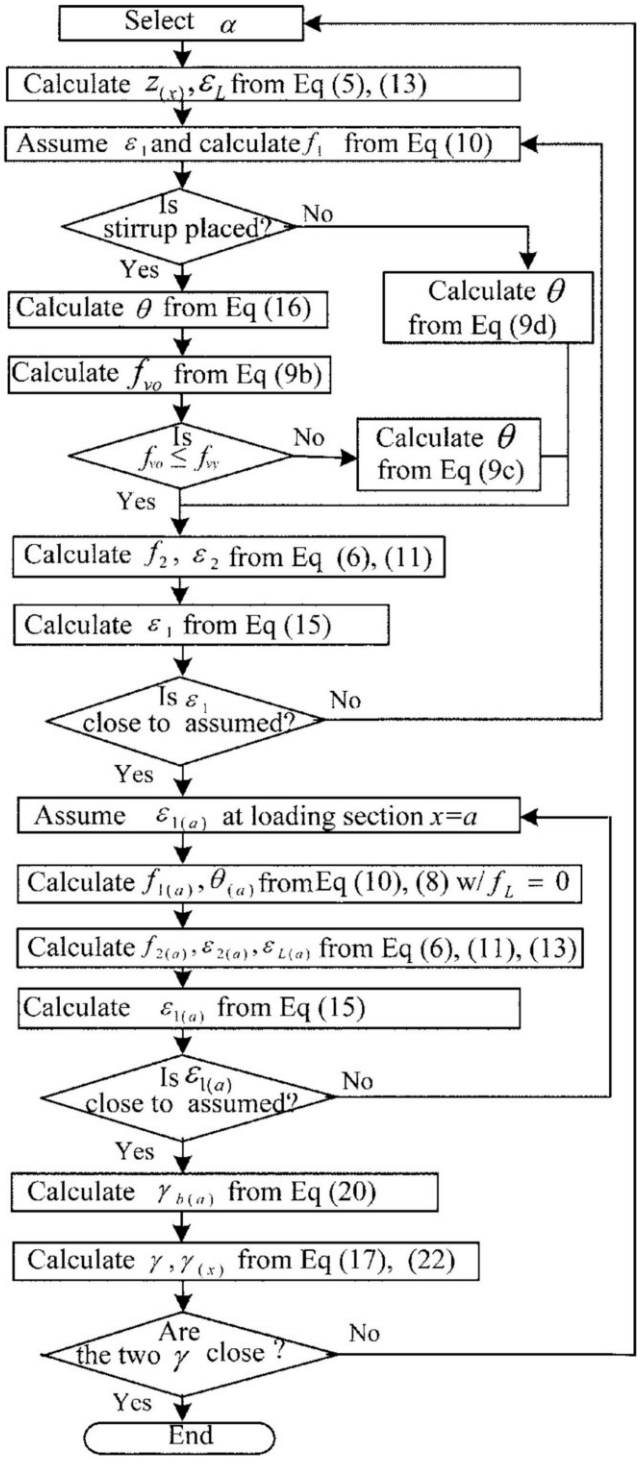

Figure 2-12 Iterative solution proposed by Kim and Jeong (2011) for calculation of arch action contribution factor

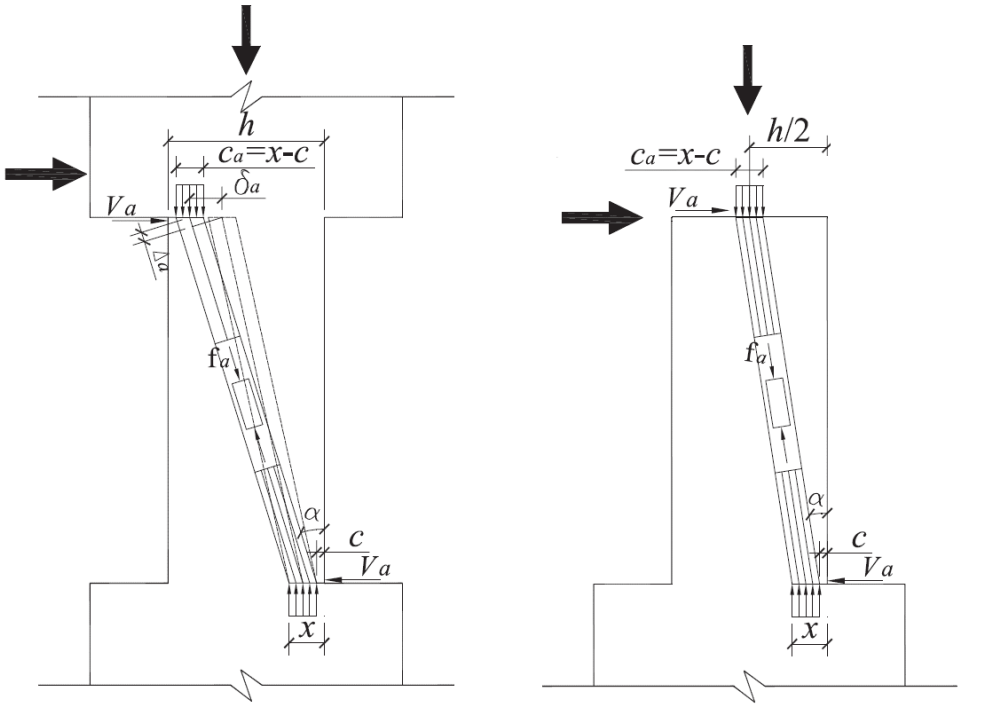

Figure 2-13 Arch action mechanism considered by Pan and Li (2013) (figure was reproduced from the study of Pan and Li (2013))

2.3 Concluding remarks

Based on the review of the existing shear hinge models in the research literature, the following shortcomings are identified that need to be addressed:

- Most of the existing shear hinge models have a limited application range or require extensive calibration (ASCE/SEI-41, 2007; LeBorgne and Ghannoum, 2014).
- Most of the models neglect axial-flexural-shear interaction effects (Elwood, 2004; Pincheira et al., 1999) or require using an analysis tool for calculation of the shear force-shear deformation response (LeBorgne and Ghannoum, 2014).
- None of the existing models accounts for second-order material effects in cracked reinforced concrete (e.g., aggregate interlock and compression softening in concrete) which are known to have significant effect on the shear behavior.

- The existing models mostly focused on the shear strength and cannot provide the full shear force-deformation response (Kim et al., 1999; Pan and Li, 2013).

This study aims to address these limitations by developing a series of rational plastic hinge models capable of accurately calculating the nonlinear shear response of a wide range of RC beams and columns. The proposed models account for the second-order material effects and the interaction between shear and other sectional force components. They are also computationally efficient and do not require any iteration making them suitable for system-level analysis of shear-critical RC structures.

Chapter 3: A Shear Hinge Model for Analysis of Reinforced Concrete Beams

3.1 Introduction

This chapter was written based on a journal paper recently published in the ACI Structural Journal (Tabkhi and Sadeghian, 2021a). It presents a comprehensive shear hinge model for RC beams capable of capturing advanced mechanisms such as interactions between shear force and bending moment, effects of nonlinear stress and strain distributions through the section, and compression softening effect in concrete. The model provides closed-form equations for five key points on the shear force-shear deformation response by satisfying the compatibility, equilibrium, and constitutive relationships. By comparing the performance of the model against test results, other analysis methods, and design codes at the component- and system-level, the effectiveness of the model in capturing the shear behavior is demonstrated.

3.2 Development of the model

The proposed lumped plasticity model estimates the shear force versus shear strain relationship by calculating five key points on the response: flexural cracking, shear cracking, yielding of shear reinforcement, ultimate shear strength, and shear failure. Figure 3-1 shows a schematic representation of the shear force-shear strain response used in the model including the key points.

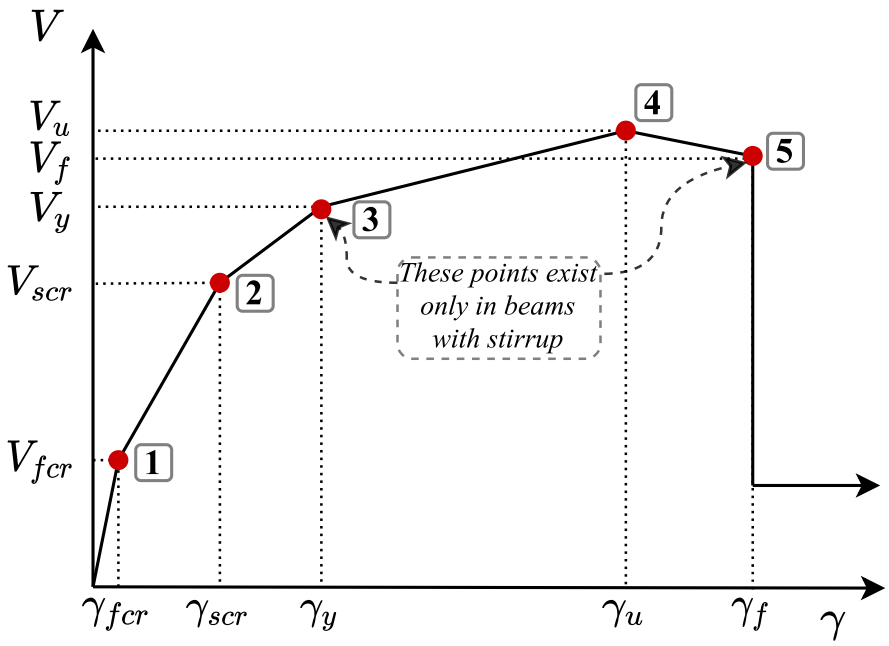

Figure 3-1 Schematic shear force-shear strain response of the proposed model

A 2D panel element is used to simulate the nonlinear shear behavior of the beam in a concentrated manner, as shown in Figure 3-2. Unlike 1D spring elements used in most existing plastic hinge models, using a 2D panel element enables capturing interactions between axial, flexural, and shear forces. To calculate the shear force and shear displacement at each key point of the response, closed-form equations are developed based on the Modified Compression Field Theory (MCFT) (Vecchio and Collins, 1986). MCFT is a smeared rotating crack model that treats stresses and strains in an average sense and allows cracks to gradually reorient as a result of change in loading or material behavior. Over the past 40 years, MCFT has been extensively verified against experimental tests, adapted to structural design codes, and implemented into various types of finite element and sectional analysis software (Sadeghian and Vecchio, 2018). These efforts have shown the ability of MCFT for computing the response of RC structures, particularly under shear. This study, for the first time, extends the application of this valuable theory to analysis of

shear-critical RC members using the lumped plasticity approach. The formulation of MCFT used in the derivation of closed-form equations for the plastic hinge model are shown in Figure 3-2.

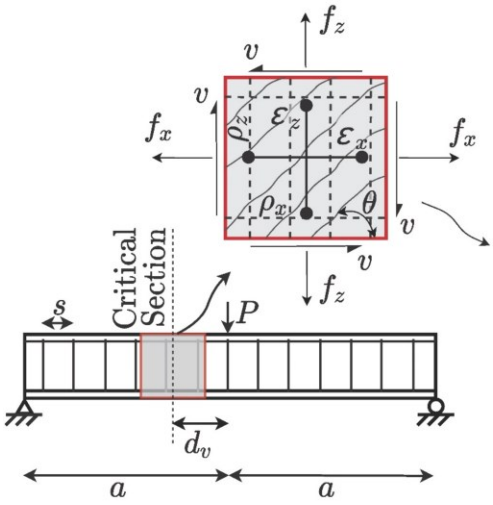

$$\textit{Equilibrium}: \begin{cases} f_x = \rho_x f_{sx} + f_{c1} - v\cot(\theta) & (3\text{-}1) \\ f_z = \rho_z f_{sz} + f_{c1} - v\tan(\theta) & (3\text{-}2) \\ v = \dfrac{f_{c1} + f_{c2}}{\tan(\theta) + \cot(\theta)} & (3\text{-}3) \end{cases}$$

$$\textit{Geometric Conditions}: \begin{cases} \tan^2(\theta) = \dfrac{\varepsilon_x + \varepsilon_2}{\varepsilon_z + \varepsilon_2} & (3\text{-}4) \\ \varepsilon_1 = \varepsilon_x + \varepsilon_z + \varepsilon_2 & (3\text{-}5) \\ \gamma_{xz} = 2(\varepsilon_x + \varepsilon_2)\cot(\theta) & (3\text{-}6) \end{cases}$$

$$\textit{Stress-Strain Relationships}: \begin{cases} f_{sx} = E_s\varepsilon_x \le f_{yx} & (3\text{-}7) \\ f_{sz} = E_s\varepsilon_z \le f_{yz} & (3\text{-}8) \\ f_{c2} = \dfrac{f'_c}{0.8 + 170\varepsilon_1}\left[2\dfrac{\varepsilon_2}{\varepsilon_0} - \left(\dfrac{\varepsilon_2}{\varepsilon_0}\right)^2\right] & (3\text{-}9) \end{cases}$$

Figure 3-2 Representing shear behavior of beam in a concentrated manner with a panel element formulated based on MCFT equations

The model considers the nonlinear distribution of various parameters, such as crack inclination (θ), shear strain (γ), and shear stress (v) through the section in an average sense. Using a large number of sectional analyses performed based on the MCFT model on a wide range of shear-critical RC beams, the nonlinear distribution of each parameter in different stages of the response is determined. The models are selected such that they cover a wide range of important parameters such as concrete compressive strength (from 20 MPa (2900 psi) to 100 MPa (14500 psi)), yield strength of reinforcing bars (from 300 MPa (43500 psi) to 600 MPa (87000 psi)), beam height (from 200 mm (7.87 in) to 2000 mm (78.74 in)), cross-sectional dimensions ratio (h/b) (from 0.8 to 8.0), and the transverse reinforcement ratio (ρ_z) between 0.00% and 2.25%. Simple equations are developed to approximate the nonlinear distribution with an average value for the entire 2D panel representing the shear

hinge in the beam. This approach enables to develop a relatively simple model for lumped plasticity analysis that can capture nonlinearity effects with reasonable accuracy. The typical distribution of shear strain, longitudinal strain and crack inclination along the beam height found from sectional analyses based on the MCFT model are shown in Figure 3-3. In the following, the development of closed-form equations for the key points of the response is discussed.

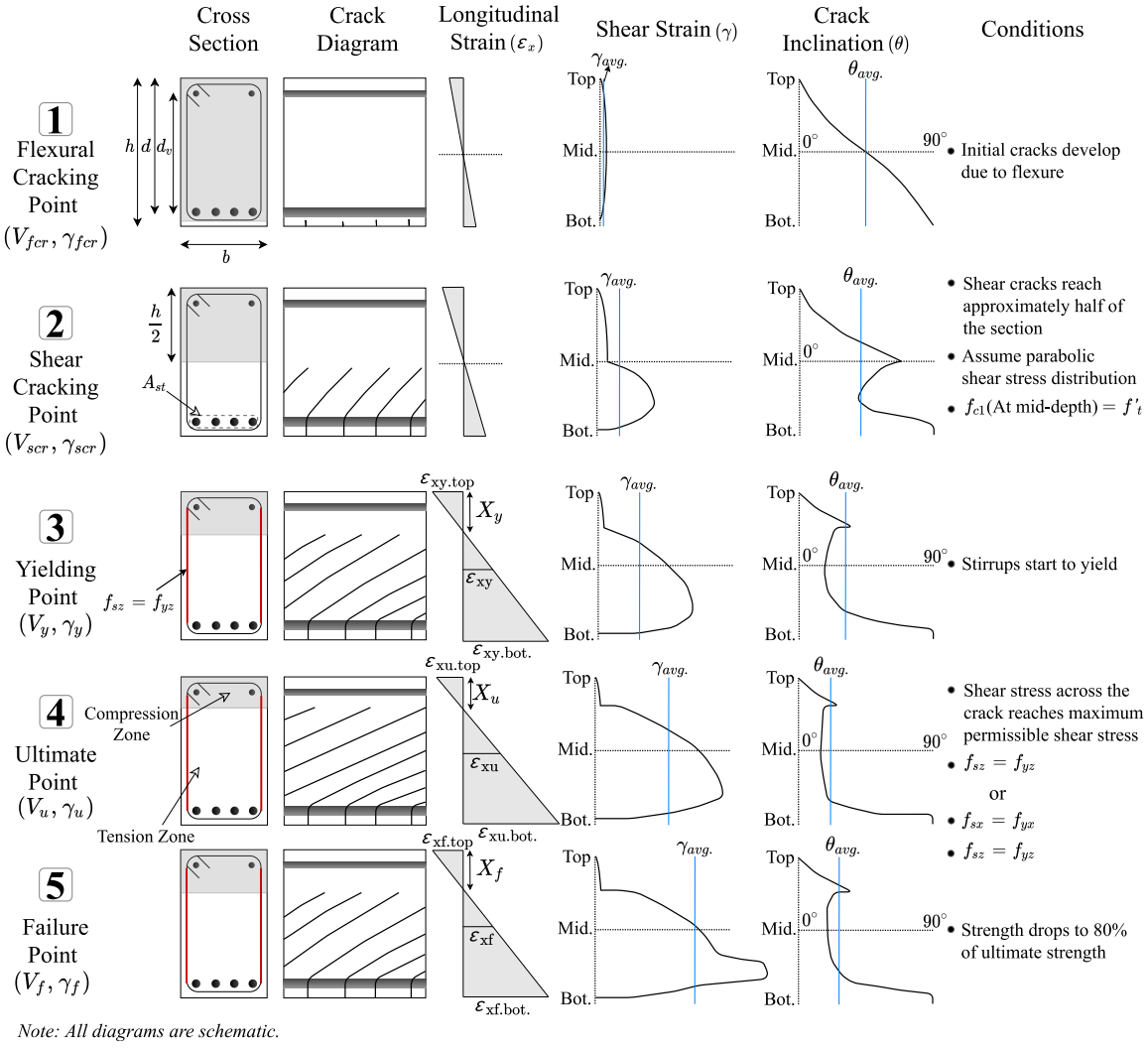

Figure 3-3 Variations of longitudinal and shear strains and crack direction through the section at five key points of the response

3.2.1 Ultimate point

The shear strength (V_u) is calculated based on the shear design provisions of the Canadian concrete design code, CSA A23.3 (2019), with some modifications. According to CSA A23.3, which is developed based on the MCFT model, the shear strength of a beam section can be expressed as:

$$V_r = V_c + V_s = \beta\sqrt{f_c'}bd_v + \frac{A_{st}f_{yt}d_v}{s}\cot(\theta_u) \qquad (3-10)$$

where V_c and V_s are the shear strength of concrete and transverse reinforcement, β is the contribution factor accounting for the strength of cracked concrete, and θ_u is the inclination of crack at the peak shear stress. In the CSA A23.3 procedure, θ_u is considered to be equal to ($29+7000\varepsilon_x$), where ε_x is the longitudinal strain at mid-depth of the member. However, Bentz et al. (2006) and Esfandiari and Adebar (2009) showed that for beams with stirrups the crack direction at ultimate load not only depends on ε_x, but also on the ratio of the yielding stress in the shear reinforcement to the compressive strength of concrete ($\rho_z \times f_{yt}/f'_c$). To perform a more thorough investigation, a wide range of RC beam cross-sections with different ratios of $\rho_z \times f_{yt}/f'_c$ is analyzed in this study using Response2000 (Bentz and Collins, 2001) which is a nonlinear sectional analysis software developed based on MCFT. The relationship between θ_u and ε_x calculated for different beams as well as the code predictions are shown in Figure 3-4. It can be seen that because of neglecting the influence of stresses in concrete and steel on θ_u, CSA A23.3 provides an upper bound for θ_u which results in conservative shear strength values. Using data presented in Figure 3-4, a more refined equation for θ_u is developed for beams containing shear reinforcement (see Eq. 3-11).

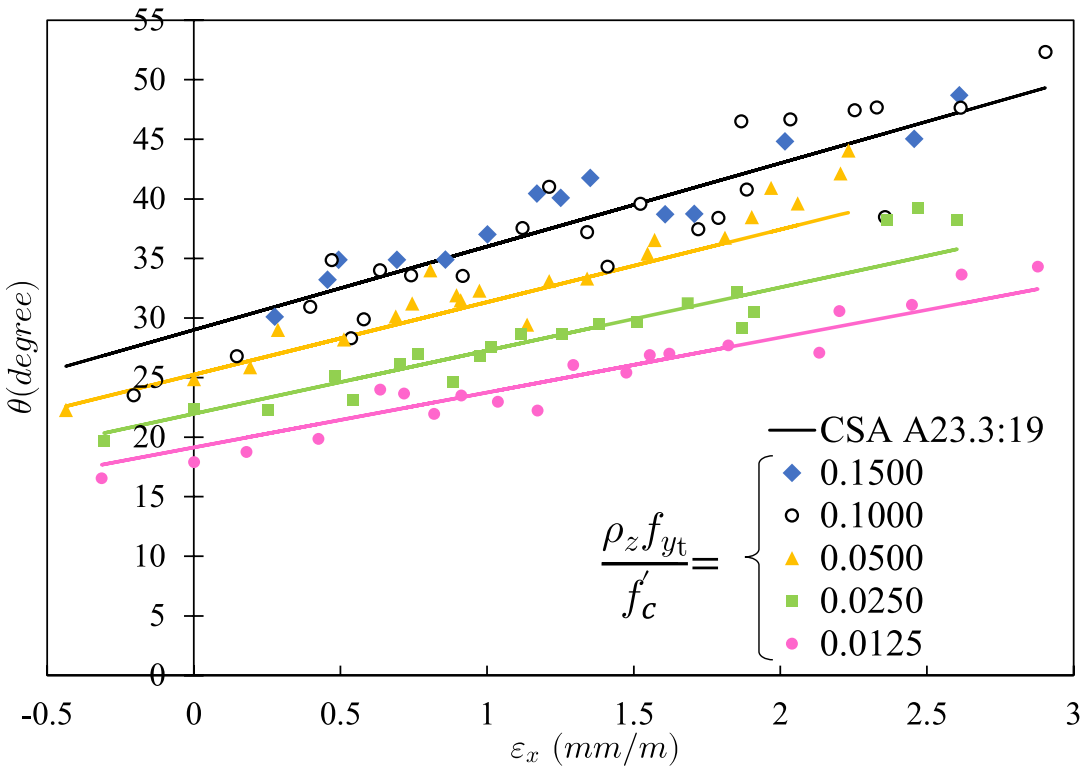

Figure 3-4 Comparison of crack inclination (θ) predicted by Response2000 and CSA A23.3 for various values of $\rho_z \times f_{yt}/f'_c$ in beams with stirrups

For beams without shear reinforcement, Bentz et al. (2006) showed that θ_u is approximately equal to $(29+7000\varepsilon_x).(0.88+s_{ze}/2500)$, where s_{ze} is the crack spacing parameter estimated using equations in Appendix A. In this study, using a parametric analytical study similar to that used for beams with stirrups, it is found that by relating θ_u to the square root of ε_x instead of ε_x, a more accurate equation for predicting θ_u can be obtained. This is shown in Figure 3-5, where the predictions of the proposed simple equation are compared with the results of the full MCFT analyses reported by Bentz et al. (2006). The proposed equations for calculating θ_u for both cases of beams with and without stirrups are shown in Eq. (3-11). All k_i coefficients are described in Appendix A.

$$\theta_u = \begin{cases} (29 + 7000\varepsilon_x).(k_6) & ; \textit{with stirrups} \\ [29 + (k_7)\sqrt{\varepsilon_x}].(k_6)) \geq 29 & ; \textit{without stirrups} \end{cases} \qquad (3-11)$$

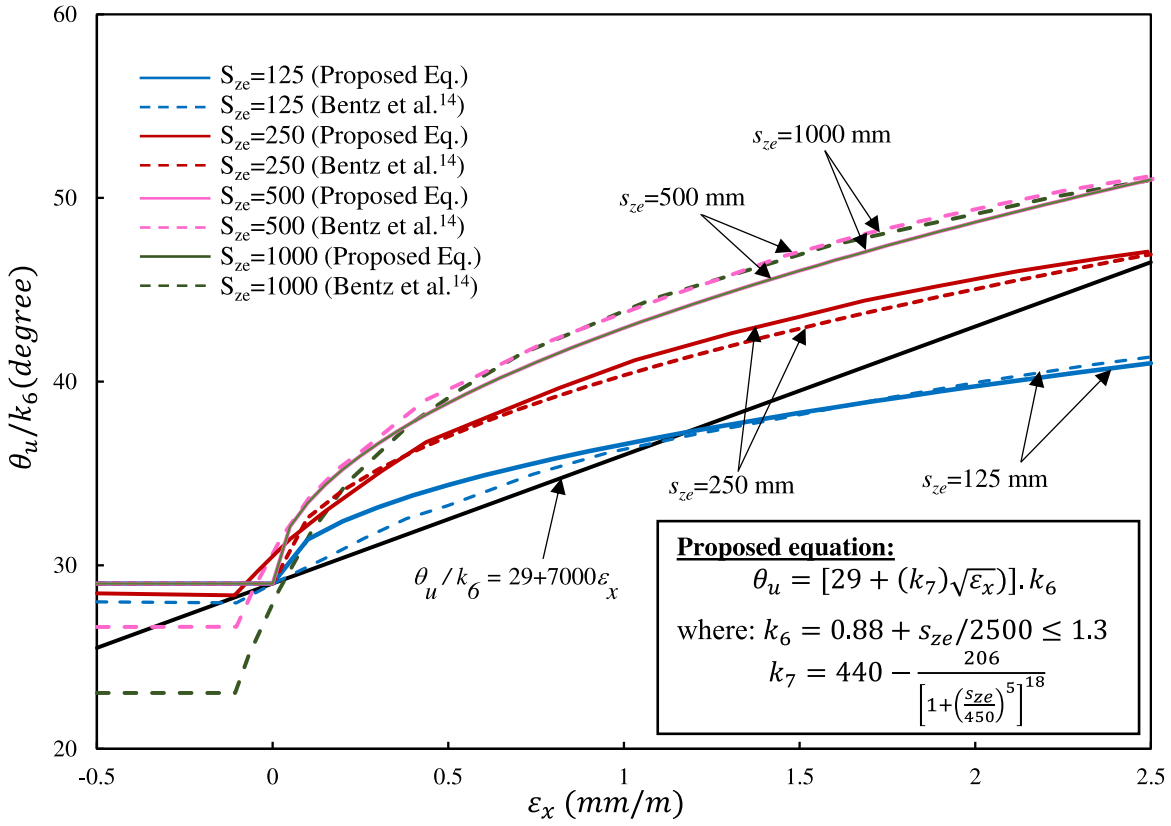

Figure 3-5 Comparison of crack inclination (θ) predicted by full-MCFT method and proposed equation in beams without stirrups

To find the shear strength in CSA A23.3, ε_x is calculated using the shear force (V_f) acting on the section. As the shear force increases, ε_x increases resulting in a lower shear strength. The relationship between the applied shear force and the shear strength of a section is shown in Figure 3-6. While this procedure works for designing a section with known sectional forces, it requires a trial-and-error procedure to be used for an analysis case where sectional forces are not known prior to the analysis. This trial-and-error procedure is explained in Section 3.3. In this study, by recognizing that the maximum applicable shear force on a section (V_u) occurs when the shear resistance becomes equal to the applied shear force $(V_r=V_f)$ (see Figure 3-6) and by estimating $cot(\theta_u)$ as $(1.73-300\varepsilon_x)/(\rho_z \times f_{yt}/f'_c)^{0.23}$, a

new equation is derived to express the shear strength solely in terms of cross-section dimensions and material properties of the beam:

$$V_u = \frac{k_1 k_3 - k_4}{2k_1 k_4} + \sqrt{\left(\frac{k_1 k_3 - k_4}{2k_1 k_4}\right)^2 + \frac{k_2 + k_3}{k_1 k_4}} \qquad (3-12)$$

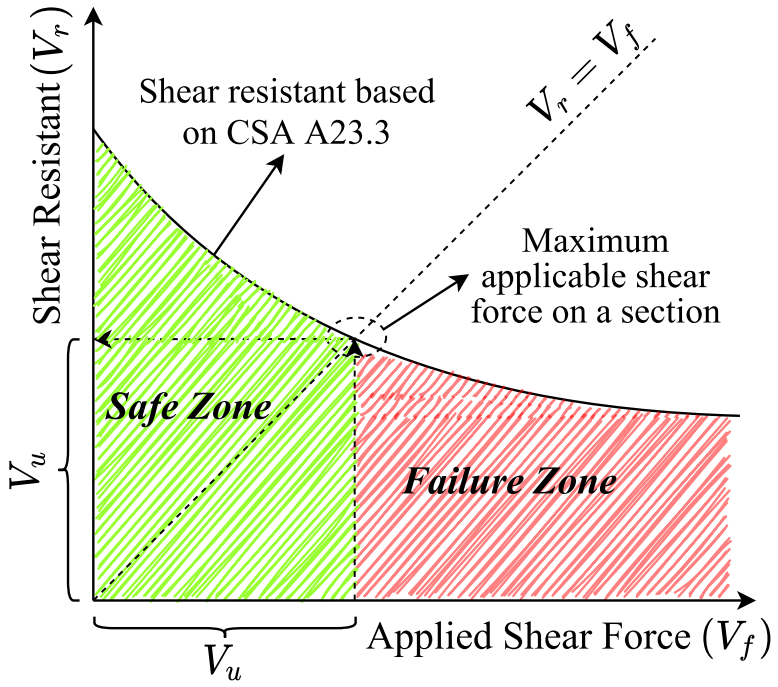

Figure 3-6 Variation of shear strength with applied shear force according to CSA A23.3

In some cases where the flexural capacity of the beam is low, the longitudinal reinforcement may yield before beam reaches its ultimate shear capacity. When the transverse and longitudinal reinforcements both yield, there would not be additional capacity in the reinforcing bars to equilibrate the diagonal compression force in the concrete resulting in a shear strength lower than that predicted by Eq. (3-12). For these cases, Esfandiari and Adebar (2009) proposed an equation to calculate the shear strength of RC beam sections:

$$V_u = \sqrt{(\alpha k_{15})^2 + 2k_{15} A_s f_{yl}} - \alpha k_{15} \qquad (3-13)$$

where α is the ratio of the bending moment to the shear force times the effective shear depth ($M/(V \times d_v)$). In this study, the minimum value of Eqs. (3-12) and (3-13) is taken as the shear strength for the lumped plasticity analysis.

The ultimate shear strain (γ_u) is found from Eq. (3-6) of the original MCFT model multiplied by a factor accounting for the effective shear strain depth in beams (k_9), as the shear strain in the compression zone is almost equal to zero (see Figure 3-3):

$$\gamma_u = 2(\varepsilon_{xu} + \varepsilon_{2u}).\cot(\theta_u).k_9 \qquad (3-14)$$

where ε_{xu} and ε_{2u} are the longitudinal strain at mid-depth and average principle compressive strain of the section at the peak shear stress, and θ_u is the crack direction at the peak shear stress which can be determined from Eq. (3-11). CSA A23.3 (2019) approximates ε_{xu} to be equal to one-half of the strain in the flexural tensile reinforcement by assuming that the longitudinal strain at the top of the section is negligible. This is generally a conservative assumption that may be reasonable for calculating the shear strength, but it can result in inaccurate shear strain predictions. To obtain a more accurate estimation of ε_{xu}, the longitudinal strain at the top of the section needs to be considered which requires estimating the height of the compression zone (X_u) (see Figure 3-3). X_u can be calculated by using Eq. (3-15) developed based on the equilibrium of the compression and tension forces in the section. According to Bentz and Collins (2006), the tension force in the reinforcement is equal to $M_u/d_v + 0.5\cot(\theta_u).V_u$. In beams with stirrups, the typical range of θ_u varies between 20 and 35 degrees, while in beams without stirrups θ_u is generally higher than 40 degrees. For simplicity, $0.5\cot\theta_u$ can be assumed to be equal to 1.0 and 0.0 for beams with and without stirrups, respectively. Additionally, the compression force in the concrete is determined to be $0.72f'_c bX_u$ from the equivalent rectangular stress block procedure (Park

and Pauley, 1975). For beams without stirrups, however, the 0.72 factor is replaced with a term proportionally related to h and the square root of f'_c. Thus, X_u can be determined using Eq. (3-15). After determining X_u, ε_{xu} can be found from Eq. (3-16) by calculating k_1 and k_5 factors using equations provided in Appendix A.

$$X_u = \begin{cases} \dfrac{\min\left((\alpha+1)V_u\,,A_{sl}.f_{yl}\right)}{0.72f'_c.b} & ;\ with\ stirrups \\ \dfrac{\min\left(\alpha V_u\,,A_{sl}.f_{yl}\right)}{\left[56\left(h.\sqrt{f'_c}\right)^{-0.7}\right]f'_c.b} & ;\ without\ stirrups \end{cases} \qquad (3-15)$$

$$\varepsilon_{xu} = \left|\frac{k_1 V_u}{750}.k_5\right| \qquad (3-16)$$

If imperial units are being used, the 56 in Eq. (3-15) should be replaced by 33.

The second parameter in Eq. (3-14) for determining γ_u is ε_{2u}. To calculate this parameter, first the principal compressive stress in concrete (f_{c2u}) is determined from Eq. (3-3) of the original MCFT model (see Figure 3-2). In this equation, the average principal tensile stress in concrete (f_{c1u}) is neglected considering that concrete is heavily cracked at this stage of the response. Thus, f_{c2u} can be expressed as:

$$f_{c2u} = v_u(tan\theta_u + cot\theta_u) \qquad (3-17)$$

f_{c2u} can also be determined from Eq. (3-9) of the original MCFT model which represents compressive stress-strain response of concrete based on the Hognestad (1951) model while including the compression softening effect. By equating Eq. (3-17) to Eq. (3-9) and using Mohr's circle of strains, the following equation can be found for ε_{2u}:

$$\varepsilon_{2u} = k_8.\varepsilon_0 \qquad (3-18)$$

where ε_0 is the strain corresponding to the compressive peak strength of concrete, and k_8 is a factor provided in Appendix A in terms of the concrete material properties, ε_{xu}, v_u, and θ_u.

3.2.2 Yielding point

The shear force corresponding to the yielding of stirrups (V_y) is found from Eq. (3-2) of the original MCFT by assuming clamping stresses in the beam are negligible ($f_z=0$) (Bentz et al., 2006), and multiplying the stress with the effective shear area:

$$V_y = \frac{\rho_z f_{yt} + f_{c1y}}{tan\theta_y}.b.d_v \qquad (3-19)$$

f_{c1y}, which is the principal tensile stress in concrete when stirrups yield, is assumed to be equal to 20% of the concrete tensile strength ($0.2f'_t$). This assumption is made by incorporating the original formulation of the MCFT model and the post-cracking tension stiffening model of Tamai et al. (1988). According to Eq. (3-5) of the original MCFT, the principal tensile strain in concrete at the yielding point (ε_{1y}) will be in the same order as the yielding strain of stirrups (ε_{zy}) considering that ε_{zy} is relatively larger than ε_{xy} and ε_{2y} at this stage of the response. Assuming that the typical yielding strain of stirrups (ε_{zy}) is about 0.002 and using the tension stiffening model of Tamai et al. (1988), f_{c1y} can be approximated as $0.2f'_t$. It worth mentioning that because of the relatively gentle slope of the post-peak tensile response of concrete due to the tension stiffening effect, the influence of approximations made in determining f_{c1y} is insignificant.

To estimate θ_y in Eq. (3-19), the relationship between V and θ after the flexural cracking point (point 1) and before reaching the peak point (point 4) in the response is investigated for a wide range of RC beam sections using Response2000. It is found that the relationship

can be expressed in the form of Eq. (3-20), where "n" is the shape factor, that can be varied from 0.5 to 1.0 in various beam sections. For simplicity, the shape factor at the yielding point is considered as 1.0, resulting in a linear relationship between V and θ. Eq. (3-20) can be further simplified by approximating the shear force at the formation of flexural cracks (V_{fcr}) as 10% of the shear strength (V_u), and estimating the initial crack direction (θ_{fcr}) as 45° which is a reasonable assumption for reinforced concrete sections. Applying these simplifications and rearranging Eq. (3-20), results in Eq. (3-21) for θ_y.

$$\left(\frac{\theta_{fcr}-\theta}{\theta_{fcr}-\theta_u}\right)^n+\left(\frac{V_u-V}{V_u-V_{fcr}}\right)^n=1 \qquad (3-20)$$

$$\theta_y=45°-(45°-\theta_u)\left(\frac{1.11V_y}{V_u}-0.11\right) \qquad (3-21)$$

By substituting θ_y from Eq. (3-21) into Eq. (3-19), the shear force at the yielding point (V_y) can be found as:

$$V_y=\begin{cases}\left|\dfrac{k_{11}}{2k_{12}}\right| & ; \quad k_{10}k_{12}>\left(\dfrac{k_{11}}{2}\right)^2,\theta_u\neq 45 \\ \dfrac{\frac{k_{11}}{2}-\sqrt{\left(\frac{k_{11}}{2}\right)^2-k_{10}k_{12}}}{k_{12}} & ; \quad k_{10}k_{12}\leq\left(\dfrac{k_{11}}{2}\right)^2,\theta_u\neq 45 \\ k_{10} & ; \quad \theta_u=45\end{cases} \leq V_u \qquad (3-22)$$

The calculation of shear strain at the yielding point is similar to that described for the peak shear strain and can be determined using Eq. (3-23).

$$\gamma_y=2\left(\varepsilon_{xy}+\varepsilon_{2y}\right).\cot\left(\theta_y\right).k_{13}\leq\gamma_u \qquad (3-23)$$

where ε_{xy} is estimated by calculating the average of longitudinal strains at the top and bottom of the section ($\varepsilon_{xy.top}$ and $\varepsilon_{xy.bot.}$), as shown in Eq. (3-24). $\varepsilon_{xy.top}$ is approximately equal to the top longitudinal strain at the peak point ($\varepsilon_{xu.top}$). Using this approximation, and

ε_{xu} and X_u calculated in the previous section, $\varepsilon_{xy.top}$ and $\varepsilon_{xy.bot}$ can be determined from Eqs. (3-25) and (3-26), respectively.

$$\varepsilon_{xy} = \left|\frac{\varepsilon_{xy.bot.} - \varepsilon_{xy.top}}{2}\right| \leq \varepsilon_{xu} \qquad (3-24)$$

$$\varepsilon_{xy.top} = \frac{k_1 V_u}{750} . \frac{X_u}{d - X_u} \qquad (3-25)$$

$$\varepsilon_{xy.bot.} = \frac{k_1 V_y}{750} \qquad (3-26)$$

The last parameter that needs to be determined in Eq. (3-23) is ε_{2y}. Using the results of the parametric study discussed above ε_{2y} is related to ε_{2u}:

$$\varepsilon_{2y} = \varepsilon_{2u} . \left(1 - \sqrt{1 - \frac{V_y}{V_u}}\right)^2 \qquad (3-28)$$

where ε_{2u} can be calculated using Eq. (3-18). Finally, the parameter k_{13} in Eq. (3-23) is defined to account for the effective shear strain depth as previously described for k_9 factor used for the ultimate point.

3.2.3 Flexural cracking point

The flexural cracking point is where the first crack perpendicular to the longitudinal axis of the beam develops. The flexural cracking moment is equal to $f'_t \times bh^2/6$. Therefore, the shear force corresponding to the cracking moment (V_{fcr}) can be determined according to Eq. (3-29).

$$V_{fcr} = \frac{0.33\sqrt{f'_c} bh^2}{6\alpha \mathrm{d_v}} \qquad (3-29)$$

The shear strain corresponding to the flexural cracking (γ_{fcr}) point is simply determined by dividing the shear force by the initial shear stiffness, as follows:

$$\gamma_{fcr} = \frac{V_{fcr}}{G.b.d_v} \qquad (3-30)$$

3.2.4 Shear cracking point

After the section cracks, as the shear force increases, cracks start to rotate towards the concrete compression strut forming diagonal shear cracks. According to the results of the parametric study, when the diagonal shear cracks approximately reach the mid-depth of the section, the neutral axis is located at the mid-depth of the section. In this study, this point is defined as the "shear cracking point" (see Figure 3-1 and Figure 3-3). Assuming a parabolic shear stress distribution through the section height, the average shear stress (v_{scr}) will be equal to two-thirds of the shear stress at the mid-depth of the section ($v_{scr.mid.}$):

$$v_{scr} = \frac{2}{3} v_{scr.mid.} \qquad (3-31)$$

According to Eq. (3-3) of the original MCFT, $v_{scr.mid.}$ can be determined from the principle tensile and compressive stresses in concrete ($f_{c1.scr.mid.}$, $f_{c2.scr.mid.}$) and the crack inclination ($\theta_{scr.mid.}$) at the mid-depth of the section. Substituting Eq. (3-3) into Eq. (3-31) results in the following equation for the shear cracking force (V_{scr}):

$$V_{scr} = \frac{2}{3} \frac{f_{c1.scr.mid.} + f_{c2.scr.mid.}}{\tan(\theta_{scr.mid.}) + \cot(\theta_{scr.mid.})} b d_v \qquad (3-32)$$

where $f_{c1.scr.mid.}$ can be estimated as $f_t' = 0.33\sqrt{f_c'}\ MPa\ \left(4\sqrt{f_c'}\ psi\right)$ since the shear cracking point is defined as when the concrete tensile stress at the mid-depth of the section reaches the cracking stress. $f_{c2.scr.mid.}$ is relatively small compared to $f_{c1.scr.mid.}$ at the shear cracking point. Nevertheless, using the results of the parametric study, the following relationship between $f_{c2.scr.mid.}$, f'_c and α can be found:

$$f_{c2.scr.mid.} = \frac{7.7 f_c'}{(\alpha f_c')^{1.6}} \qquad (3-33)$$

If f'_c is expressed in imperial units, the 7.7 factor in Eq. (3-33) should be replaced by 22000. $\theta_{scr.mid.}$ can also be found by calculating the average crack direction (θ_{scr}) and considering

the distribution of the crack direction through the section height at the shear cracking point, as shown in Figure 3-7. It can be seen that the distribution of crack direction can be approximated with a parabolic curve at the top half of the section and a constant value at the bottom half of the section. Using the weighted average concept, the crack direction at mid-depth can be estimated as about 1.5 times the average crack direction through the section:

$$\theta_{scr.mid.} = 1.5\theta_{scr} \qquad (3-34)$$

θ_{scr} is determined with the same concept as that provided for Eq. (3-20) at the yielding point assuming that V_{scr}/V_u equals to 0.4 and 0.7 for beams with and without stirrups, respectively:

$$\theta_{scr} = \begin{cases} 30° + 0.33\theta_u \;\; ; \;\; with\ stirrups \\ 15° + 0.67\theta_u \;\; ; \;\; without\ stirrups \end{cases} \qquad (3-35)$$

The results of the sectional parametric study showed that the influence of the initial assumption for V_{scr}/V_u on the final value of V_{scr} is insignificant.

The shear cracking strain (γ_{scr}) is simply estimated by dividing the shear force by 75% of the initial shear stiffness of concrete, as presented in Eq. (3-36). The shear stiffness at this point can vary from $G.b.d_v$ to $0.5G.b.d_v$. For simplicity, the average value of this range which is $0.75G.b.d_v$ is used for the model.

$$\gamma_{scr} = \frac{V_{scr}}{0.75G.b.d_v} \qquad (3-36)$$

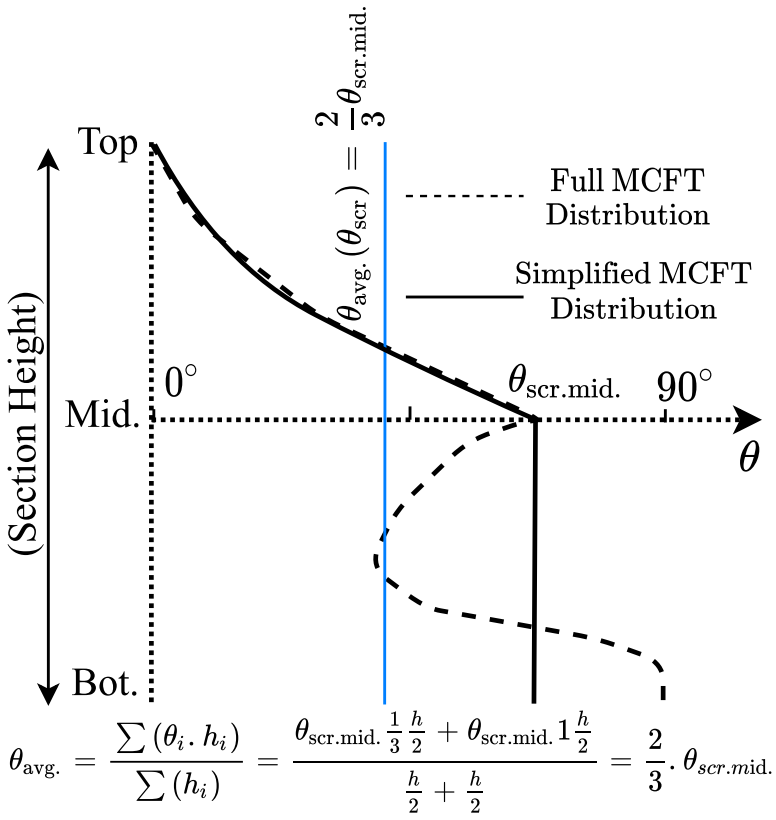

Figure 3-7 Variation of crack direction through section at shear cracking point

3.2.5 Failure point

For beams without stirrups or beams with stirrups that do not have adequate flexural reinforcement, the post-peak response is assumed to be negligible due to the brittle nature of the failure. For beams that contain stirrups and have adequate flexural reinforcement, a post-peak response is calculated to consider the residual shear strength and ductility of the beam after reaching the ultimate shear strength point. For these beams, the shear stress at failure is considered as 80% of the ultimate shear strength based on the recommendations from the literature (Park and Ang, 1985). To find the shear strain, it is assumed that the principal compressive strain in concrete at failure (ε_{2f}) is equal to the strain corresponding to the peak compressive strength of concrete (ε_0). Using this assumption and Eq. (3-6) of the original MCFT, the shear strain at failure can be found from Eq. (3-37).

$$\gamma_f = 2(\varepsilon_{xf} + \varepsilon_0).\cot(\theta_f).k_{14} \qquad (3-37)$$

Solving Eq. (3-37) requires estimating the average longitudinal strain (ε_{xf}) and the average crack direction (θ_f) at failure. It can be seen from various sectional analysis results that values of ε_x and θ at the post-peak response are approximately equal to those corresponding to the same shear force at the pre-peak response. Thus, values of ε_x and θ at the failure point are approximated with the pre-peak values at 80% of the shear strength. ε_{xf} can be found from the longitudinal strain at the top and bottom of the section ($\varepsilon_{xf.bot.}$ and $\varepsilon_{xf.top}$) using Eq. (3-38).

$$\varepsilon_{xf} = \left|\frac{\varepsilon_{xf.bot.} - \varepsilon_{xf.top}}{2}\right| \geq \varepsilon_{xu} \qquad (3-38)$$

where $\varepsilon_{xf.top}$ is equal to $\varepsilon_{xy.top}$ as the top longitudinal strain does not vary significantly from the yielding point to the failure point, and can be calculated using Eq. (3-25). Also, $\varepsilon_{xf.bot}$ can be calculated using Eq. (3-26) by replacing V_y with $0.8V_u$. The next parameter required to calculate the shear strain at failure is θ_f which can be estimated by replacing V_y with $0.8V_u$ in Eq. (3-21). This results in the following simplified equation for θ_f.

$$\theta_f = 10° + 0.78\,\theta_u \qquad (3-39)$$

Finally, the parameter k_{14} is defined to account for the effective shear strain depth as previously described for k_9 and k_{13} factors used for the ultimate and yielding points, respectively.

The step-by-step procedure on how to use the above-mentioned equations to calculate the five key points and generate the shear force-shear strain relationship is demonstrated in Figure 3-8.

3.3 Verification at the component-level

A total of 11 shear-critical beams experimentally tested by Podgorniak-Stanik (1998), Frosch (2000), Cladera (2002) and Sherwood (2008) and one flexural-critical beam tested by Kassem et al. (2011) were selected to assess the performance and accuracy of the proposed model. To provide an unbiased comparison of the results, different beams were selected for the verification study than those considered in the previous section for the derivation of model equations. The main characteristics of the beams are shown in Table 3-1. The beam sections covered a wide range of key design parameters to provide a comprehensive assessment of the proposed model. All beams were simply supported and subjected to a point load at the mid-span, except for "ST-6" beam that was loaded under two symmetrical point loads.

Table 3-1 Parameters of RC beams considered for the verification study

Researcher	Beam	f'_c (MPa)	f_{yl} (MPa)	f_{yt} (MPa)	b (mm)	h (mm)	d (mm)	a (mm)	s (mm)	A_{sl} (mm^2)	A_{st} (mm^2)	$\frac{V_{u,exp.}}{V_{u,cal.}}$
Kassem et al. (2011)	ST-6	40.8	460	460	200	300	235	875	80	600	200	1.04
Podgorniak-Stanik (1998)	BN50	37.0	483	-	300	500	450	1350	-	1100	-	1.14
	BH50	99.0	483	-	300	500	450	1350	-	1100	-	0.93
	BN100	37.0	550	-	300	1000	925	2700	-	2100	-	0.93
Sherwood (2008)	S-10H	77.3	494	-	122	330	280	810	-	285	-	1.03
	L-10H	73.6	452	-	300	1510	1400	4050	-	3500	-	0.97
Podgorniak-Stanik (1998)	BM100	46.0	550	508	300	1000	925	2700	600	2100	142.6	1.11
Frosch (2000)	V1&V2	36.5	475	483	457	914	851	2553	372	3870	142.6	1.04
Sherwood (2008)	S-10HS	77.3	502	496	122	330	280	810	160	458	19.6	1.13
	L-10HS	73.6	452	494	300	1510	1400	4050	235	5600	71.3	1.07
Cladera (2002)	H50/4	49.9	500	540	200	400	351	1080	210	2098	100.6	1.04
	H100/4	87.0	500	540	200	400	351	1080	210	2098	100.6	0.99

(Note: 1 mm = 0.0394 in.; 1 MPa = 0.1450 ksi.)

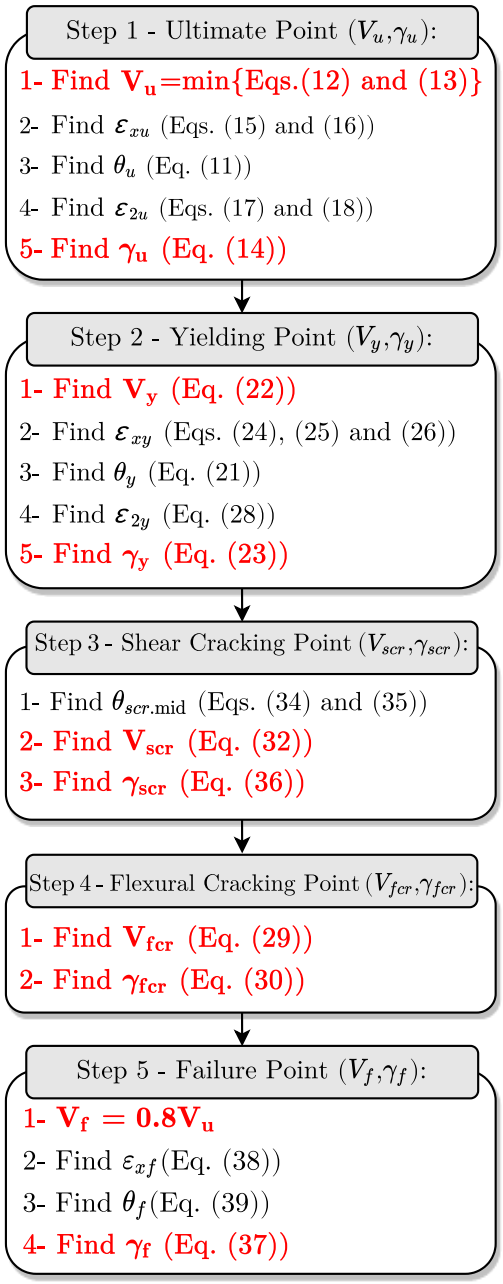

Figure 3-8 Step-by-step procedure for calculation of the five key points for the proposed model

The beams were modeled in the OpenSees software (Mazzoni et al., 2006) using 2-noded frame elements each having a series of fibers representing the nonlinear behavior at the section-level. As mentioned previously, the frame element in OpenSees is not capable of capturing the shear behavior in an RC member, as it is designed to consider only the biaxial flexural and axial behavior. To account for shear effects, the proposed shear hinge model

was added to the FE model using *ZeroLength* elements (see Figure 3-9). A *ZeroLength* element (i.e., shear hinge) was placed on each side of the beam at d_v distance away from the applied load. This is considered to be the critical section because the shear force distribution is constant throughout the beam and the largest bending moment occurs at the midspan under the loading plate. As the bending moment increases the longitudinal strain increases resulting in a lower shear strength and a more critical section (i.e., shear force-bending moment interaction effect). Because of the high concentrated compressive force under the loading plate, the shear-critical section is typically assumed to be at the d_v distance away from the loading plate. This location correlates reasonably well with the location of diagonal shear cracks observed in experimental tests. It should be noted that this location is only suitable for simply supported beams subjected to a concentrated load at the midspan. For beams with other types of boundary or loading conditions, the location of shear hinge might be different and should be selected based on the shear force and bending moment diagrams. A multi-linear uniaxial material model was assigned to the *ZeroLength* elements. The response of the material model was defined using the values of the shear force and shear deformation at each key point obtained from the procedure described in Figure 3-8. The shear deformation was calculated by multiplying the shear strain by 1.5 times the section height (h) as recommended by Guner (2008).

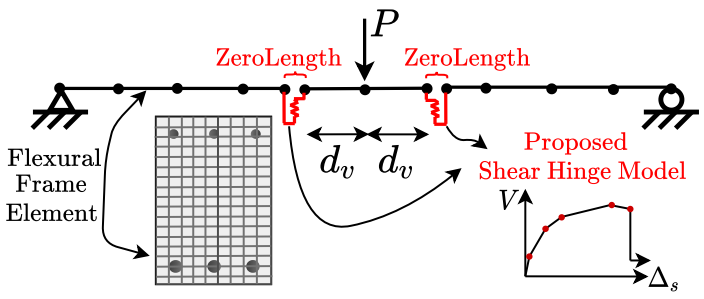

Figure 3-9 OpenSees model of beam with the proposed shear hinge model

Figure 3-10 shows the comparison of load-deflection responses of the beams obtained from: 1) the experiment; 2) OpenSees with and without the proposed shear hinge model; 3) OpenSees with a shear hinge model defined according to the ASCE-41 (2017) backbone curves; and 4) VecTor5 (Guner and Vecchio, 2008), a distributed plasticity analysis software with shear analysis capability. Before investigating the shear-critical beams, a flexural-critical beam (ST-6) was analyzed to verify the modeling procedure in OpenSees. It can be seen from Figure 3-10 that the results of OpenSees models with and without the shear hinge for the flexural-critical beam were nearly identical and correlated well with the experimentally reported data. Thus, implementing shear hinges into the OpenSees model did not have any effect on the behavior of the flexural-critical beam as expected. It worth noting that for this beam the shear deformations were negligible compared to flexural deformations.

After verifying the FE modeling procedure in OpenSees, the ability of the proposed shear hinge model to capture shear behavior was investigated. It can be seen from Figure 3-10 that the OpenSees model with the proposed shear hinge computed force-displacement relationships of the shear-critical beams reasonably well. In general, the model was able to capture the initial elastic response, reduction in stiffness due to concrete cracking or yielding of the transverse reinforcement, peak strength and deformation, and failure due to shear. In some cases (H50/4 and H100/4), the model overestimated the initial stiffness, resulting in relatively more stiff responses with somewhat lower deflections. The overestimation of the initial stiffness for these two beams was common for all analysis methods including the ASCE-41 shear hinge model and VecTor5. One reason for this could be that these beams might had already been in their cracked state prior to the test due to the shrinkage effect which resulted in a lower initial stiffness compared to an uncracked beam.

Another reason could be the inherent variation in the behavior of shear-critical test specimens due to the complexity and variability associated with shear mechanisms. An example of this variation can be seen in the experimentally reported peak strengths of V1 and V2 beams which had identical material and structural characteristics.

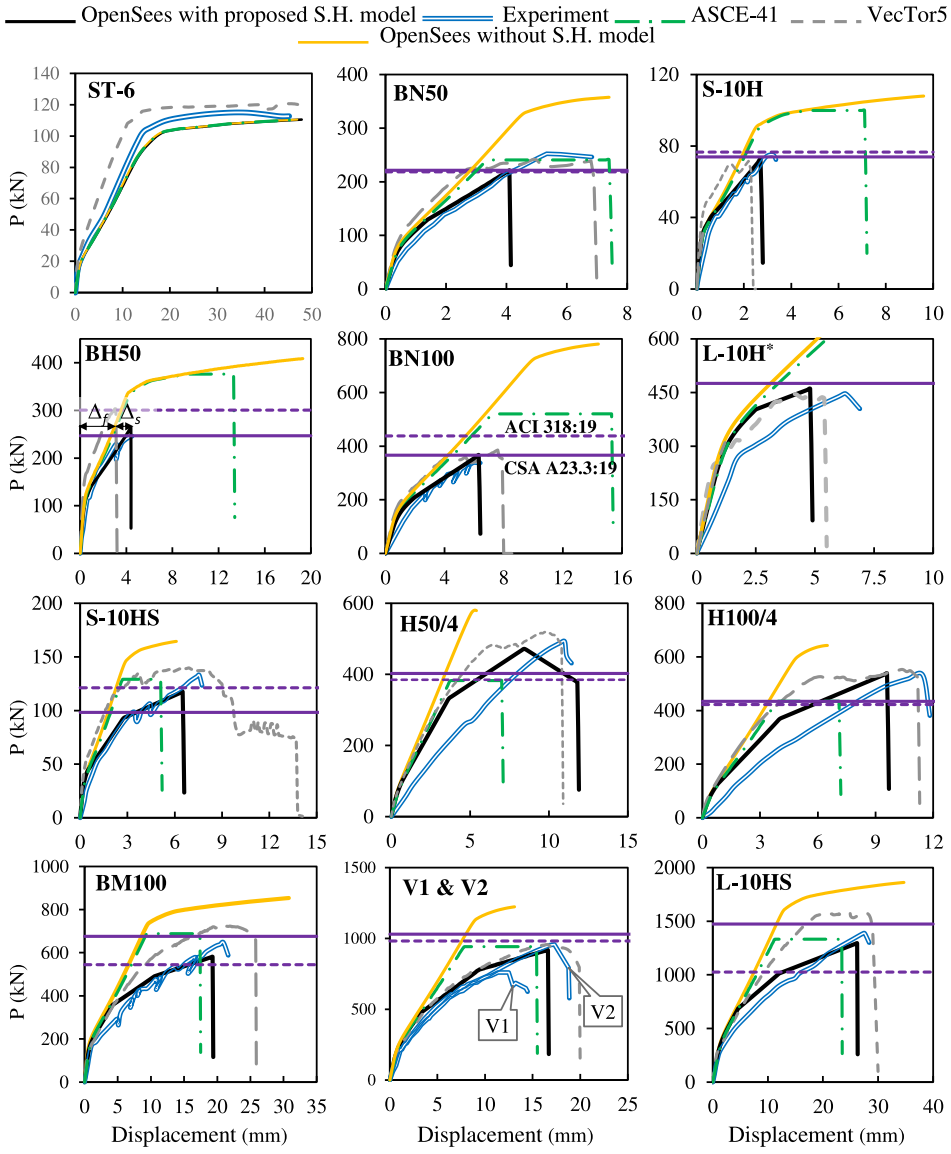

Note: Curves of L-10H beam for the OpenSees without S.H. and ASCE-41 models are not shown completely for clarity of the figure. The peak load and the corresponding displacement for these two models are [1278.1 kN, 68.8 mm] and [1016.4 kN, 23.8 mm], respectively. Also, the ACI 318:19 prediction for peak strength for this beam is 941.9 kN.

Figure 3-10 Comparison of force-displacement curves between OpenSees models with and without proposed shear hinge, experiment, OpenSees with ASCE-41 shear hinge model, and VecTor5

As shown in Figure 3-10, the OpenSees model without the shear hinge couldn't account for shear effects, leading to significant overestimation of the peak strength and deformation. For this model, the analysis continued until the beam reached its flexural capacity resulting in wrong failure modes. It should be mentioned that frame elements with fiber sections in OpenSees are not intended to capture the shear behavior or to be used for analysis of shear-critical structures. The reason this modeling approach is included in this study is to demonstrate the consequence of using frame elements in OpenSees for structures with considerable shear effects and the importance of enhancing these elements with shear modeling capability.

Comparison of the load-deflection responses calculated by VecTor5 which considers shear effects using a distributed plasticity approach with those obtained from the proposed lumped plasticity shear hinge model in Figure 3-10 demonstrated a good agreement between the results. Although the lumped plasticity model is based on a relatively less complicated analysis approach where the nonlinearity effects due to shear are concentrated at the hinge locations, it can be seen that this approach resulted in the same or even higher level of accuracy compared to VecTor5. This can be due to an approximation made in the formulation of VecTor5 which assumes a predefined shear strain distribution (either parabolic or uniform) through the section for the entire analysis. This assumption, however, is only accurate for the initial stages of the response. After concrete starts to crack, shear strains at the cracked layers become considerably larger than those at the uncracked layers resulting in a more complicated strain distribution. With the proposed shear hinge model, on the other hand, the actual shear strain distribution in different stages of the response was

considered in the derivation of the model equations in an average sense (see Figure 3-3) which led to more accurate results for most of the analysis cases.

The performance of the proposed model was also evaluated against another shear hinge model defined based on the ASCE-41 backbone curves and implemented into OpenSees. It can be seen from Figure 3-10 that this model could not accurately capture the strength and ductility of beams without stirrups particularly if they had relatively high depth or high concrete compressive strength. One reason for this is the inability of the ASCE-41 model to consider the size effect which is known to have significant influence on the response of beams with no or little shear reinforcement (Collins et al., 2020). For beams containing stirrups, the load-deflection responses calculated by the ASCE-41 model generally showed better agreement with the experimental results.

The shear strength of the beam sections predicted by the CSA A23.3 (2019) and ACI-318 (2019) design codes are also shown in Figure 3-10. For the calculation of shear strength of beams with high strength concrete, f'_c was limited to 70 MPa and 80 MPa (10.15 ksi and 11.60 ksi) as recommended by the ACI-318 and CSA A23.3 codes, respectively. The peak strength calculated by the proposed shear hinge model and CSA A23.3 for beams without stirrups were close to each other and showed better agreement with the experimental results when compared to the peak strength obtained from ACI-318. For beams with stirrups, the proposed shear hinge model computed the peak strength of beams more accurately than both of the design codes.

For the calculation of the peak shear strength based on the CSA A23.3 code equation, a trial-and error procedure was performed. First, an initial value of V_f was assumed, and

based on the value of α (the ratio of the bending moment to the shear force times the effective shear depth) that is constant for a particular section in a beam, the value of ε_x was calculated. Based on the calculated ε_x, the values of β and θ_u were computed, and finally the shear resistance (V_r) was found. The V_r was then compared with the initially assumed V_f, and this procedure continued until V_f and V_r converged.

3.4 Verification at the system-level

The application of the proposed model at the system-level was investigated on a two-storey, single-span RC frame with shear-critical beams tested by Duong et al. (2007). The geometry of the frame, as well as cross-section dimensions and reinforcement details, are shown in Figure 3-11.

The base shear versus lateral roof displacement responses reported from the experimental test and calculated by the analysis procedures mentioned in the previous section are shown in Figure 3-12. It can be seen that there was a good agreement between the results of the OpenSees model with the proposed shear hinge model, the VecTor5 model, and the experiment. Both analytical models captured the damage sequence and failure mode of the frame accurately. First, the first-storey beam failed in shear causing a significant drop in the load-deflection response which shortly followed by the shear failure of the second-storey beam resulting in complete failure of the frame. In Figure 3-12, the reason for the sharp drop in the calculated result of the OpenSees analysis with the proposed shear hinge model at the system-level is due to assuming a sudden drop in the post-peak response of the proposed shear hinge model at the member-level. Once a shear-critical member fails, because of the sudden drop in its shear resistance (see Figure 3-1) it no longer contributes

to the stiffness of the system. As a result, an abrupt reduction in the force-displacement curve at the system-level would be yielded.

The other two analytical models (OpenSees model without shear hinge and OpenSees model with ASCE-41 shear hinge) both significantly overestimated the peak strength and ductility. The OpenSees model without shear hinge only computed the flexural response of the frame and neglected the shear behavior as expected. The OpenSees model with the ASCE-41 shear hinge captured the shear failure, but significantly overestimated the peak shear strength and ductility of the frame. One reason for the overestimation of the results is that the ASCE-41 model does not take into account the influence of yielding of longitudinal reinforcement on the shear capacity as discussed in the derivation of the ultimate strength equation in the Model Development section. The overestimation in the strength led to significantly higher lateral roof deformations, especially because at this stage of the response the flexural reinforcement at the base of the columns was yielded.

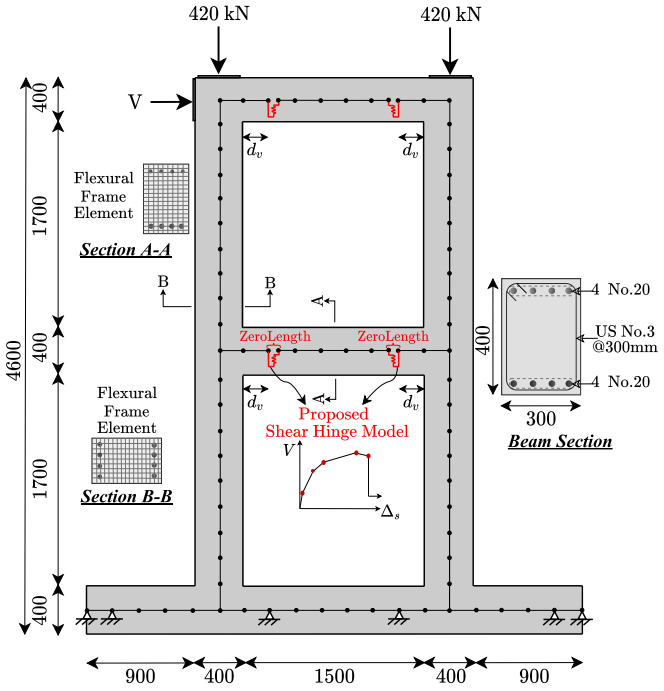

Figure 3-11 Lumped plasticity model of Duong et al. (2007) test frame (1 mm = 0.0394 in.; 1 kN = 0.225 kip)

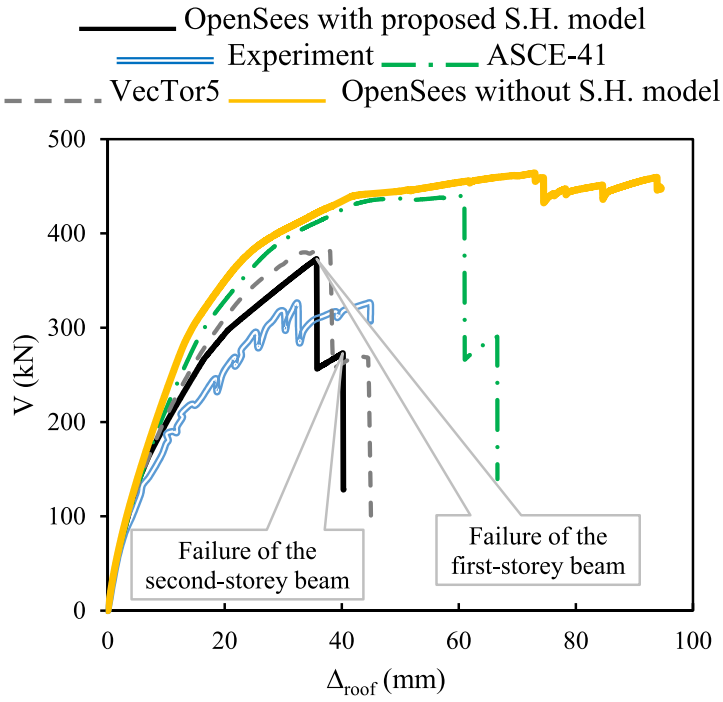

Figure 3-12 Comparison of base shear versus lateral roof displacement for Duong et al. (2007) test frame (1 mm = 0.0394 in.; 1 kN = 0.225 kip)

3.5 Summary and conclusions

A nonlinear lumped plasticity model was developed based on the Modified Compression Field Theory (MCFT) to capture the shear behavior of RC beams. The compatibility, equilibrium, and constitutive relationships of the original MCFT model, which requires a complicated trial-and-error procedure, were simplified into closed-form equations using a wide range of parametric studies on shear-critical RC beams. Nonlinear distribution of stresses, strains, and crack direction through the section at different stages of the response was considered in the development of the model equations. Using the proposed model, the shear force and shear deformation values at five key stages of the response can be calculated enabling detailed representation of the shear behavior. By implementing the proposed model into OpenSees, its performance was assessed against experimental tests, the ASCE-41 lumped plasticity model, and a distributed plasticity model at both the component- and system-level. It was demonstrated that the proposed model can compute the failure mode and load-deflection response of the test specimens with better accuracy compared to the other two modeling approaches. The analysis results also highlighted the consequences of using a frame-type analysis procedure like OpenSees for shear-critical structures without giving special consideration to modeling shear effects. Lastly, the ultimate shear strength values estimated from the proposed model were compared against those obtained from the CSA A23.3 and ACI-318 design codes. It was shown that although the basis of the proposed model is similar to CSA A23.3 for the calculation of the ultimate shear strength, the model provided more accurate results because of the improvements made in the formulation.

After successful application of MCFT to various design procedures and nonlinear finite element and sectional analysis programs over the last forty years, this study for the first time demonstrated that this viable theory can also be highly effective for the analysis of shear-critical RC structures using the lumped plasticity approach. Considering the computational efficiency of the lumped plasticity approach, the proposed shear hinge model will be beneficial for the analysis of large RC structural systems. It enables to accurately take into account the nonlinear shear response of structures while using computationally efficient frame-type analysis procedures.

3.6 Notation

A_{sl}= area of tensile longitudinal reinforcement

A_{st}= area of transverse reinforcement

a= shear span

b= beam width

d= effective depth

d_v= effective shear depth, taken as the greater of $0.9d$ or $0.72h$

E_s= modulus of elasticity of steel

f'_c= cylindrical compressive strength of concrete

f_{c1}= principal tensile stress in concrete

f_{c2}=principal compressive stress in concrete

f_{sx}=average stress in x-reinforcement

f_{sz}= average stress in z-reinforcement

f'_t= modulus of rupture of concrete

f_x= stress applied to element in x-direction

f_{yl} (f_{yx})= yield strength of longitudinal reinforcement

f_{yt} (f_{yz})= yield strength of transverse reinforcement

f_z= stress applied to element in z-direction

G= initial shear modulus of concrete

h= beam height

n= shape factor used in Eq. (3-20)

s= spacing of transverse reinforcement

s_z= crack spacing parameter, as defined in CSA A23.3

s_{ze}= equivalent value of s_z that allows for influence of aggregate size

V_c= shear resistance provided by concrete

V_f= shear force acting on a section

V_r= shear resistance

V_s= shear resistance provided by transverse reinforcement

V= shear force

v= shear stress

v_c= shear stress in concrete

v_{ci}= shear stress on crack surfaces

X= distance from extreme compression fiber to neutral axis

$\alpha = \frac{M}{V d_v}$

β= contribution factor accounting for strength of cracked concrete

Δ_f= flexural deformation

Δ_s= shear deformation

ε_0= strain in concrete at peak stress f'_c

ε_1= principal tensile strain in concrete

ε_2= principal compressive strain in concrete

ε_x= longitudinal strain

ε_z= transverse strain

γ= shear strain

θ= angle between crack inclination and x-axis

ρ_x= longitudinal reinforcement ratio

ρ_z= transverse reinforcement ratio

Subscripts “u”, “f”, “y”, “scr” and “fcr” are related to each of the five key points in the model. Also, subscripts “mid.”, “top” and “bot.” show the location of the parameter through the height of the section. Parameters without the location subscripts, indicate the average value through the height. For example, θ_y denotes the average crack inclination angle at the yielding point, and $f_{c1.scr.mid.}$ denotes the principal tensile stress in concrete at the mid-depth of the section at the shear cracking point.

Chapter 4: A Shear Hinge Model for Analysis of Reinforced Concrete Columns

4.1 Introduction

This chapter was written based on a journal paper that was recently accepted for publication in the ACI Structural Journal. It presents a rational shear hinge model for nonlinear analysis of RC columns that is capable of capturing advanced mechanisms in reinforced concrete and axial-flexure-shear interaction effects. The model is developed based on fundamental equations of equilibrium and compatibility in conjunction with well-recognized constitutive material models enabling its application to a wide range of structures. The accuracy and application range of the model are assessed by analyzing a large number of shear-critical RC columns with various design parameters and comparing the results against those obtained from experimental tests and detailed finite element analyses. The effectiveness of the proposed model for system-level analysis is also shown by modeling a multi-storey frame structure.

4.2 Development of the model

Similar to the shear hinge model developed for beams and described in Chapter 3, a multi-linear curve for shear force versus shear strain relationship is proposed for columns, as shown in Figure 4-1. Four key points on this curve are considered, representing the various stages of the shear response: concrete cracking, yielding of transverse reinforcement, ultimate shear strength, and shear failure. As shown in Figure 4-1, the key points considered for the beam and column model have two major differences. First, the shear cracking point in the beam model is removed from the column model. In the beam model, this point was defined as when diagonal shear cracks approximately reach the mid-depth

of the section. Because of the presence of axial compressive load in columns, however, the tensile zone in the section becomes relatively small, and the shear cracks typically do not reach the mid-depth prior to yielding of the transverse reinforcement (see Figure 4-1). This change also makes the model simpler without affecting its accuracy.

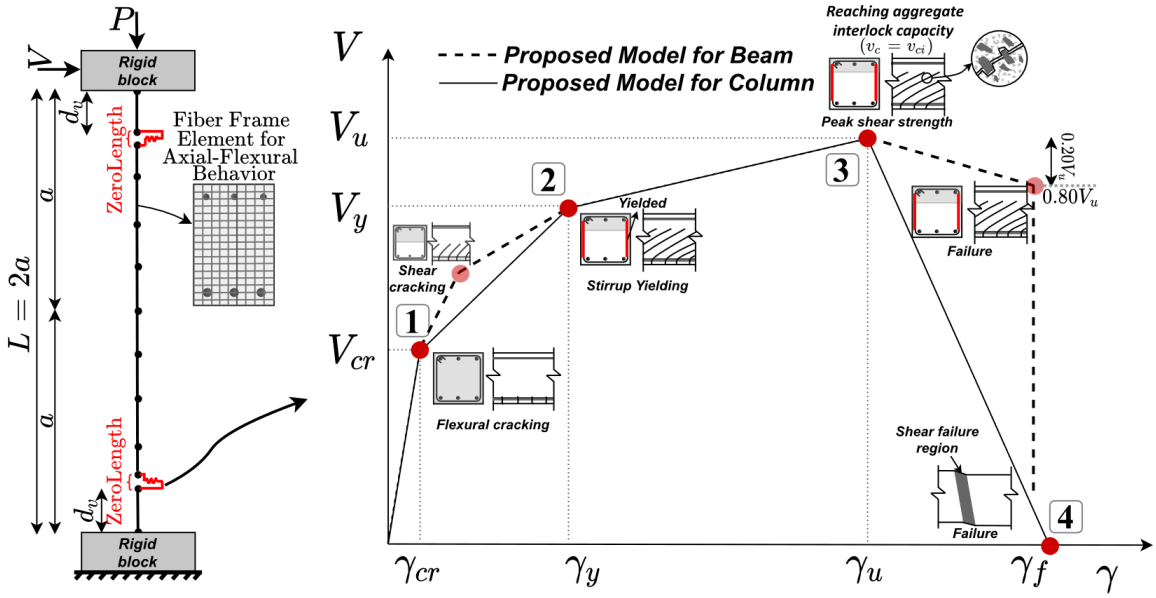

Figure 4-1 Schematic shear force-shear strain curves for the shear hinge models proposed for beams and columns

The second change is in the definition of the post-peak response. For beams, the failure point was defined as a point where there was a 20% reduction in the peak shear strength which was then followed by an abrupt decline in the response. This definition was considered acceptable as there has not been much research done on the post-peak response of shear-critical beams. In comparison, there are a few studies dedicated to the failure point of shear-critical columns. The model proposed by Elwood and Moehle (2005) developed based on the shear friction theory, and the model proposed by Tran and Li (2015) formulated based on the energy concept are two examples of these studies. The post-peak

response of shear-critical columns will be discussed in more detail in the Failure Point section.

In general, there are two main differences between the characteristic behavior of RC beams and columns that need to be investigated. First, the presence of axial load on columns affects their shear behavior by changing the magnitude and distribution of strains, stresses, and the concrete crack inclination. In this study, the effect of axial load is considered in conjunction with the other sectional forces (bending moment and shear force) by modifying the equilibrium and compatibility equations used for the development of the beam shear hinge model. This enables accounting for the axial-flexural-shear interaction effects which is critical for accurate prediction of the shear behavior in RC columns. The second difference is the confinement effect in RC columns due to the lateral pressure produced by the transverse reinforcement. Although the confinement effect in columns can have a substantial impact on the flexural and axial response, its influence on the shear behavior can be neglected. This is because shear cracks in columns are typically initiated as vertical cracks along the tension reinforcement and then extend towards the compression reinforcement as diagonal cracks. The parts of the cross-section that are mostly affected by shear cracks are often under high tensile strains and therefore confinement has not much of an influence on their behavior. Confinement mainly affects the behavior in the compression zone of the column which can be critical for the axial and flexural response since concrete crushing may take place in this zone. In this study, the confinement effect is considered in defining the concrete material properties of nonlinear fiber sections of frame elements used for modeling columns.

As shown in Figure 4-2, and similar to the procedure considered for beams, a 2D panel element is considered at the critical section of the column to represent the nonlinear shear behavior in a concentrated form. The critical section is defined d_v (i.e., effective shear depth) away from the section having maximum shear force, which is approximately the location of diagonal shear cracks observed in experimental tests and is consistent with the shear-critical section defined in the Canadian Concrete Design code (CSA A23.3, 2019). In cases where the shear force is constant throughout the column length (e.g., cantilever columns), the critical section is d_v away from the section having the largest bending moment. This is because as the bending moment increases, the longitudinal strain increases, which reduces the ability of concrete to carry shear forces resulting in a lower shear strength for the cross-section (CSA A23.3, 2019; Bentz et al., 2006).

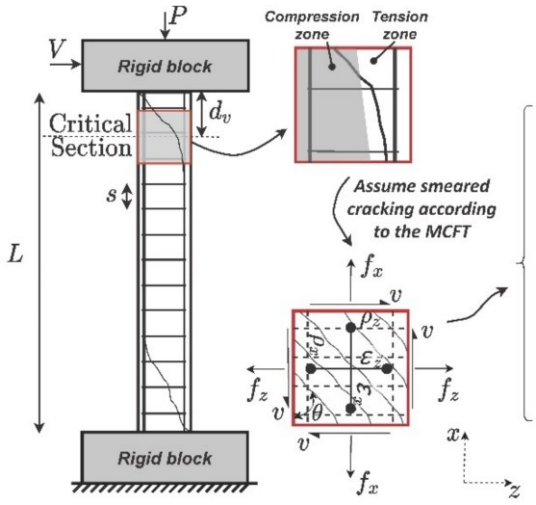

$$\textit{Equilibrium}: \begin{cases} f_x = \rho_x f_{sx} + f_{c1} - v\cot(\theta) & (4\text{-}1) \\ f_z = \rho_z f_{sz} + f_{c1} - v\tan(\theta) & (4\text{-}2) \\ v = \dfrac{f_{c1} + f_{c2}}{\tan(\theta) + \cot(\theta)} & (4\text{-}3) \end{cases}$$

$$\textit{Geometric Conditions}: \begin{cases} \tan^2(\theta) = \dfrac{\varepsilon_x + \varepsilon_2}{\varepsilon_z + \varepsilon_2} & (4\text{-}4) \\ \varepsilon_1 = \varepsilon_x + \varepsilon_z + \varepsilon_2 & (4\text{-}5) \\ \gamma_{xz} = 2(\varepsilon_x + \varepsilon_2)\cot(\theta) & (4\text{-}6) \end{cases}$$

$$\textit{Stress-Strain Relationships}: \begin{cases} f_{sx} = E_s\varepsilon_x \le f_{yx} & (4\text{-}7) \\ f_{sz} = E_s\varepsilon_z \le f_{yz} & (4\text{-}8) \\ f_{c2} = \dfrac{f'_c}{0.8 + 170\varepsilon_1}\left[2\dfrac{\varepsilon_2}{\varepsilon_0} - \left(\dfrac{\varepsilon_2}{\varepsilon_0}\right)^2\right] & (4\text{-}9) \end{cases}$$

Figure 4-2 Estimating shear behavior of an RC column in a concentrated form with a 2D panel element formulated based on MCFT

By evaluating the stresses and strains on the 2D panel and using the original MCFT formulation, closed-form equations are derived to calculate the shear force and shear strain

of each key point of the shear response demonstrated in Figure 4-1. The original MCFT formulation, which are based on the equilibrium and compatibility conditions and stress-strain relationships, are shown in Figure 4-2. The development of closed-form equations requires estimating stresses, strains, and crack inclination at the critical section of the column. By analyzing a wide range of column cross-sections using the Response2000 sectional analysis software (Bentz and Collins, 2001) and VecTor2 FE program (Wong et al., 2013), the nonlinear distribution of longitudinal strain (ε_x), shear strain (γ), and crack inclination (θ) along the section height is determined. Figure 4-3 shows an example of the nonlinear distribution of each parameter at different stages of the structural response. As it can be seen in this figure, the average value of the nonlinear distribution of each parameter is estimated using the equivalent area approach and then used for the development of closed-form equations. Unlike the original MCFT model which is complicated and requires a trial-and-error procedure, the closed-form equations enable direct calculation of shear response allowing the application of MCFT to the lumped plasticity analysis. Details of the closed-form equations developed for each key point of the shear response are discussed below. The similarities and differences between the equations proposed for columns and those previously developed for beams are highlighted.

4.2.1 Ultimate point

Similar to the beam model, the shear strength (V_u) of columns is calculated based on the Canadian Concrete Design Code, CSA A23.3 (2019), with a few modifications. Eq. (4-10) shows the relationship provided in the code for computing the shear strength of an RC section which includes the contributions of both the concrete and the transverse reinforcement (V_c and V_s, respectively).

$$V_u = V_c + V_s = \beta\sqrt{f_c'}bd_v + \frac{A_{st}f_{yt}d_v}{s}\cot(\theta_u) \qquad (4-10)$$

where θ_u and β are the crack inclination at the ultimate shear stress and the contribution factor accounting for the strength of cracked concrete, respectively. Both parameters are a function of the longitudinal strain at mid-height of the section (ε_{xu}) which can be calculated based on sectional forces (bending moment, shear force and axial load) using Eq. (4-11) (Bentz et al., 2006). This equation is simplified by defining two factors (k_1 and k'_1) which account for the effects of bending moment (M) and axial load (P), and will be also used in the rest of the equations presented in this study. All the k factors defined in this study are provided in Appendix B.

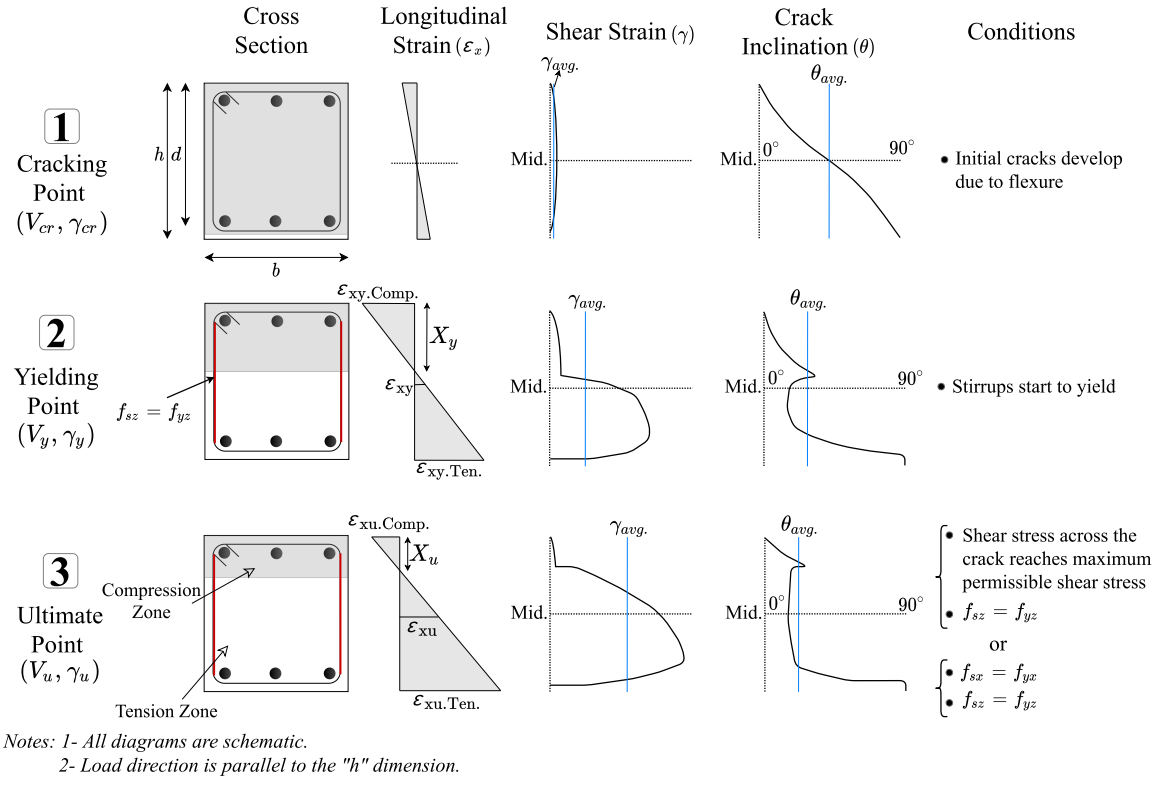

Figure 4-3 Variations of longitudinal and shear strains and crack direction through the section at the first three key points of the response

$$\varepsilon_{xu} = \frac{(1+\alpha)V_u + 0.5P}{2A_{sl}E_s} = \left|\frac{k_1 V_u + k_1'}{1500}\right| \qquad (4-11)$$

In Eq. (4-11), α is the ratio of the bending moment to the shear force multiplied by the effective shear depth ($M/V.d_v$). Once ε_{xu} is calculated based on the sectional forces, θ_u can be found using Eq. (4-12). This equation was originally proposed for the beam model as described in Chapter 3. It improves the crack inclination relationship of the CSA A23.3 design code by adding the k_6 factor in the equation to account for the effects of the yielding stress of the shear reinforcement (f_{yt}) and the compressive strength of concrete (f_c') on θ_u.

$$\theta_u = (29 + 7000\varepsilon_{xu}).(k_6) \qquad (4-12)$$

Figure 4-4 shows that this equation is also valid for columns. In this figure, the average value of the crack inclination angle along the cross-section of 12 shear-critical columns obtained from the VecTor2 nonlinear FE analysis software (Wong et al., 2013) are compared against the angle computed from Eq. (4-12). Over the last thirty years, VecTor2 has been extensively verified against experimental data of various shear-critical structural components (Sadeghian and Vecchio, 2018) and therefore can be considered as a reliable FE analysis tool for evaluating the performance of the proposed shear hinge model. It can be seen from Figure 4-4 that the average θ_u values correlate well, demonstrating the validity of the proposed equation for the calculation of θ_u of RC columns. Structural details of the RC columns considered in this study are summarized in Table 4-1.

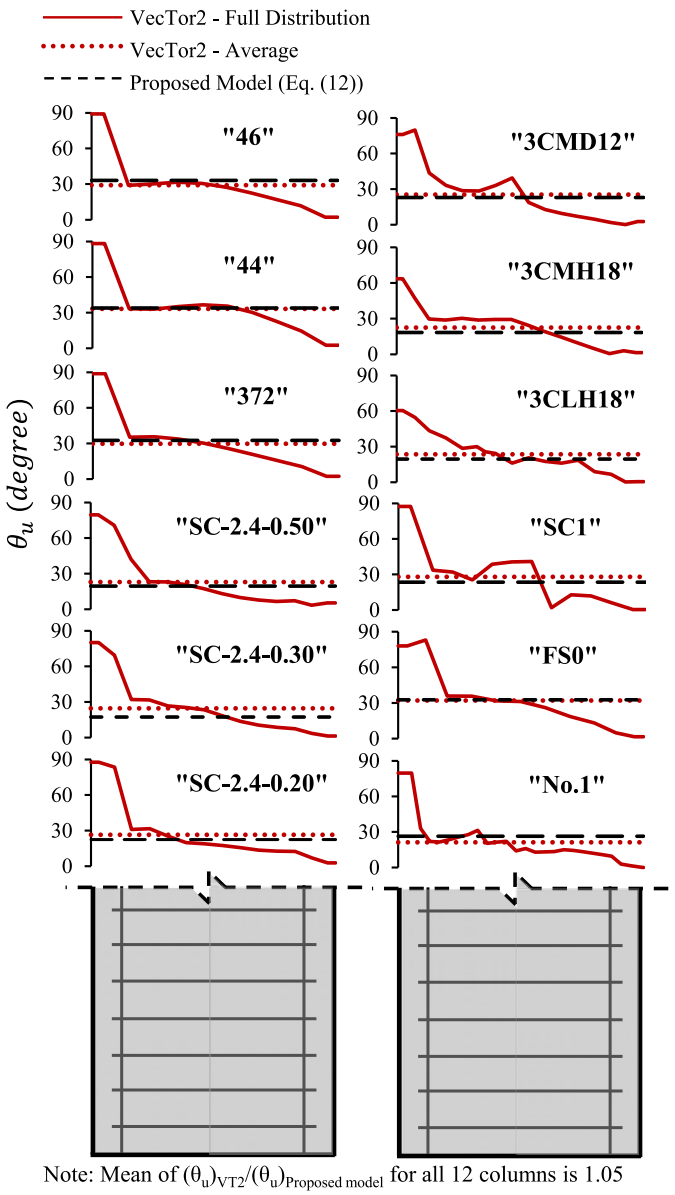

Figure 4-4 Comparison of the average crack inclination angle along the cross-section for 12 shear-critical RC columns computed by VecTor2 and the proposed model

By substituting Eq. (4-11) into Eq. (4-12) and Eq. (4-12) into Eq (4-10) and following the same procedure as that described for the beam model, the shear strength of the column cross-section can be derived solely as a function of material properties and section dimensions as expressed in Eq. (4-13). In this equation, setting the axial load factor (k'_1) to zero results in the shear strength equation previously proposed for the beam model.

$$V_u = \frac{k_1 k_3 - k_4(1 + k'_1)}{2k_1 k_4} + \sqrt{\left(\frac{k_1 k_3 - k_4(1 + k'_1)}{2k_1 k_4}\right)^2 + \frac{k_2 + k_3(1 + k'_1)}{k_1 k_4}} \qquad (4-13)$$

Esfandiari and Adebar (2009) showed that yielding of the longitudinal reinforcement can limit the shear strength of RC members. Based on their work, the authors proposed Eq. (4-14) to calculate the shear strength of beams with low amount of flexural reinforcement (see Chapter 3 for more details):

$$V_u = \sqrt{(\alpha k_{15})^2 + 2k_{15} A_{sl} f_{yl}} - \alpha k_{15} \qquad (4-14)$$

Application of this equation to RC columns requires two modifications. First, the contribution of concrete to the shear strength was neglected in Eq. (4-14) and needs to be considered for columns. As previously discussed, the tension zone in columns is typically smaller than that in beams due to the axial load effect and therefore there is more contribution from the concrete to the shear strength in columns. In this study, the concrete contribution is considered by adding the $\beta\sqrt{f'_c} b d_v$ term to Eq. (4-14). To be on the conservative side, the β factor is taken as 0.05 which is the minimum value recommended by CSA A23.3 (2019). The second modification is to include the effect of axial load, in addition to the shear force and bending moment, in the derivation of Eq. (4-14). As a result of these two modifications, the following equation is proposed for the calculation of shear strength in RC columns with low amount of flexural reinforcement:

$$V_u = \sqrt{(\alpha k_{15})^2 + 2k_{15} A_{sl} f_{yl} - k_{15} P} - \alpha k_{15} + 0.05\sqrt{f'_c} b d_v \qquad (4-15)$$

The minimum value of Eqs. (4-13) and (4-15) is taken as the shear strength of RC column sections for the lumped plasticity analysis.

The shear strain at the ultimate point (γ_u) can be found from Eq. (4-16) which is derived by modifying Eq. (4-6) of the original MCFT method (see Figure 4-2) to account for the effective shear strain depth in the section as discussed for the beam model in Chapter 3. Since Eq. (4-16) is determined solely based on the compatibility and strain transformation relationships, it can be used for columns as well.

$$\gamma_u = 2(\varepsilon_{xu} + \varepsilon_{2u}).\cot(\theta_u).k_9 \qquad (4-16)$$

In Eq. (4-16), ε_{xu} is the longitudinal strain at the mid-depth of the section, ε_{2u} is the average principle compressive strain of the section, θ_u is the average crack inclination angle, and k_9 is a modification factor to account for the shear strain distribution over the depth. All these parameters are calculated at the peak shear stress (i.e., the ultimate point) and are affected by the axial load in columns. ε_{xu} can be calculated from Eq. (4-17) which is similar to the equation used for the beam model developed based on the equilibrium requirements. The main difference in the calculation of ε_{xu} is the addition of the k'_1 factor to the equation to account for the effect of axial load. In addition, a lower bound is considered to ensure that the value of ε_{xu} would not fall below the limit of longitudinal strain under pure axial load condition.

$$\varepsilon_{xu} = \frac{k_1 V_u + k'_1}{750}.k_5 \geq \frac{P}{bh(0.5E_c + \rho_x E_s)} \qquad (4-17)$$

In Eq. (4-17), the k_5 factor is a function of the compression zone depth in the section (X_u) which can be calculated using Eq. (4-18) developed based on the equilibrium of compression and tension forces in the section with the consideration of axial load.

$$X_u = \frac{\sqrt{C\varepsilon_0\left[bdf'_c\varepsilon_{xu.Ten.} + \frac{C\varepsilon_0}{2}\right]} - \frac{C}{2}}{bf'_c\varepsilon_{xu.Ten.}} \qquad (4-18)$$

$$C = T - P = \min\{(1+\alpha)V_u + 0.5P\ , A_{sl}f_{yl}\} - P \qquad (4-19)$$

where C and T are the summation of the forces acting on the compression and tension sides of the neutral axis, respectively, and P is the applied compressive axial load which should be considered with a negative sign. A more accurate and complicated version of Eq. (4-18) that considers the effect of the longitudinal compression reinforcement is provided in Appendix B. In Eq. (4-18), $\varepsilon_{xu.Ten.}$ is the strain of the tension reinforcement at the peak shear stress which can be computed using Eq. (4-20) developed by Bentz and Collins (2006).

$$\varepsilon_{xu.Ten.} = \frac{k_1 V_u + k_1'}{750} \qquad (4-20)$$

The second variable in Eq. (4-16) is ε_{2u} which can be calculated by finding the principal compressive stress in the concrete (f_{c2u}). Using Eq. (4-3) of the original MCFT method and neglecting the principal tensile stress in the concrete (f_{c1u}) because of high tensile strains at this stage of the response, f_{c2u} can be expressed as:

$$f_{c2u} = v_u(tan\theta_u + cot\theta_u) \qquad (4-21)$$

For the beam model, f_{c2u} and θ_u in Eq. (4-21) represented the average values of concrete stress and crack angle for the entire cross-section. While this approach works well for beams, its application to columns requires some modifications. Because of the axial load, the compression depth of the section in columns is considerably larger than that in beams. To consider the contribution of the stresses in the compression zone to the average f_{c2u} of the section more accurately, instead of applying Eq. (4-21) to the entire cross-section, f_{c2u} values of the compression and tension zones of the section are calculated separately using Eqs. (4-22a) and (4-22b). The weighted average technique is then used to compute the average f_{c2u} of the section as expressed in Eq. (4-23).

$$f_{c2u.Ten.} = v_u(tan\theta_{u.Ten.} + cot\theta_{u.Ten.}) \qquad (4-22a)$$

$$f_{c2u.Comp.} = v_u\left(tan\theta_{u.Comp.} + cot\theta_{u.Comp.}\right) \qquad (4-22b)$$

$$f_{c2u} = \frac{f_{c2u.Comp.}X_u + f_{c2u.Ten.}(h - X_u)}{h} \qquad (4-23)$$

where $\theta_{u.Ten.}$ and $\theta_{u.Comp.}$ are the average crack inclination angle in the tension and compression zones of the section, respectively. The distribution of f_{c2u} and θ_u along the section height obtained from the VecTor2 model as well as the average values for the tension and compression zones estimated by the proposed lumped plasticity model are shown in Figure 4-5. To determine $\theta_{u.Ten.}$ and $\theta_{u.Comp.}$, the distribution of the crack angle along the section is simplified into a constant and a parabolic distribution for the tension and compression zones, respectively. Using the simplified distributions and the average θ_u of the section calculated from Eq. (4-12), $\theta_{u.Ten.}$ and $\theta_{u.Comp.}$ can be estimated from Eq. (4-24).

$$\theta_{u.Ten.} = \frac{\theta_u}{1 - \frac{2X_u}{3h}} \qquad (4-24a)$$

$$\theta_{u.Comp.} = \frac{\theta_{u.Ten.}}{3} \qquad (4-24b)$$

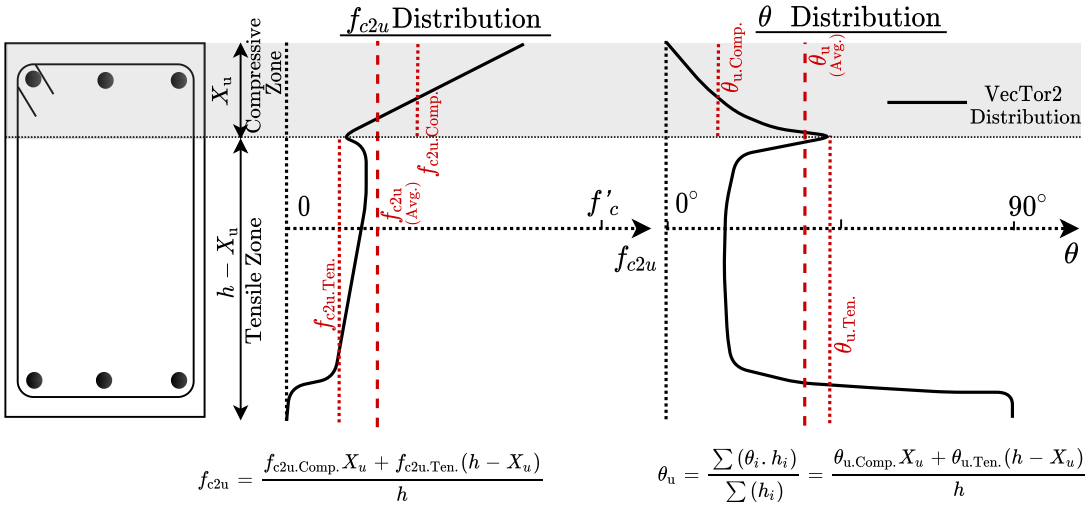

Figure 4-5 Variation of principal compressive stress and crack direction through section at the ultimate point

By equating Eq. (4-23) to Eq. (4-9) of the original MCFT method, which represents the compressive stress-strain response of concrete based on the Hognestad (1951) model while accounting for the compression softening effect (see Figure 4-2), Eq. (4-25) can be derived for calculation of the principal compressive strain in concrete (ε_{2u}).

$$\varepsilon_{2u} = \max\{k_8, 1 - \sqrt{1 - \frac{f_{c2u}}{f_c'}}\} \times \varepsilon_0 \qquad (4-25)$$

The overall concept for calculating ε_{2u} is the same for both the beam and column models. The only difference between the two models is in the consideration of the compression softening effect. As the axial compressive load increases in a column section, the principal tensile strain in concrete (ε_1) reduces, and as a result the reduction factor for the compression softening effect that is equal to $1/(0.8+170\varepsilon_1)$ (see Eq. (4-9)) may become greater than 1.0 which is not correct. Therefore, the maximum reduction factor for the compression softening effect is limited to 1.0 which occurs when the principal tensile strain in concrete is extremely low and the compression softening effect is negligible. This limit is included in the derivation of Eq. (4-25).

4.2.2 Yielding point

The shear force corresponding to the yielding of the transverse reinforcement (V_y) can be found using Eq. (4-26) which is derived from Eq. (4-2) of the original MCFT method as described in Chapter 3 for the beam model.

$$V_y = \frac{\rho_z f_{yt} + f_{c1y}}{tan\theta_y}.b.d_v \qquad (4-26)$$

In Eq. (4-26), the effect of axial load is considered in the calculation of the principal tensile stress in concrete (f_{c1y}) which is estimated from the principal tensile strain (ε_{1y}). From Eq. (4-5) of the original MCFT shown in Figure 4-2, ε_{1y} equals to the summation of the yielding

strain of stirrups (ε_{zy}), the longitudinal strain at the yielding point (ε_{xy}), and the principal compressive strain in concrete at the yielding point (ε_{2y}). Considering that ε_{zy} is typically around 0.002 and is relatively greater than ε_{xy} and ε_{2y} at this stage of the response, f_{c1y} can be estimated as $0.2f'_t$ (20% of the concrete tensile strength) based on the tension stiffening model of Tamai et al. (1988). As shown in Chapter 3, this approach works well for beams where the compression depth of the section (X_u) is relatively small compared to the tension zone. However, the compression depth of the section in columns is generally much larger than that in beams because of the axial load effect, and therefore the contribution of ε_{2y} and ε_{1y} becomes more significant in comparison with ε_{zy}. This effect is taken into account in the calculation of f_{c1y} by including the ratio of the compression depth to the total height of the column section (X_u/h) as can be seen in Eq. (4-27).

$$f_{c1y} = \left(0.2 + 0.3\frac{X_u}{h}\right) f'_t \qquad (4-27)$$

The next parameter that needs to be calculated in Eq. (4-26) is θ_y. For the beam model described in Chapter 3, a linear relationship was found between the crack angle and shear strength at the yielding point (θ_y and V_y) and those calculated at the ultimate point (θ_u and V_u). The application of this linear relationship, which is expressed in Eq. (4-28), to RC columns can be evaluated by computing the crack angle and shear strength of 12 shear-critical columns that were previously mentioned in the Ultimate Point section using the VecTor2 FE analysis software. It can be seen from Figure 4-6 that the FE analysis results correlate well with the predictions of Eq. (4-28) demonstrating that this equation is applicable to columns as well.

$$\theta_y = 45° - (45° - \theta_u)\left(\frac{1.11V_y}{V_u} - 0.11\right) \qquad (4-28)$$

Substituting Eq. (4-28) into Eq. (4-26), the following equation can be derived for V_y:

$$V_y = \begin{cases} \left|\frac{k_{11}}{2k_{12}}\right| & ; \quad k_{10}k_{12} > \left(\frac{k_{11}}{2}\right)^2, \theta_u \neq 45 \\ \frac{\frac{k_{11}}{2} - \sqrt{\left(\frac{k_{11}}{2}\right)^2 - k_{10}k_{12}}}{k_{12}} & ; \quad k_{10}k_{12} \leq \left(\frac{k_{11}}{2}\right)^2, \theta_u \neq 45 \\ k_{10} & ; \quad \theta_u = 45 \end{cases} \leq V_u \qquad (4-29)$$

The shear strain at the yielding point (γ_y) can be calculated with a similar approach to that described for the shear strain at the peak point (γ_u):

$$\frac{V_y}{G.b.d_v} \leq \gamma_y = 2(\varepsilon_{xy} + \varepsilon_{2y}).\cot(\theta_y).k_{13} \leq \gamma_u \qquad (4-30)$$

where ε_{xy} is the longitudinal strain at the mid-depth of the cross-section and ε_{2y} is the principal compressive strain in the concrete both calculated at the yielding point. Similar to the procedure used for beams, ε_{xy} can be calculated as the average of longitudinal strain at the outermost tensile and compressive fibers of the section ($\varepsilon_{xy.Ten.}$ and $\varepsilon_{xy.Comp.}$), as shown in Eq. (4-31):

$$\frac{P}{bh(0.5E_c + \rho_x E_s)} \leq \varepsilon_{xy} = \left|\frac{\varepsilon_{xy.Ten.} - \varepsilon_{xy.Comp.}}{2}\right| \leq \varepsilon_{xu} \qquad (4-31)$$

$\varepsilon_{xy.Comp.}$ is approximately equal to the longitudinal strain in the outermost compressive fiber of the section at the peak point ($\varepsilon_{xu.Comp.}$) as described in Chapter 3. Therefore, similar to the procedure used at the peak point, $\varepsilon_{xy.Comp.}$ can be computed using Eq. (4-32). $\varepsilon_{xy.Ten.}$ can also be determined from Eq. (4-33), which is exactly the same as Eq. (4-20) used for the peak point, except that V_u is replaced by V_y.

$$\varepsilon_{xy.Comp.} = \frac{k_1 V_u + k'_1}{750} . \frac{X_u}{d - X_u} \qquad (4-32)$$

$$\varepsilon_{xy.Ten.} = \frac{k_1 V_y + k'_1}{750} \qquad (4-33)$$

To calculate ε_{2y} in Eq. (4-30), a linear relationship between the principal compressive strain in the concrete and the shear force calculated at the yielding point and the peak point of the response is derived. This relationship, which is expressed in Eq. (4-34) and shown in Figure 4-6, is found by regression analysis of data obtained from FE analysis of the aforementioned 12 RC column specimens with VecTor2. In Figure 4-6, in addition to the linear relationship derived for columns, the results of the parabolic relationship previously found for beams in Chapter 3 are also shown. It can be seen that the data points calculated by VecTor2 for columns correlate better with the linear equation.

$$\varepsilon_{2y} = 0.9\varepsilon_{2u}.\left(\frac{V_y}{V_u}\right) \qquad (4-34)$$

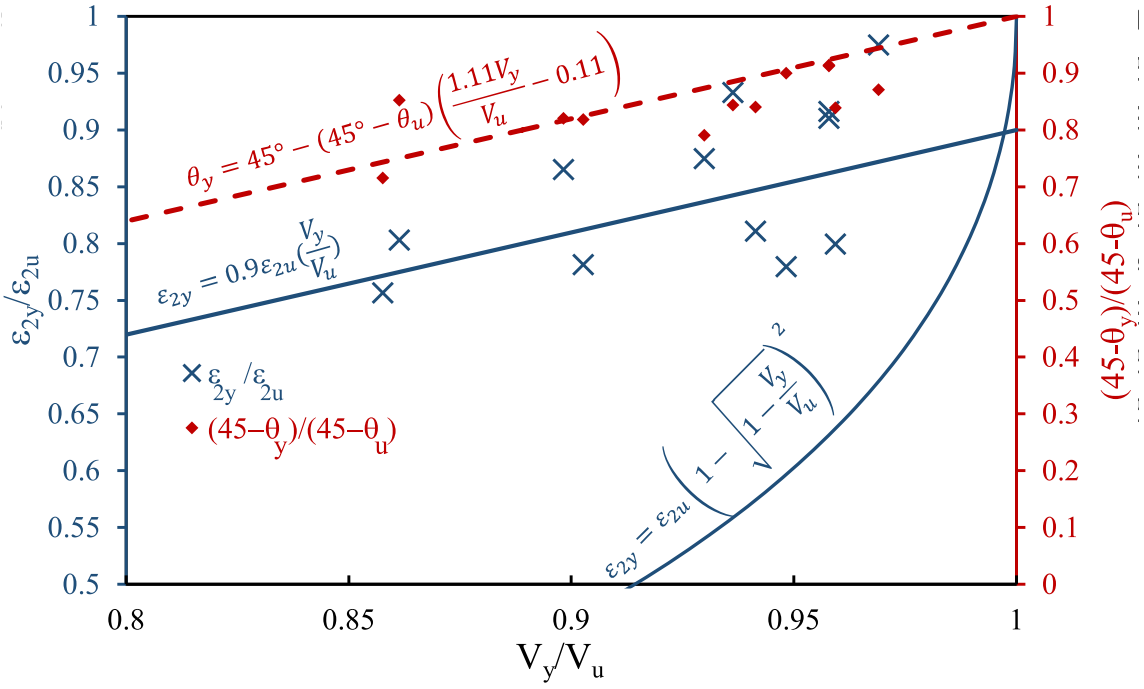

Figure 4-6 Relationship between the principal compressive strain in concrete, crack direction, and shear strength at the yielding point and the ultimate point of response

Finally, the parameter k_{13} in Eq. (4-30) is defined to account for the effective shear strain depth as previously described for k_9 factor used in Eq. (4-16) for the ultimate point.

4.2.3 Cracking point

The cracking point is when initial flexural cracks develop in a section prior to the development of the shear crack. Flexural cracks develop when the longitudinal stress due to the bending moment and axial load in the section (*M/S-P/A*) reaches the concrete tensile strength (f'_t). Using the relationship between stresses and the parameter $\alpha=M/V.d_v$ which relates the bending moment to the shear force, Eq. (4-35) can be derived for the shear force at the cracking point. Setting P=0 in this equation leads to the formula previously developed for the beam model in Chapter 3.

$$V_{cr} = \frac{0.33\sqrt{f_c'}bh^2 - Ph}{6\alpha \mathrm{d_v}} \qquad (4-35)$$

The shear strain at the cracking point (γ_{cr}) can simply be calculated by dividing the shear force by the initial shear stiffness (G):

$$\gamma_{cr} = \frac{V_{cr}}{G.b.d_v} \qquad (4-36)$$

4.2.4 Failure point

The post-peak response of shear-critical RC columns can be assumed to be linear with the ultimate shear strain (γ_f) occurring at the zero shear force as recommended by Elwood et al. (2007). γ_f can be calculated from Eq. (4-37) proposed by Elwood and Moehle (2005) based on a shear-friction model.

$$\gamma_f = 0.04\frac{1+\cot^2\theta_f}{\cot(\theta_f)\left(1-P\frac{s}{A_{st}f_{yt}d_v}\right)}\frac{a}{2h} \qquad (4-37)$$

where θ_f is the crack inclination angle at the failure point which is suggested to be taken as 30° for columns with axial load ratios less than 20%, and 25° for columns with higher axial

load ratios. As the axial compressive load increases, the longitudinal strain reduces, which leads to a lower crack inclination angle.

Figure 4-7 summaries all the above-mentioned equations into a four-step procedure for the calculation of the shear force and shear strain at key points of the proposed plastic hinge model.

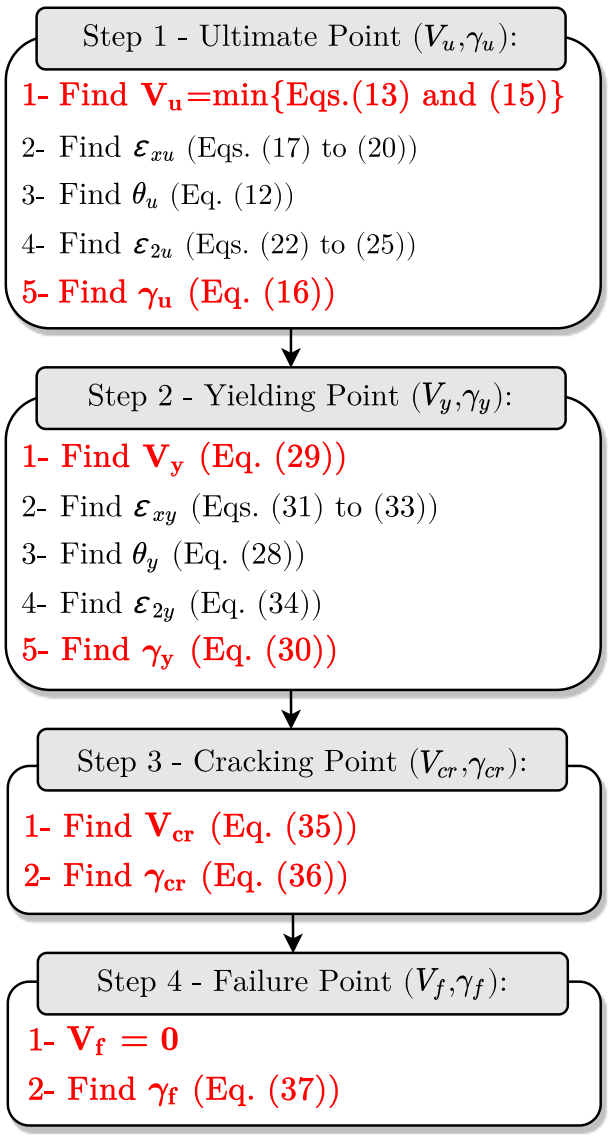

Figure 4-7 Step-by-step procedure for calculation of the four key points for the proposed model

4.3 Verification against experimental test results

The performance and accuracy of the proposed model were assessed by comparing the results of 12 shear-critical RC columns experimentally tested by Tran (2010), Kokusho (1973), Lynn (2001), Imai and Yamamoto (1986), Yoshimura and Yamanaka (2000), Zimos et al. (2020), and Ikeda (1968). The key characteristics of the columns, including dimensions, material properties, rebar area, axial load, and boundary conditions, are shown in Table 4-1. The columns were selected from various test programs with different sets of design parameters allowing thorough performance assessment of the proposed model. Shear behavior played a significant role in the response of all the selected columns.

Table 4-1 Parameters of RC columns considered for the verification study

Researcher	Column	f'_c (MPa)	f_{yl} (MPa)	f_{yt} (MPa)	b (mm)	h (mm)	d (mm)	a (mm)	s (mm)	A_{sl} (mm^2)	A_{st} (mm^2)	$\frac{P}{f'_c A_g}$	BC
Tran (2010)	SC-2.4-0.20	22.6	408.0	392.6	350	350	309	850	125	2513	56.5	0.200	DC
	SC-2.4-0.30	49.3	409.0	392.6	350	350	306	850	125	3927	56.5	0.300	DC
	SC-2.4-0.50	24.2	408.0	392.6	350	350	309	850	125	2513	56.5	0.500	DC
Kokusho (1973)	372	19.9	524.0	351.6	200	200	170	500	100	532	68.4	0.197	C
Lynn (2001)	3CLH18	26.9	331.0	399.9	457	457	394	1473	457	6334	143.2	0.089	DC
	3CMH18	27.6	331.0	399.9	457	457	394	1473	457	6334	143.2	0.262	DC
	3CMD12	27.6	331.0	399.9	457	457	394	1473	305	6334	244.4	0.262	DC
Imai and Yamamoto (1986)	No. 1	27.1	318.0	336.0	400	500	443	825	100	5322	127.2	0.072	C
Yoshimura and Yamanaka (2000)	FS0	27.0	387.0	355.0	300	300	255	900	75	3438	138.6	0.260	C
Zimos et al. (2020)	SC_1	32.8	565.0	565.0	300	300	254	832	320	2413	100.5	0.061	C
Ikeda (1968)	44	19.6	434.0	558.0	200	200	173	500	100	796	58.4	0.100	C
	46	19.6	434.0	558.0	200	200	173	500	100	796	58.4	0.200	C

The OpenSees software (Mazzoni et al., 2006) was used to model the columns with 2-noded frame type elements. The nonlinear axial and flexural behavior of the columns were

considered through a series of fibers defined along the cross-section. Since frame elements with fiber sections cannot account for the shear effects in RC members, a *ZeroLength* element with a multi-linear uniaxial material behavior was added to each shear span of the columns as shown in Figure 4-1. The multi-linear response of the uniaxial material model assigned to the zero length elements was defined based on the shear force and shear deformation values computed by the proposed plastic hinge model according to the equations presented in the previous section. The shear deformation was computed by multiplying the shear strain by the shear plastic hinge length, which can be estimated as the length of the projection of the shear crack along the longitudinal axis of the member ($d_v cot(\theta)$) (Salgado and Guner, 2018). Knowing that the crack inclination angle in columns ranges between 15 and 35 degrees, the plastic hinge length can be approximated as twice the section height ($2h$).

In Figure 4-8, the lateral force-displacement responses of the columns computed by the OpenSees model with the proposed shear hinge elements were compared against the results of experimental tests and VecTor2. It can be seen that the force-displacement results of the OpenSees model that included the shear hinge model were in good agreement with the experimental results in terms of stiffness, peak strength, and displacement. The proposed modeling approach provided the same level of accuracy as the VecTor2 nonlinear FE analysis software with much less modeling and computing effort. Therefore, it can be regarded as a promising analysis approach for shear-critical RC structures. To demonstrate the consequences of neglecting the shear effects, the results of OpenSees model without including shear hinge elements are also shown in Figure 4-8. As expected, neglecting the shear behavior resulted in significant overestimation of strength and ductility for the shear-

critical columns. Since the frame elements with fiber sections cannot capture shear failure, the analysis continued until the fibers failed due to flexural and axial load effects resulting in highly unsafe results.

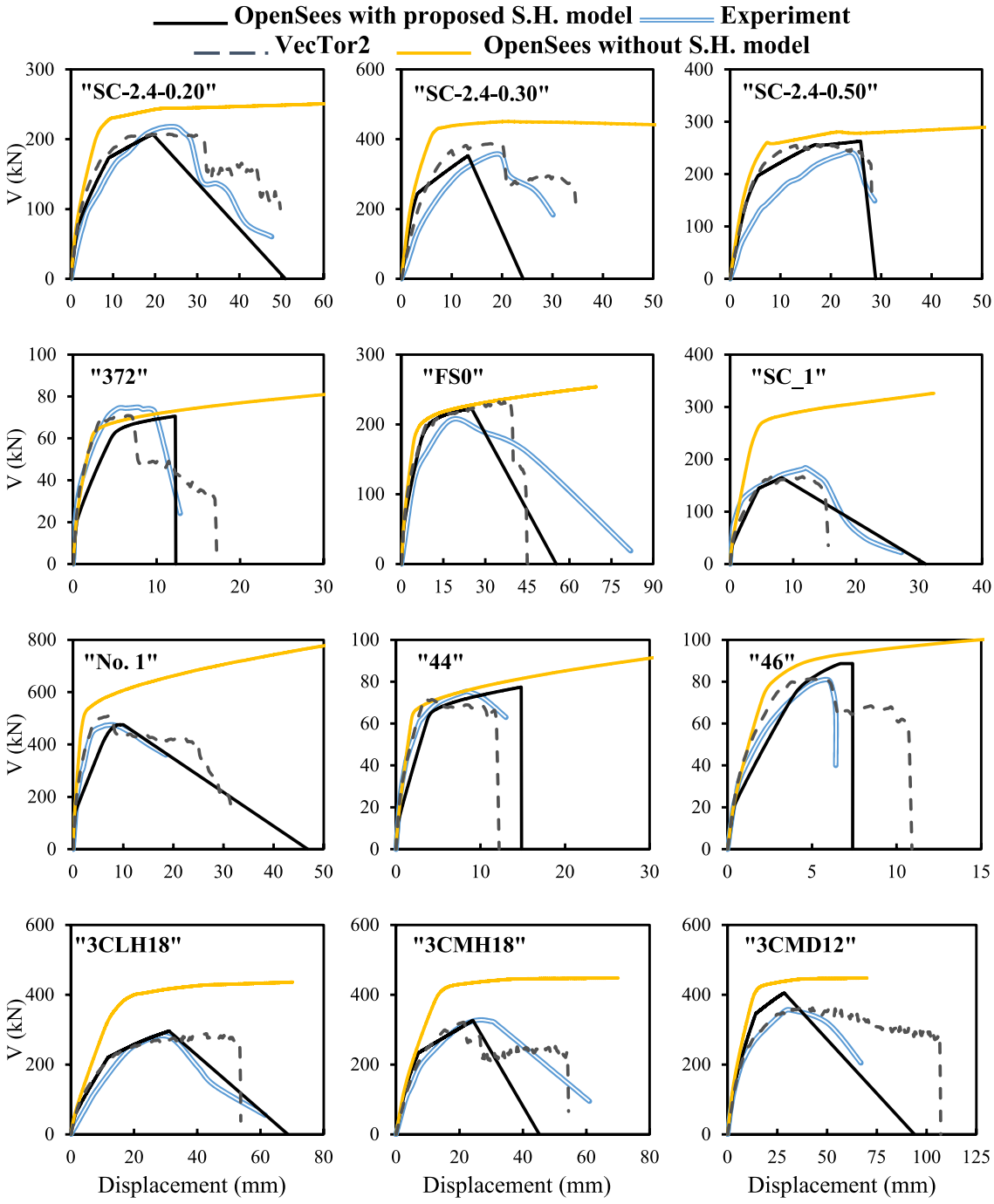

Figure 4-8 Comparison of force-displacement responses between OpenSees models with and without shear hinge elements, experiment, and VecTor2 (1 mm = 0.0394 in.; 1 kN = 0.225 kip)

4.4 Parametric study

To further verify the accuracy of the proposed shear hinge model and evaluate its application range, a comprehensive parametric study was conducted by modeling and analysis of 48 shear-critical cantilever RC columns. The VecTor2 FE analysis software was used to assess the performance of the proposed shear hinge model under various geometrical, material and loading conditions. The selected columns varied in terms of six key design parameters; namely, the cylindrical compressive strength of concrete (f'_c), the ratio of the applied axial load to the axial capacity of the concrete section (P/f'_cA_g), the transverse reinforcement ratio (ρ_z), the ratio of the shear span to the section effective depth (a/d), cross-section dimensions (b or h), and the aspect ratio of cross-section (b/h). The total area of longitudinal reinforcement and the yield strength of all reinforcements are assumed to be 4200 mm^2 (6.51 in^2) and 400 MPa (58.02 ksi), respectively. Other characteristics of the columns are shown in Table 4-2.

The characteristics of the load-deflection responses of the abovementioned columns were evaluated by determining five performance indicators for each response: 1) shear strength (V_u), 2) displacement corresponding to the peak strength (Δ_u), 3) shear force at the yielding of the transverse reinforcement (V_y), 4) area under the pre-peak portion of the response ($A_{pre\text{-}peak}$), and 5) total area under the load-deflection response (A_{total}). For each performance indicator, the ratio between the prediction of the proposed lumped plasticity analysis approach and the finite element analysis (LP-to-FE) was computed.

To identify the application range and the limitations of the proposed lumped plasticity model, the variation of LP-to-FE ratios for the five performance indicators are presented

in Figure 4-9 as a function of design variables considered in the parametric study. Figure 4-9(a) shows the performance of the model as f'_c varies from 20 MPa to 80 MPa (2.90 ksi to 11.60 ksi). It can be seen that for all values of the f'_c the LP-to-FE ratios for all performance indicators were close to 1.0, meaning that the predictions of the lumped plasticity model agreed well with the FE analysis results. However, the accuracy of the model reduced as the concrete compressive strength increased above 50 MPa (7.25 ksi). This was expected because the Hognestad's equation was used for the concrete compressive stress-strain relationship in the development of the proposed model, which is not an ideal constitutive material model for predicting the response of high-strength concrete members.

Table 4-2 Properties of RC columns used for parametric study (1 mm = 0.0394 in.; 1 kN = 0.225 kip; 1 MPa = 0.1450 ksi)

Model	f'_c (MPa)	P/f'_cA_g	ρ_z (%)	a/d	h (mm)	b/h	Model	f'_c (MPa)	P/f'_cA_g	ρ_z (%)	a/d	h (mm)	b/h
C1	30	0.20	0.20	2.39	400	1.00	C25	30	0.20	0.08	2.39	400	1.00
C2	20	0.20	0.20	2.39	400	1.00	C26	30	0.20	0.07	2.39	400	1.00
C3	25	0.20	0.20	2.39	400	1.00	C27	30	0.20	0.20	1.19	400	1.00
C4	35	0.20	0.20	2.39	400	1.00	C28	30	0.20	0.20	1.49	400	1.00
C5	40	0.20	0.20	2.39	400	1.00	C29	30	0.20	0.20	1.79	400	1.00
C6	45	0.20	0.20	2.39	400	1.00	C30	30	0.20	0.20	2.09	400	1.00
C7	50	0.20	0.20	2.39	400	1.00	C31	30	0.20	0.20	2.69	400	1.00
C8	60	0.20	0.20	2.39	400	1.00	C32	30	0.20	0.20	2.99	400	1.00
C9	70	0.20	0.20	2.39	400	1.00	C33	30	0.20	0.20	3.58	400	1.00
C10	80	0.20	0.20	2.39	400	1.00	C34	30	0.20	0.20	4.48	400	1.00
C11	30	0.05	0.20	2.39	400	1.00	C35	30	0.20	0.20	5.97	400	1.00
C12	30	0.10	0.20	2.39	400	1.00	C36	30	0.20	0.20	2.39	250	1.00
C13	30	0.30	0.20	2.39	400	1.00	C37	30	0.20	0.20	2.39	300	1.00
C14	30	0.40	0.20	2.39	400	1.00	C38	30	0.20	0.20	2.39	500	1.00
C15	30	0.50	0.20	2.39	400	1.00	C39	30	0.20	0.20	2.39	600	1.00
C16	30	0.60	0.20	2.39	400	1.00	C40	30	0.20	0.20	2.39	800	1.00
C17	30	0.70	0.20	2.39	400	1.00	C41	30	0.20	0.20	2.39	1000	1.00
C18	30	0.80	0.20	2.39	400	1.00	C42	30	0.20	0.20	2.39	1200	1.00
C19	30	0.20	0.80	2.39	400	1.00	C43	30	0.20	0.20	2.39	1500	1.00
C20	30	0.20	0.40	2.39	400	1.00	C44	30	0.20	0.20	2.39	400	0.50
C21	30	0.20	0.27	2.39	400	1.00	C45	30	0.20	0.20	2.39	400	0.75
C22	30	0.20	0.16	2.39	400	1.00	C46	30	0.20	0.20	2.39	400	1.25
C23	30	0.20	0.13	2.39	400	1.00	C47	30	0.20	0.20	2.39	400	1.50
C24	30	0.20	0.10	2.39	400	1.00	C48	30	0.20	0.20	2.39	400	2.00

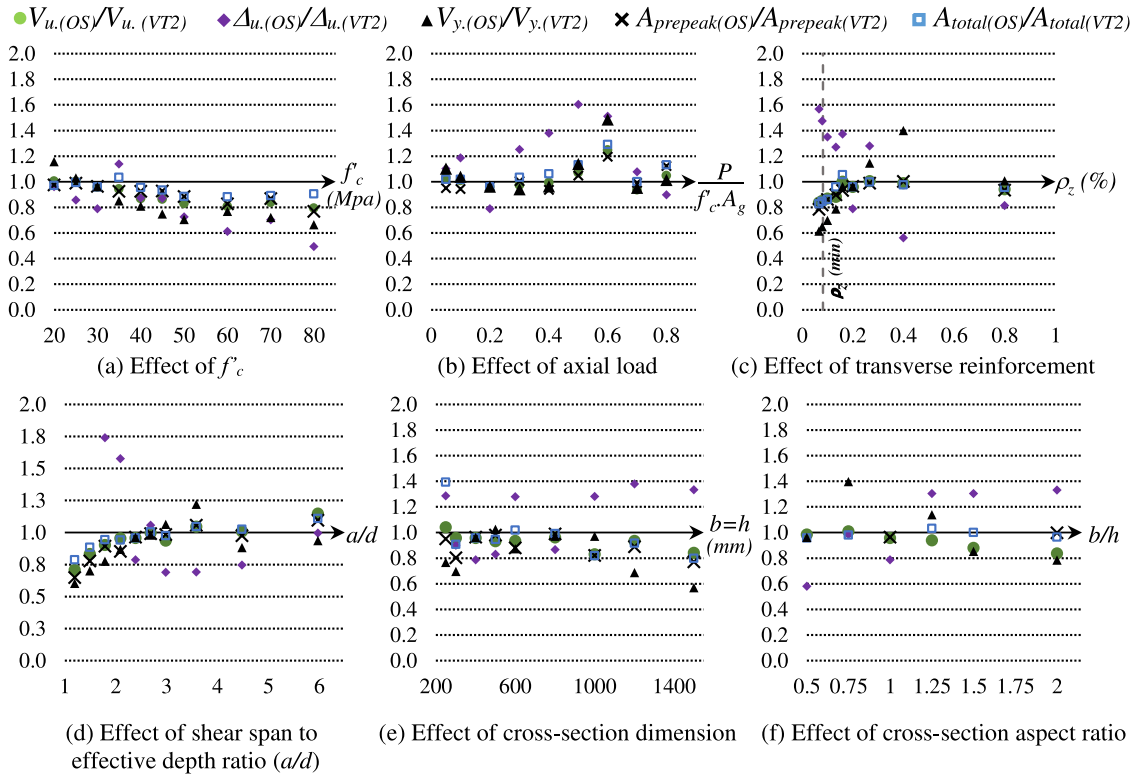

Figure 4-9 Performance of the proposed shear hinge model for RC columns with various design parameters (1 mm = 0.0394 in.; 1 kN = 0.225 kip)

The effect of axial load is shown in Figure 4-9(b). It can be seen that the proposed model accurately calculated almost all the performance indicators for axial load ratios ranging from 0.05 to 0.8. The only inconsistency was in the predictions of Δ_u for columns with axial load ratios between 0.4 and 0.6, where Δ_u was overestimated to some extent by the proposed model. Nevertheless, this did not affect the overall performance of the model for these columns as the rest of the performance indicators including the total area and the area under the pre-peak response were predicted with good accuracy. From Figure 4-9(c), it can be seen that the proposed model calculated the response of RC columns that contained at least the minimum amount of shear reinforcement specified according to the CSA A23.3 design code (CSA, 2019) reasonably well.

Figure 4-9(d) shows the performance of the model for shear span-to-depth ratios *(a/d)* from about 1 to 6. It can be seen than as the *a/d* reduced below 2 the accuracy of the proposed model started to deteriorate. This is because the model was developed based on the assumption of plane sections remain plane (i.e., beam action) and the arch action which occurs in deep members was not considered in its formulation. The effect of size and the aspect ratio of the cross-section were investigated in Figure 4-9(e) and Figure 4-9(f). It is shown that the proposed model was able to calculate the shear response of RC columns with cross-section sizes varying from 250 mm (9.84 in.) to 1500 mm (59.06 in.) and aspect ratios between 0.5 to 2.0 with good accuracy. For larger cross-sections, the accuracy of the model was slightly lower which could be due to the size effect in concrete.

4.5 Verification at system-level

The effectiveness of the proposed shear hinge model for the system-level performance assessment of RC structures was evaluated by analyzing a four-storey three-span frame structure representing an RC building constructed in the late 1990s in Vancouver, Canada. The geometry of the frame as well as properties of member cross-sections are shown in Figure 4-10(a). The frame was designed according to the requirements of CSA A23.3-94 (1994) which was the applicable design code at the time of construction. However, due to the improvements made in the Canadian design practice over the last 25 years, the frame does not meet some of the requirements of the current edition of the code (CSA A23.3-19 (2019)). One of the most noticeable changes in the Canadian design code has been the addition of stringent requirements for volumetric transverse reinforcement in columns located in seismic regions. The lack of these requirements in the older versions of CSA A23.3 design code has raised concerns about the safety of some existing RC structures under earthquakes.

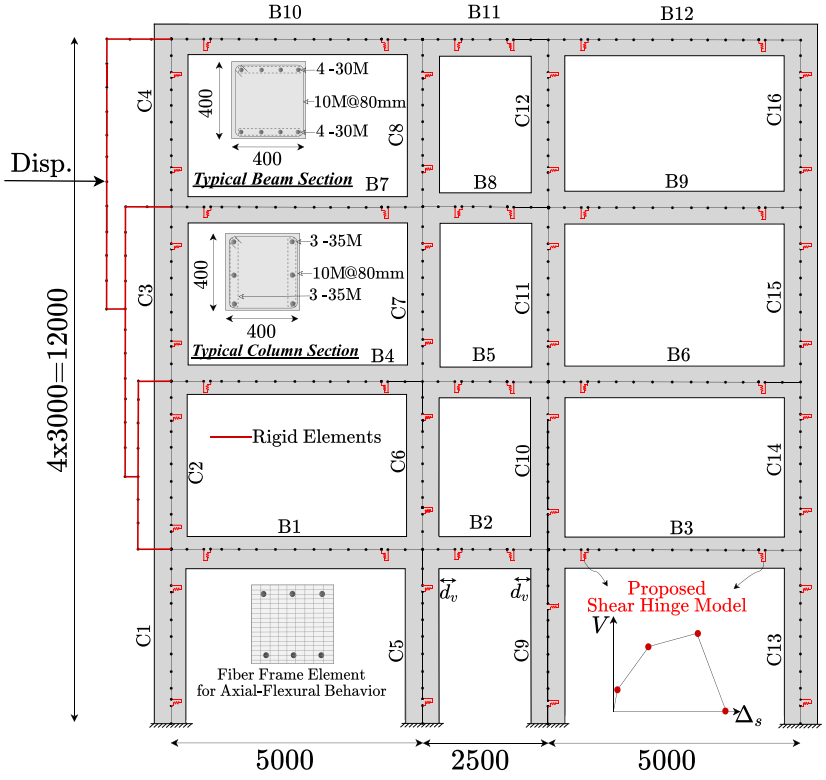

(a)

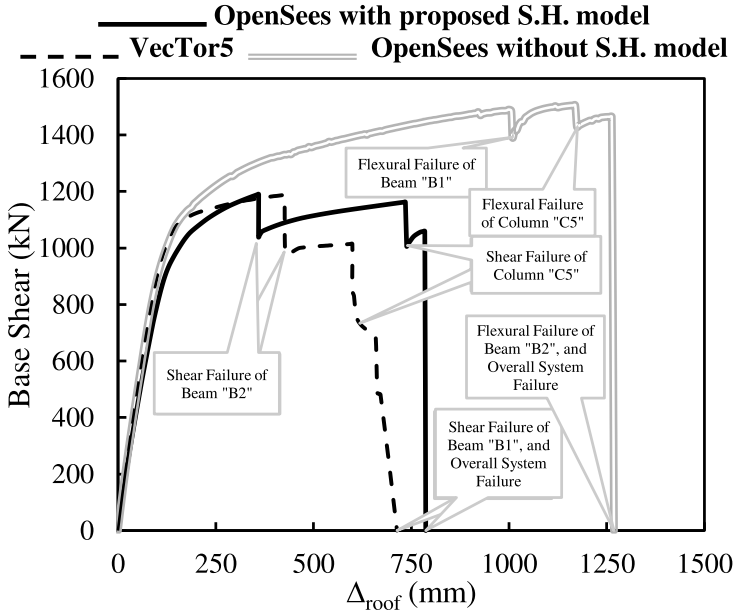

(b)

Figure 4-10 a) System-level OpenSees model and b) the base shear versus lateral roof displacement responses of the RC frame (1 mm = 0.0394 in.; 1 kN = 0.225 kip)

The structure was modeled using frame-type fiber-based elements in OpenSees and VecTor5 (Guner and Vecchio, 2008) software. VecTor5 is a distributed plasticity analysis software for RC frames, developed based on the MCFT model (Vecchio and Collins, 1986). Unlike most frame-type analysis software, the fiber-based elements in VecTor5 can capture nonlinearity effects due to shear in addition to the flexural and axial behavior. In the OpenSees model, the shear behavior was considered based on the lumped plasticity models presented in this chapter and Chapter 3, while the flexural and axial behavior were considered using the distributed plasticity approach with fiber-based elements. To consider shear effects, zero length elements with shear hinge models were added to the ends of columns and beams of the frame as shown in Figure 4-10(a).

Pushover analyses were conducted on the OpenSees and VecTor5 models to simulate the seismic loads on the structure. The frame was subjected to a monotonically increasing lateral displacement applied through a series of rigid elements attached to the frame structure using simply supported connections. The location of the applied lateral load and the configuration of the rigid elements were selected such that the lateral seismic force distribution in the structure was proportional to the floor level height and the mass of each storey (Calvi et al., 2002). Gravity loads (dead, live and snow) for a typical residential building as defined in NBCC:1995 (Canadian Commission on Building and Fire Codes, 1995) were also applied on the beams.

The base shear versus the lateral roof displacement response is shown in Figure 4-10(b) for three different analysis cases: the OpenSees analysis with and without the shear hinge models and the VecTor5 analysis. It can be seen in Figure 4-10(b) that both the force-deflection responses and also the sequence of failure obtained from VecTor5 and the

OpenSees model with the shear hinges were similar. Both analysis methods predicted that the structural collapse was initiated by the shear failure of the shorter beam in the first storey (*B2*), followed by the shear failure of the adjacent column *C5* and beam *B1* which then resulted in complete collapse of the structural system. As shown in Figure 4-10(b), the OpenSees model without the shear hinges resulted in a completely different damage sequence and mode of failure along with considerable overestimation of the strength and ductility of the frame. In terms of the analysis time, the OpenSees model with the shear hinges was about 78% faster than the VecTor5 model where the shear behavior was considered in a distributed manner. For larger structural systems or 3D models, the difference between the analysis time of the two modeling methods is expected to be even higher.

4.6 Summary and conclusion

A new lumped plasticity model was developed based on the MCFT method to predict the response of shear-critical RC columns. The model represents the nonlinear shear behavior of columns in a concentrated manner through a set of closed-from equations derived by simplifying the complex procedure of the original MCFT method. The model formulation takes into account the shear-flexure-axial interaction effects and complex material mechanisms in reinforced concrete such as tension stiffening and compression softening. Moreover, it considers the nonlinear distribution of stresses, strains and the crack inclination through the section height in an average sense.

The accuracy of the proposed model was verified through analysis of 12 shear-critical RC columns tested by different researchers using the OpenSees software. It was shown that the model can calculate the response of shear-critical columns reasonably well in terms of

strength, ductility and stiffness. The analysis results also indicated that neglecting the nonlinearity effects due to shear can result in significant overestimation of the peak strength and ductility leading to unsafe predictions. Afterwards, using a comprehensive parametric study on columns with various design parameters, the application range and the limitations of the model were identified. The design parameters that were investigated included material properties, loading condition, and cross-sectional details. The model performed well for almost all RC columns except those with a shear span to effective depth ratio of less than 2.0 which was expected as the arch action was not considered in the model formulation. Also, the accuracy of the model was reduced for high strength concrete columns or columns with transverse reinforcement ratios less than the minimum value specified by the Canadian design code (CSA A23.3, 2019). Finally, the effectiveness of the proposed model for the system-level analysis of RC structures was evaluated by modeling a multi-storey frame structure with shear-critical members. The results demonstrated that the proposed lumped plasticity model can effectively consider nonlinear shear deformations and shear failure modes in RC frames with the same level of accuracy as the distributed plasticity method but with considerably less computational time.

The use of the proposed shear hinge model for columns and the previously developed model for beams will assist engineers to evaluate the safety and performance of large RC structures while considering the nonlinear shear behavior of different structural members in an accurate and practical manner. The proposed shear hinge models can be easily used with any type of frame analysis software without requiring any changes to the software formulation.

4.7 Notation

$A_{pre\text{-}peak}$= area under the pre-peak portion of the response

A_{sl}= area of tensile longitudinal reinforcement

A_{st}= area of transverse reinforcement

A_{total}= total area under the load-deflection response

a= shear span

b= beam width

C= summation of the forces acting on the compression side of the cross-section

d= effective depth

d_v= effective shear depth, taken as the greater of $0.9d$ or $0.72h$

E_s= modulus of elasticity of steel

f'_c= cylindrical compressive strength of concrete

f_{c1}= principal tensile stress in concrete

f_{c2}=principal compressive stress in concrete

f_{sx} and f_{sz}=average stress in longitudinal and transverse reinforcements

f'_t= modulus of rupture of concrete

f_x and f_z= stress applied to element in x and z directions

f_{yl}= yield strength of longitudinal reinforcement

f_{yt}= yield strength of transverse reinforcement

G= initial shear modulus of concrete

h= beam height

P= axial compressive load (negative sign for compression)

s= spacing of transverse reinforcement

s_z= crack spacing parameter, as defined in CSA A23.3

s_{ze}= equivalent crack spacing that allows for influence of aggregate size

T= summation of the forces acting on the tension side of the cross-section

V_c= shear resistance provided by concrete

V_s= shear resistance provided by transverse reinforcement

V= shear force

v= shear stress

v_c= shear stress in concrete

v_{ci}= shear stress on crack surfaces

X= distance from extreme compression fiber to neutral axis

β= contribution factor accounting for strength of cracked concrete

ε_0= strain in concrete at f'_c

ε_1= principal tensile strain in concrete

ε_2= principal compressive strain in concrete

ε_x= longitudinal strain

ε_z= transverse strain

γ= shear strain

θ= angle between crack inclination and x-axis

ρ_x and ρ_z= longitudinal and transverse reinforcement ratios

Subscripts “u”, “f”, “y”, and “cr” are related to each of the four key points in the model.

Chapter 5: Consideration of Shear Behavior in Macro-Modeling of Deep Reinforced Concrete Members

5.1 Introduction

This chapter presents a shear plastic hinge model developed based on the beam-arch action mechanism for nonlinear analysis of deep RC members. The contribution of web concrete and transverse reinforcement (i.e., beam action) to the shear response is considered based on the Modified Compression Field Theory, while the contribution of the inclined concrete compression chord (i.e., arch action) is taken into account using the compatibility condition for shear deformations. The model is capable to calculate the shear force and deformation at different stages of the response while considering important material effects in RC and interactions between internal force components. Through a comprehensive verification and parametric study, it is demonstrated that the model is able to accurately compute the shear behavior in various deep RC members. Lastly, the effectiveness of the proposed model for system-level analysis of structures is evaluated by modeling a multi-storey RC shear wall with coupling beams. The analysis results show that shear deformations can have a great influence on the performance of the structure as a whole in addition to the behavior at the component-level.

5.2 Model Description

As shown in Figure 5-1, a multilinear shear force-displacement response consisting of four key points is considered for the proposed model where each point represents a major change in the member behavior (cracking in concrete, yielding in transverse reinforcement, peak shear stress, and failure). Based on equilibrium and compatibility conditions, closed-form equations are derived to calculate the shear force and displacement at each key point

of the response while considering both beam and arch action mechanisms. The equations for the beam action are obtained by evaluating the relationships between stresses and strains based on the MCFT theory for a 2D panel representing a section of the deep member (see Figure 5-2(b)). These equations are similar to those proposed by the authors for slender members in Chapters 3 and 4. The contribution of the inclined concrete compression strut, known as arch action, is taken into account by investigating the compatibility condition according to the Pan and Li (2013) model, as shown in Figure 5-2 (c). Once the nonlinear shear force-displacement response is determined, it can be implemented into the structural model using spring elements located at the ends of the deep member (see Figure 5-2 (a)). A description of closed-form equations developed for each key point of the response is provided in the following sections.

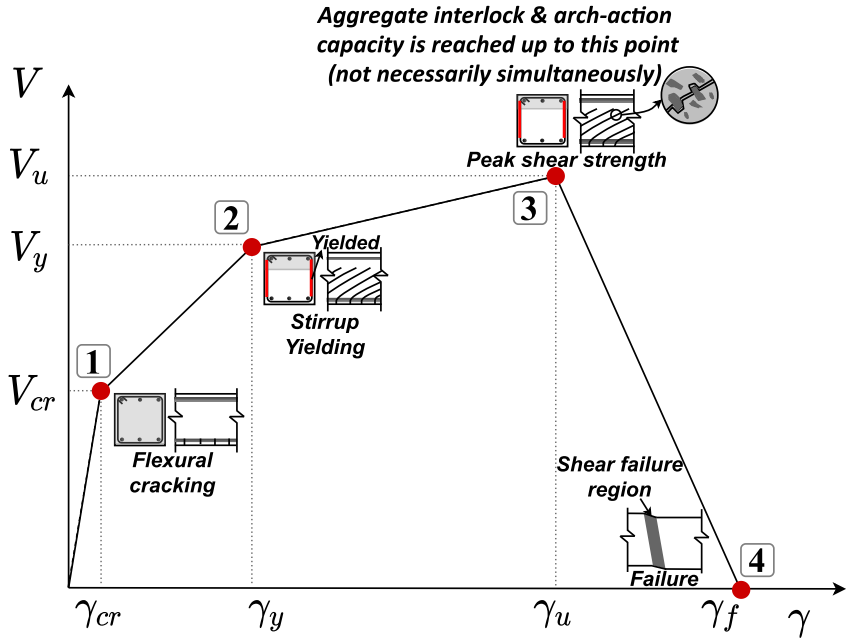

Figure 5-1 The general shear response curve for the proposed model

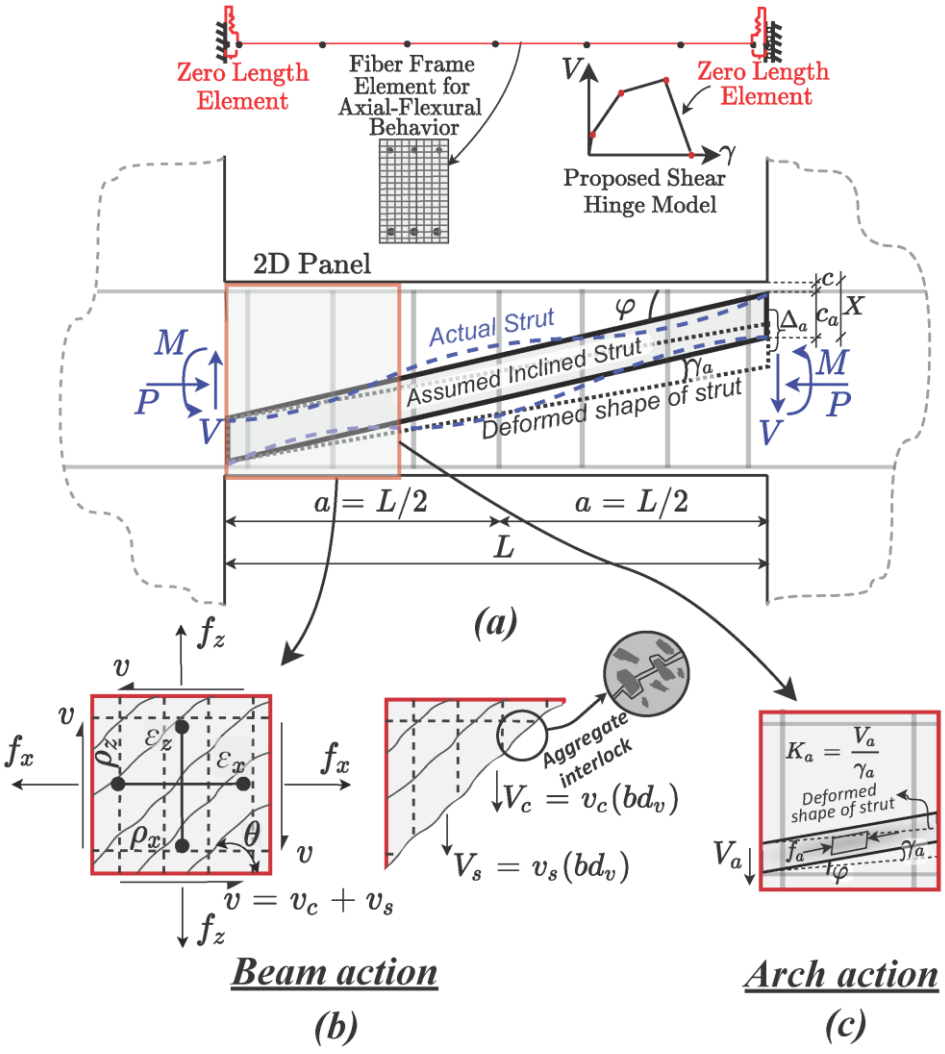

Figure 5-2 a) The actual and assumed inclined strut, and the location of proposed shear hinge b) 2D panel representing stresses and strains due the beam action c) Contribution of arch action to stresses and strains of the 2D panel

5.2.1 Peak point

According to Chapter 4, the shear capacity of a section due to the beam action (V_{ub}) can be computed using Eq. (5-1), which accounts for the shear force carried by the concrete web and transverse reinforcement. In this equation, the shear strength equals to the minimum value of two expressions. The first one is developed based on the shear design provisions of CSA A23.3 code (2019) with some refinements to the calculation of the concrete crack

inclination. The second expression in Eq. (5-1) limits the shear strength for members with low amount of flexural reinforcement as it has been shown that yielding of both longitudinal and transverse reinforcement can prevent the member from reaching its full shear capacity (see Chapter 3).

$$V_{ub} = min\begin{cases} \dfrac{k_1k_3 - k_4(1+k'_1)}{2k_1k_4} + \sqrt{\left(\dfrac{k_1k_3 - k_4(1+k'_1)}{2k_1k_4}\right)^2 + \dfrac{k_2 + k_3(1+k'_1)}{k_1k_4}} \\ \sqrt{(\alpha k_{15})^2 + 2k_{15}A_{sl}f_{yl} - k_{15}P} - \alpha k_{15} + 0.05\sqrt{f'_c}bd_v \end{cases} \qquad (5-1)$$

where P, f'_c, b, and d_v are the axial load, uniaxial compressive strength of concrete, member width, and effective shear depth, respectively. k factors used in Eq. (5-1) and the rest of the equations presented in this chapter are all defined in Appendix C.

The contribution of the arch action to the shear strength of an RC member can be calculated from a compatibility equation between deformations due to the beam action and the arch action:

$$\frac{V_{ub}}{K_{ub}} = \frac{V_{ua}}{K_{ua}} \qquad (5-2)$$

where V_{ub} and V_{ua} are the shear strength of the beam and arch action at the peak point. K_{ub} and K_{ua} are also the shear stiffness of the cross-section due to the beam and arch action, respectively. K_{ua} equals to V_{ua} divided by the projection of shear strain induced by the diagonal compression strut in the vertical direction (i.e., $\gamma_a = \Delta_a/(L \times sin(\varphi))$ that is the shear strain perpendicular to the longitudinal axis of the member, as can be seen in Figure 5-2(a). From Eq. (5-2) and considering the ratio of K_{ua}/K_{ub} according to the Pan and Li model (2013), V_{ua} can be computed using Eq. (5-3). Finally, the total shear capacity of the member

(V_u) that is the summation of shear contribution due to the beam action (V_{ub}) and the arch action (V_{ua}) can be calculated according to Eq. (5-4).

$$V_{ua} = V_{ub}\frac{K_{ua}}{K_{ub}} = V_{ub}\left[\frac{c_{au}\sin^2\varphi_u\cos^2\varphi_u}{n\rho_z d_v\cot^2\theta_u}(1+n\rho_z\csc^4\theta_u)\right] \qquad (5-3)$$

$$V_u = V_{ub}+V_{ua} = V_{ub}\left(1+\frac{K_{ua}}{K_{ub}}\right) = V_{ub}\left(1+\frac{c_{au}\sin^2\varphi_u\cos^2\varphi_u}{n\rho_z d_v\cot^2\theta_u}(1+n\rho_z\csc^4\theta_u)\right) \qquad (5-4)$$

where c_{au} is the effective strut depth as shown in Figure 5-2(a) and can be taken as the compression zone depth (X_u) minus the concrete cover, where X_u can be calculated using Eq. (5-5) proposed in Chapter 4.

$$X_u = \frac{\sqrt{C\varepsilon_0\left[bdf_c'\varepsilon_{xu.Ten.}+\frac{C\varepsilon_0}{2}\right]}-\frac{C}{2}}{bf'_c\varepsilon_{xu.Ten.}} \qquad (5-5)$$

where C and $\varepsilon_{xu.Ten}$ represent the force acting in the compression zone of the section and longitudinal strain of the tensile reinforcement, respectively, and can be calculated using equations provided in Appendix C. In Eq. (5-4), φ_u is the inclination of the diagonal compression strut as shown in Figure 5-2(a) and can be calculated according to Eq. (5-6) as suggested by Pan and Li (2013).

$$\varphi_u = \begin{cases}\tan^{-1}\left[\dfrac{h-X_u}{L}\right] & ;\ Double\ curvature\ members\\ \tan^{-1}\left[\dfrac{h-X_u}{2L}\right] & ;\ Single\ curvature\ members\end{cases} \qquad (5-6)$$

In Eq. (5-4), θ_u is the average crack inclination angle at the peak point which can be computed using Eq. (5-7). This is an improved version of the CSA A23.3 equation that enables to account for the effect of concrete compressive strength and transverse reinforcement on θ_u through the k_6 factor, in addition to the influence of longitudinal strain

(ε_{xu}) which is the only parameter considered in the code equation (see Chapter 3 and 4 for more details).

$$\theta_u = (29 + 7000\varepsilon_{xu}).(k_6) \qquad (5-7)$$

where ε_{xu} is the longitudinal strain at the mid-depth of the section and can be computed using Eq. (5-8) developed in Chapter 4 based on the study of Bentz and Collins (2006):

$$\varepsilon_{xu} = \frac{k_1 V_{ub} + k_1'}{750}.k_5 \geq \frac{P}{bh(0.5E_c + \rho_x E_s)} \qquad (5-8)$$

The shear strain at the peak point (γ_u) can be calculated using Eq. (5-9) that is derived based on the principles of Mohr's circle.

$$\gamma_u = 2(\varepsilon_{xu} + \varepsilon_{2u}).\cot(\theta_u).k_9 \qquad (5-9)$$

where k_9 is a factor that accounts for the influence of effective shear strain depth, and ε_{2u} is the average principle compressive strain of the section at the peak point which can be estimated from Eq. (5-10).

$$\varepsilon_{2u} = \max\{k_8, 1 - \sqrt{1 - \frac{f_{c2u}}{f_c'}}\}.\varepsilon_0 \qquad (5-10)$$

In Eq. (5-10), ε_0 is the strain corresponding to the uniaxial compressive strength of concrete and f_{c2u} is the principal compressive stress in the concrete which can be calculated using the equations provided in Appendix C. Knowing ε_{2u}, ε_{xu} and θ_u, the shear strain at the peak point can be determined from Eq. (5-9).

To validate the proposed model, the shear strength of a short column with a cross-section similar to the "SC-1.7-0.20" specimen tested by Tran (2010) is calculated for various *a/d* ratios using the above equations and the VecTor2 nonlinear FE analysis software. Details of the cross-section are provided in Table 5-1. To better evaluate the model, the beam

action is decoupled from the arch action and contributions of the concrete web (V_{uc}), transverse reinforcement (V_{us}), and inclined concrete strut (V_{ua}) to the total shear strength (V_u) are calculated separately and presented in Figure 5-3. It can be seen that the results of the proposed model for all three contributing factors and the total shear strength are in good agreement with the FE results for different a/d ratios. Also, as expected the contribution of the arch action becomes much more notable as the shear span to depth ratio decreases. For example, the contribution of V_{ua} to the total shear capacity is about 22% for a/d of 2.0, while this percentage increases to nearly 69% as a/d reduces to 0.5 resulting in significant increase in the total shear strength (the beam action remains almost the same for different a/d ratios).

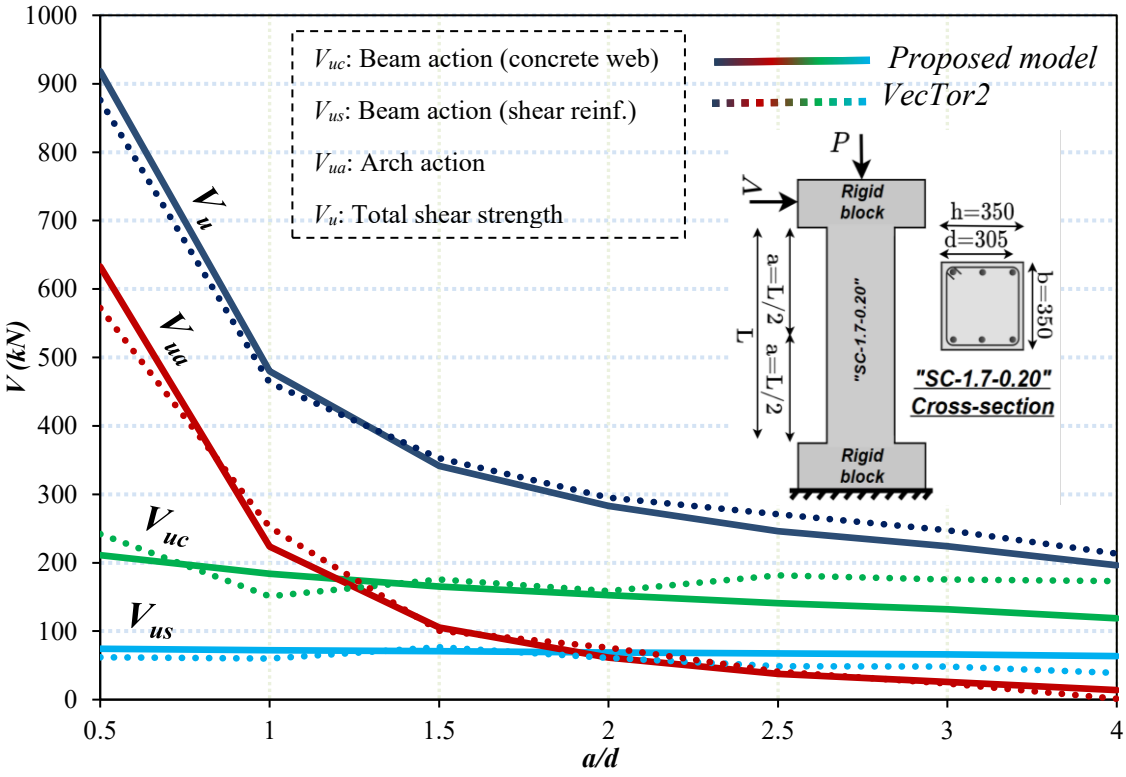

Figure 5-3 Comparison of different shear resisting mechanisms computed by VecTor2 and the proposed model for RC columns with various *a/d* ratios

5.2.2 Yielding point

The shear force at the yielding point due to the beam action (V_{yb}) can be calculated using Eq. (5-11). This equation was proposed by the authors for slender members in Chapter 4 based on the original formulation of the MCFT method (Vecchio and Collins, 1986) and the evaluation of the relationship between the shear force and crack inclination at the ultimate and yielding points for a wide range of RC cross-sections.

$$V_{yb} = \begin{cases} \left|\frac{k_{11}}{2k_{12}}\right| & ; \quad k_{10}k_{12} > \left(\frac{k_{11}}{2}\right)^2, \theta_u \neq 45 \\ \frac{\frac{k_{11}}{2} - \sqrt{\left(\frac{k_{11}}{2}\right)^2 - k_{10}k_{12}}}{k_{12}} & ; \quad k_{10}k_{12} \leq \left(\frac{k_{11}}{2}\right)^2, \theta_u \neq 45 \\ k_{10} & ; \quad \theta_u = 45 \end{cases} \leq V_u \qquad (5-11)$$

The equations for calculating all the *k* factors are provided in Appendix C. The arch action at the yielding point is considered using a similar approach employed for the peak point. For the calculation of the shear stiffness ratio between the beam and arch action (K_{ya}/K_{yb}), the K_{yb} is taken as the shear force (V_{yb}) due to the beam action divided by the corresponding shear strain (γ_y).

$$K_{yb} = \frac{V_{yb}}{\gamma_y} \qquad (5-12)$$

The shear strain at the yielding point (γ_y) can be calculated using Eq. (5-13) which is developed based on the Mohr's circle of strains, similar to Eq. (5-9) used for the peak point.

$$\frac{V_y}{G.b.d_v} \leq \gamma_y = 2\left(\varepsilon_{xy} + \varepsilon_{2y}\right).\cot\left(\theta_y\right).k_{13} \leq \gamma_u \qquad (5-13)$$

where ε_{xy} is the longitudinal strain at the mid-depth of the cross-section, ε_{2y} is the average principal compressive strain in the concrete, and θ_y is the average crack inclination angle. These parameters can be calculated using Eqs. (5-14) to (5-16) derived based on the

procedure explained in Chapters 3 and 4 for the yielding point of the previously developed models.

$$\frac{P}{bh(0.5E_c + \rho_x E_s)} \leq \varepsilon_{xy} = \left|\frac{\varepsilon_{xy.Ten.} - \varepsilon_{xy.Comp.}}{2}\right| \leq \varepsilon_{xu} \qquad (5-14)$$

$$\varepsilon_{2y} = 0.9\varepsilon_{2u}.\left(\frac{V_{yb}}{V_{ub}}\right) \qquad (5-15)$$

$$\theta_y = 45° - (45° - \theta_u)\left(\frac{1.11V_{yb}}{V_{ub}} - 0.11\right) \qquad (5-16)$$

$\varepsilon_{xy.Ten.}$ and $\varepsilon_{xy.Comp.}$ are the longitudinal strain at the outermost tensile and compressive fibers of the section.

After finding K_{yb}, K_{ya} can be calculated using Eq. (5-17) in order to determine the shear force at the yielding point due to the arch action. Eq. (5-17) is similar to Eq. (5-3) used for the calculation of the K_{ua} at the peak point. However, the effective depth and inclination of the compression strut (c_a and φ) are updated according to the compression zone depth, X, at the yielding point.

$$K_{ya} = E_c b c_{ay} \sin^2 \varphi_y \cos^2 \varphi_y \qquad (5-17)$$

In Eq. (5-17), the effective strut depth (c_{ay}) can be taken as the compression zone depth (X_y) minus the concrete cover, where X_y can be estimated from Eq. (5-18) (see Chapter 4 for more details). Also, the inclination of the compression strut (φ_y) can be calculated using Eq (5-19) which is the same as Eq. (5-6) but written in terms of X_y instead of X_u.

$$X_y = \frac{\varepsilon_{xy.Comp.}}{\varepsilon_{xy.Comp.} + \varepsilon_{xy.Ten.}} d \qquad (5-18)$$

$$\varphi_y = \begin{cases} \tan^{-1}\left[\dfrac{h - X_y}{L}\right] & ; \ Double\ curvature\ members \\ \tan^{-1}\left[\dfrac{h - X_y}{2L}\right] & ; \ Single\ curvature\ members \end{cases} \qquad (5-19)$$

Finally, knowing the shear force due to the beam action (V_{yb}) and the arch action (V_{ya}), the total shear force at the yielding point (V_y) can be calculated using Eq. (5-20).

$$V_y = V_{yb} + V_{ya} = V_{yb}\left(1 + \frac{K_{ya}}{K_{yb}}\right) = V_{yb}\left(1 + \frac{E_c b c_{ay} \sin^2 \varphi_y \cos^2 \varphi_y}{\frac{V_{yb}}{\gamma_y}}\right) \qquad (5-20)$$

5.2.3 Cracking point

The cracking point is defined as when the initial flexural cracks develop in the member. Prior to this point, the member is uncracked, and hence almost all the shear is resisted by the concrete web with nearly no contribution from the transverse reinforcement and arch action (Kim et al., 1999; Kim and Jeong, 2011). Therefore, the shear force at this point can be calculated using the beam action only, as proposed by the authors in Chapter 4 and is shown in Eq. (5-21).

$$V_{cr} = \frac{0.33\sqrt{f_c'}bh^2 - Ph}{6\alpha \mathrm{d_v}} \qquad (5-21)$$

The shear strain at the cracking point (γ_{cr}) can be calculated by simply dividing the shear stress ($V_{cr}/b.d_v$) by the initial shear stiffness (G):

$$\gamma_{cr} = \frac{V_{cr}}{G.b.d_v} \qquad (5-22)$$

5.2.4 Failure point

According to a study by Elwood et al. (2007) on shear-critical RC members, a linear response is assumed for the post-peak strength degradation of the proposed model. The strength degradation continues until there is no residual shear strength in the section which is defined as the failure point. The shear strain corresponding to the zero shear force in the post-peak response can be calculated from Eq. (5-23) proposed by Elwood and Moehle (2005).

$$\gamma_f = 0.04 \frac{1 + \cot^2 \theta_f}{\cot(\theta_f)\left(1 - P\frac{s}{A_{st} f_{yt} d_v}\right)} \frac{a}{2h} \qquad (5-23)$$

Tran and Li (2015) investigated the failure of RC structures and showed that Eq. (5-23) is valid for both slender and deep members. In this equation, θ_f is the crack inclination angle at the failure point which can be taken as 30° for members with axial load ratios less than 20%, and 25° for members with higher axial load ratios as recommended in Chapter 4.

Figure 5-4 shows the step-by-step procedure for using the proposed model to calculate the shear force-strain response of deep members. Unlike most existing models for deep members, none of the calculation steps require any iteration enabling application of the proposed model for analysis of large structural systems in a practical manner. Once the shear strain at each step is found, the shear deformation can be calculated by multiplying the shear strain by the shear plastic hinge length as shown in Eq. (5-24). The shear plastic hinge length can be considered as the shear span length of the member (a) extended by half of the effective depth of the cross-section ($d/2$) into the end support (e.g., shear walls for coupled beams), as suggested by Fisher (2016). With this definition, however, the plastic hinge length can increase up to two times the shear span length for very short members which is not realistic. To avoid this issue, the plastic hinge length is limited to $1.5a$ for members with a/d ratios equal to or less than one. In addition, an upper limit of $2h$ that is proposed by authors for slender members in Chapter 4 is considered which may govern when the a/d ratio increases.

$$\Delta_{shear} = \begin{Bmatrix} \gamma.\left(a + \frac{d}{2}\right) & , & \frac{a}{d} > 1.0 \\ \gamma.(1.5a) & , & \frac{a}{d} \leq 1.0 \end{Bmatrix} \leq \gamma.2h \qquad (5-24)$$

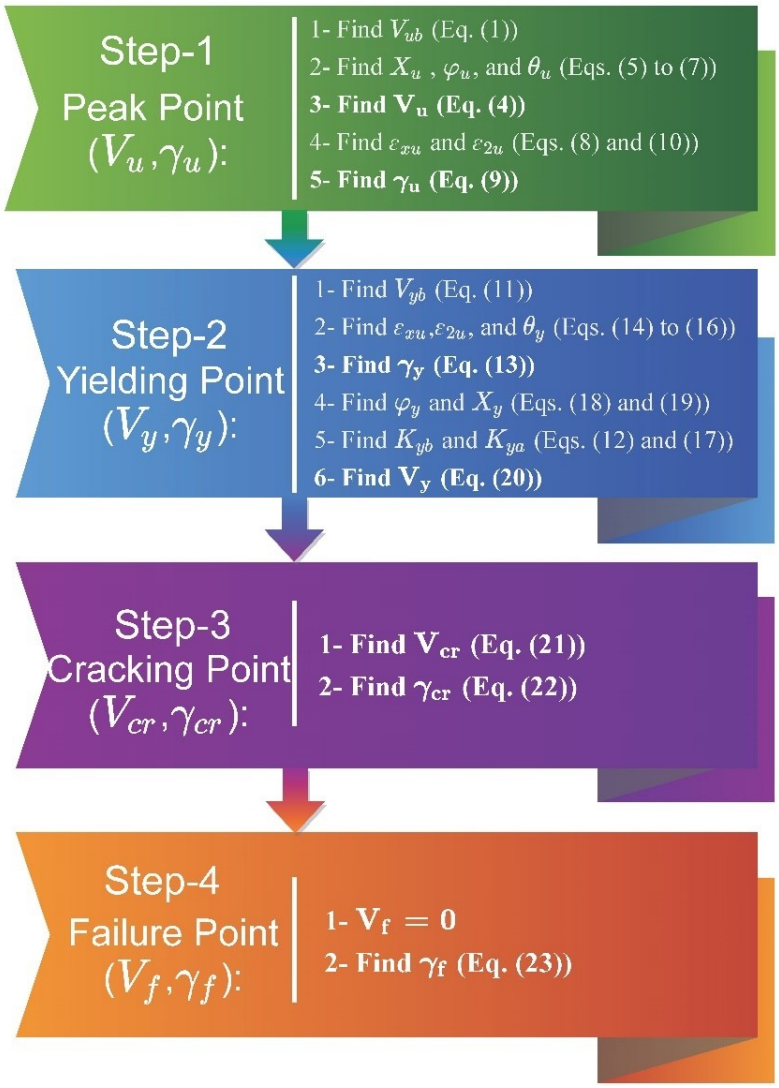

Figure 5-4 Step-by-step procedure for calculation of the four key points for the proposed model

5.3 Verification study at component-level

Coupling beams and short columns are among the most commonly used deep members in RC structures. In this study, a total of 12 deep shear-critical specimens, including 4 columns and 8 coupling beams, that were experimentally tested by various researchers were selected to evaluate the performance of the proposed model. Table 5-1 tabulates the material and geometrical properties of the specimens. The specimens were selected from various experimental test programs with a wide range of key design parameters (concrete

compressive strength, *a*/*d* ratio, longitudinal and transverse reinforcement ratios, axial load, etc.) to provide an unbiased comparison between the experimental results, proposed model and other analytical approaches.

Table 5-1 Parameters of RC columns considered for the verification study

Researcher	Specimen	f'_c (MPa)	f_{yl} (MPa)	f_{yt} (MPa)	b (mm)	h (mm)	d (mm)	$\frac{a}{d}$	s (mm)	A_{sl} (mm^2)	A_{st} (mm^2)	$\frac{P}{f'_c A_g}$	Member Type	Failure Mode
Tran (2010)	SC-1.7-0.20	27.5	408.0	392.6	350	350	305	1.97	125	2513	56.5	0.200	C	Shear
	SC-1.7-0.35	25.5	408.0	392.6	350	350	305	1.97	125	2513	56.5	0.350	C	Shear
	RC-1.7-0.20	24.5	408.0	392.6	250	490	445	1.91	125	2513	56.5	0.200	C	Shear
Umehara and Jirsa (1982)	CUS	34.9	441.0	414.0	230	410	370	1.23	89	685	56.5	0.162	C	Shear
Galano and Vignoli (2000)	P01	48.9	567.0	567.0	150	400	372	0.80	75	5322	100.5	0.000	CB	Flexure-Shear
Lim et al. (2016)	CB30-C	47.9	465.0	441.0	300	500	429	1.75	100	5564	398.0	0.000	CB	Flexure-Shear
Bristowe (2000)	NR2	41.0	433.0	428.0	300	500	448	2.00	131	3060	157.0	0.000	CB	Flexure-Shear
	NR4	41.0	433.0	428.0	300	500	448	2.00	90	3060	157.0	0.000	CB	Flexure-Shear
Fisher (2016)	CBF1	80.3	563.0	422.0	316	600	488	1.64	60	16800	400.0	0.000	CB	Shear
	CBF4	66.5	563.0	422.0	400	600	488	1.64	120	16800	400.0	0.000	CB	Shear
Barney et al. (1980)	C2	21.0	517.0	480.0	102	169	156	1.36	34	256	142.0	0.000	CB	Flexure-Shear
	C7	25.6	458.0	480.0	102	169	156	2.71	34	256	142.0	0.000	CB	Flexure-Shear

1 mm = 0.0394 in.; 1 MPa = 0.1450 ksi.
"CB" and "C" stand for the Coupling Beam and Column, respectively.

As shown in Figure 5-2(a), the proposed shear hinge model was implemented into the OpenSees analysis program (Mazzoni et al, 2006) using *ZeroLength* elements located at the end supports (shear walls for coupling beams and the foundation for short columns) to account for the nonlinear shear effects. *BeamColumn* elements with nonlinear fiber sections were also used to consider the axial-flexural behavior through the entire length of members. Thus, the shear behavior was analyzed using the lumped plasticity approach,

while the flexural and axial effects were taken into account based on the distributed plasticity analysis approach. Figure 5-5 compares the analytical and experimental load-deflection responses of the 12 deep members. The specimens were modeled using four different approaches: 1) The shear hinge model with the consideration of both the beam and arch action implemented into OpenSees, 2) The shear hinge model with the consideration of only the beam action implemented into OpenSees, 3) The peak point calculated based on the model of Pan and Li (2013), and 4) The VecTor2 nonlinear FE analysis program. As it can be seen in Figure 5-5, the load-deflection responses calculated by the proposed shear hinge model were in decent agreement with the experimental results for all specimens in terms of the shear strength, ductility, and stiffness. Also, it can be seen that neglecting the arch action effect resulted in considerable underestimation of the strength and ductility for almost all specimens demonstrating the importance of considering this mechanism for deep members. As expected, the arch action effect was more pronounced for specimens with a/d ratios less than 2.0.

As shown in Figure 5-5, the model of Pan and Li (2013) was able to predict the shear strength of specimens that experienced pure shear failure with good accuracy (e.g., SC-1.7-0.20, CBF1, CBF4). However, it overestimated the shear strength of specimens that had flexural-shear failure mode (e.g., P01, CB30-C, C2). This is because the Pan and Li model (2013) does not account for the reduction in the shear strength due to the yielding of longitudinal and transverse reinforcement prior to the opening of diagonal crack. As described in the Model Description section, the flexural-shear failure mode is considered in the shear hinge model proposed by the author using the second expression in Eq. (5-1). In terms of deformation at the peak strength, the Pan and Li model (2013) mostly

underestimated the test results for the specimens with pure shear failure mode. Also, for the specimens with flexure-shear failure, the ultimate deflection was significantly overestimated mainly due to the deficiency of the model to limit the shear strength which led to the calculation of excessive flexural deformations for the specimens. In such cases, the prediction of the Pan and Li model was not shown on the graphs to maintain the clarity of the figure. For example, the Pan and Li model predicted 122 mm as the ultimate deformation of the "P01" specimen, while the experimentally measured value was 25.94 mm. The ultimate deformation computed by the proposed shear hinge model for this specimen was 24.45 mm.

From Figure 5-5 it can be also concluded that the VecTor2 FE analysis software, which was developed based on the MCFT theory (Vecchio and Collins, 1986), calculated the load-deflection responses of the test specimens reasonably well, specially up to the peak point. Thus, this FE software can be considered as a reliable analysis tool for shear-critical deep RC members and was used for the verification purposes in the parametric study that will be described in the next section.

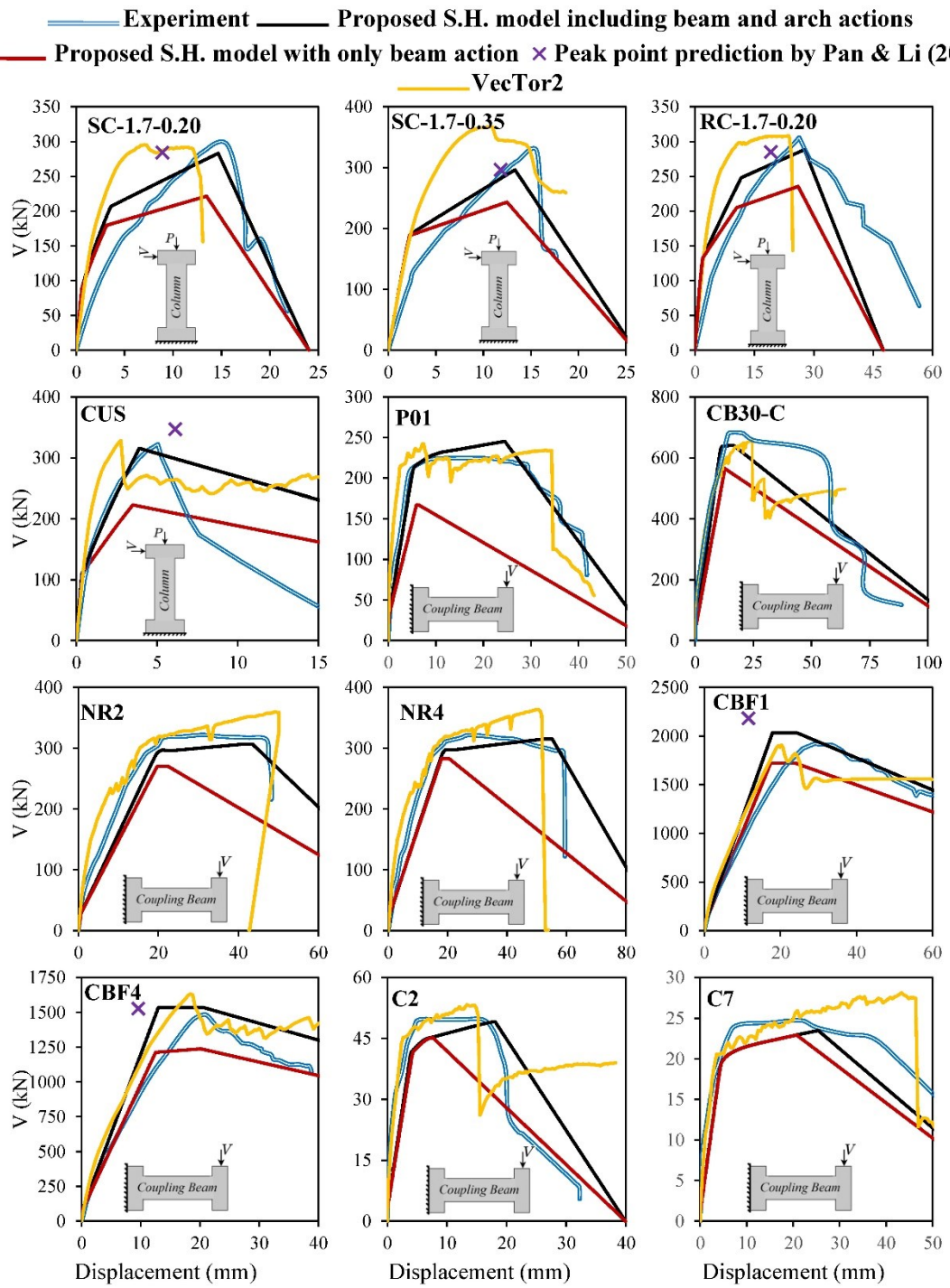

Figure 5-5 Comparison of force-displacement curves of different analytical models and experiment (1 mm = 0.0394 in.; 1 kN = 0.225 kip)

5.4 Parametric study

A total of 49 RC deep members with a wide range of design parameters were analyzed using the proposed shear hinge model and VecTor2 to evaluate the application range of the model. The design parameters investigated in the parametric study were the concrete compressive strength (f'_c), axial load ratio (P/f'_cA_g), transverse and longitudinal reinforcement ratios (ρ_z, ρ_x), cross-section depth (h), and boundary condition. The variation of these design parameters for each case study is shown in Table 5-2. The deep member "CB1" was used as the reference case, and the rest of the case studies were defined based on that by changing only one design parameter at a time. The selected members all had a width of 400 mm, a clear cover of 40 mm, rebar yield strength of 400 MPa, and were subjected to a shear force and/or an axial load at their ends. Members "CB1" to "CB10" and "CB19" to "CB48" were in double curvature bending with no axial load representing the response of coupling beams. Members "CB11" to "CB18" were also in double curvature bending but had axial load to simulate the behavior of short columns with fixed end supports. Finally, member "CB49" was in single curvature bending representing the response of a short cantilever beam.

The accuracy of the proposed shear hinge model was evaluated based on five response parameters: 1) the shear strength (V_u), 2) the deformation at the peak strength (Δ_u), 3) The shear force at the yielding point (V_y), 4) the area under the pre-peak region of the force-displacement curve ($A_{pre\text{-}peak}$), and 5) the total area under the force-displacement curve (A_{total}). The ratio of response parameters obtained from the proposed shear hinge model and the VecTor2 analysis was calculated and plotted in Figure 5-6 in terms of variation in each design parameter (f'_c, P/f'_cA_g, etc.). A response parameter ratio of one indicates an

excellent correlation between the prediction of the proposed model and VecTor2. As the ratio moves away from one, the accuracy of the proposed model to capture that particular response parameter deteriorates.

Table 5-2 Properties of RC columns used for parametric study (1 mm = 0.0394 in.; 1 kN = 0.225 kip; 1 MPa = 0.1450 ksi)

Model	f'_c (MPa)	ρ_x (%)	ρ_z (%)	a/d	P/f'_cA_g	h (mm)	Model	f'_c (MPa)	ρ_x (%)	ρ_z (%)	a/d	P/f'_cA_g	h (mm)
CB1	30	1.42	0.20	1.36	0.00	800	CB26	30	1.42	1.00	1.36	0.00	800
CB2	20	1.42	0.20	1.36	0.00	800	CB27	30	1.42	0.20	0.54	0.00	800
CB3	25	1.42	0.20	1.36	0.00	800	CB28	30	1.42	0.20	0.68	0.00	800
CB4	35	1.42	0.20	1.36	0.00	800	CB29	30	1.42	0.20	0.81	0.00	800
CB5	40	1.42	0.20	1.36	0.00	800	CB30	30	1.42	0.20	0.95	0.00	800
CB6	45	1.42	0.20	1.36	0.00	800	CB31	30	1.42	0.20	1.08	0.00	800
CB7	50	1.42	0.20	1.36	0.00	800	CB32	30	1.42	0.20	1.22	0.00	800
CB8	60	1.42	0.20	1.36	0.00	800	CB33	30	1.42	0.20	1.63	0.00	800
CB9	70	1.42	0.20	1.36	0.00	800	CB34	30	1.42	0.20	1.83	0.00	800
CB10	80	1.42	0.20	1.36	0.00	800	CB35	30	1.42	0.20	2.03	0.00	800
CB11	30	1.42	0.20	1.36	0.05	800	CB36	30	0.47	0.20	1.36	0.00	800
CB12	30	1.42	0.20	1.36	0.10	800	CB37	30	0.71	0.20	1.36	0.00	800
CB13	30	1.42	0.20	1.36	0.20	800	CB38	30	0.95	0.20	1.36	0.00	800
CB14	30	1.42	0.20	1.36	0.30	800	CB39	30	1.19	0.20	1.36	0.00	800
CB15	30	1.42	0.20	1.36	0.40	800	CB40	30	1.66	0.20	1.36	0.00	800
CB16	30	1.42	0.20	1.36	0.50	800	CB41	30	1.90	0.20	1.36	0.00	800
CB17	30	1.42	0.20	1.36	0.60	800	CB42	30	2.14	0.20	1.36	0.00	800
CB18	30	1.42	0.20	1.36	0.80	800	CB43	30	2.37	0.20	1.36	0.00	800
CB19	30	1.42	0.05	1.36	0.00	800	CB44	30	1.42	0.20	1.36	0.00	400
CB20	30	1.42	0.10	1.36	0.00	800	CB45	30	1.42	0.20	1.36	0.00	600
CB21	30	1.42	0.15	1.36	0.00	800	CB46	30	1.42	0.20	1.36	0.00	1000
CB22	30	1.42	0.25	1.36	0.00	800	CB47	30	1.42	0.20	1.36	0.00	1200
CB23	30	1.42	0.40	1.36	0.00	800	CB48	30	1.42	0.20	1.36	0.00	1500
CB24	30	1.42	0.60	1.36	0.00	800	CB49*	30	1.42	0.20	1.36	0.00	800
CB25	30	1.42	0.80	1.36	0.00	800							

* "CB49" model has the same properties as "CB1" model, except that it is cantilever, rather than double curvature.

With regards to the concrete compressive strength (f'_c), it can be seen from Figure 5-6(a) that the proposed model predicted all response parameters with good accuracy for f'_c ranging from 30 to 80 MPa. However, the accuracy of the model slightly reduced as f'_c increased beyond 40 MPa. This can be because of using the Hognestad parabola (1951) in the formulation of the model for computing the compression behavior of concrete which may not be an ideal constitutive model for analysis of high strength concrete.

The response parameters computed by the proposed model and VecTor2 were also in good correlation for all axial load ratios as shown in Figure 5-6(b). Except that the displacement at the peak strength and the area under the force-deflection response for member "CB18" which had the highest axial load ratio (P/f'_cA_g=0.80) were not calculated with the same level of accuracy as the other members. This can be attributed to the sensitivity of the results to the calculation of the compression zone depth (X_u) for cases with high axial ratios. When the axial load ratio is extremely high, the cross-section is mostly in compression and thus any approximation in the calculation of X_u can have a considerable effect on the shear strain and deformation. Nevertheless, the axial load ratio of 0.80 is an extreme case that rarely occurs in real-world problems, specially for shear-critical members. Therefore, this should not have much impact on the application range of the proposed model.

Figure 5-6(c) shows the analysis results for deep members with different ratios of transverse reinforcement. As it can be seen from this figure, the proposed model calculated the response of deep members having at least the minimum amount of shear reinforcement ($\rho_{z.min}$) as specified by CSA A23.3 (2019) reasonably well. However, the accuracy of the model started to deteriorate as the transverse reinforcement ratio became less than $\rho_{z.min}$. The shear response of these members was mainly governed by the concrete behavior which is generally more difficult to capture than the response of reinforcement.

The effect of shear span to effective depth ratio (a/d) is shown in Figure 5-6(d). It can be seen that the model overestimated the response parameters when the a/d ratio was less than one, while for members with higher a/d ratios the model slightly underestimated the response. The discrepancy between the results was mostly in the prediction of Δ_u for

members with a/d ratios less than one. This can be attributed to the approximations made in the estimation of shear plastic hinge length in Eq. (5-24) used for the calculation of the shear deformation from the shear strain. The discrepancy in shear deformation values resulted in some inaccuracies in the prediction of the area under the force-displacement response as well. However, the shear strength and the yielding force both were calculated with reasonable accuracy for all a/d ratios.

The effect of longitudinal reinforcement ratio (ρ_x) can be seen in Figure 5-6(e). The two failure modes (pure shear failure and flexural-shear failure) considered for deep members are also shown in this figure. It can be seen that members that were lightly reinforced in the longitudinal direction experienced a flexural-shear failure. According to Figure 5-6(e), the response parameters calculated by the proposed model were generally in good agreement with the VecTor2 results. However, for members close to the transition point of the failure mode ($\rho_x \approx 1\%$), the prediction of Δ_u was not as accurate as that for the other members. Through a series of sensitivity analyses, it was found that the ultimate deformation of these members was extremely sensitive to the material properties of the reinforcement, particularly at the post-yielding region. Even a small change in the material properties defined in the model can change the failure mode of these member and significantly affect their ultimate deformations.

The effect of cross-section size is also demonstrated in Figure 5-6(f). It can be seen that the proposed model worked fairly well for deep members with various cross-section dimensions. Lastly, comparison of the analysis results for the "CB1" and "CB49" members yielded a range of ratios between 0.80 and 1.15 for all five response parameters (V_u, Δ_u,

etc.) indicating that the proposed model is able to predict the response of deep members in double curvature as well as single curvature bending reasonably well.

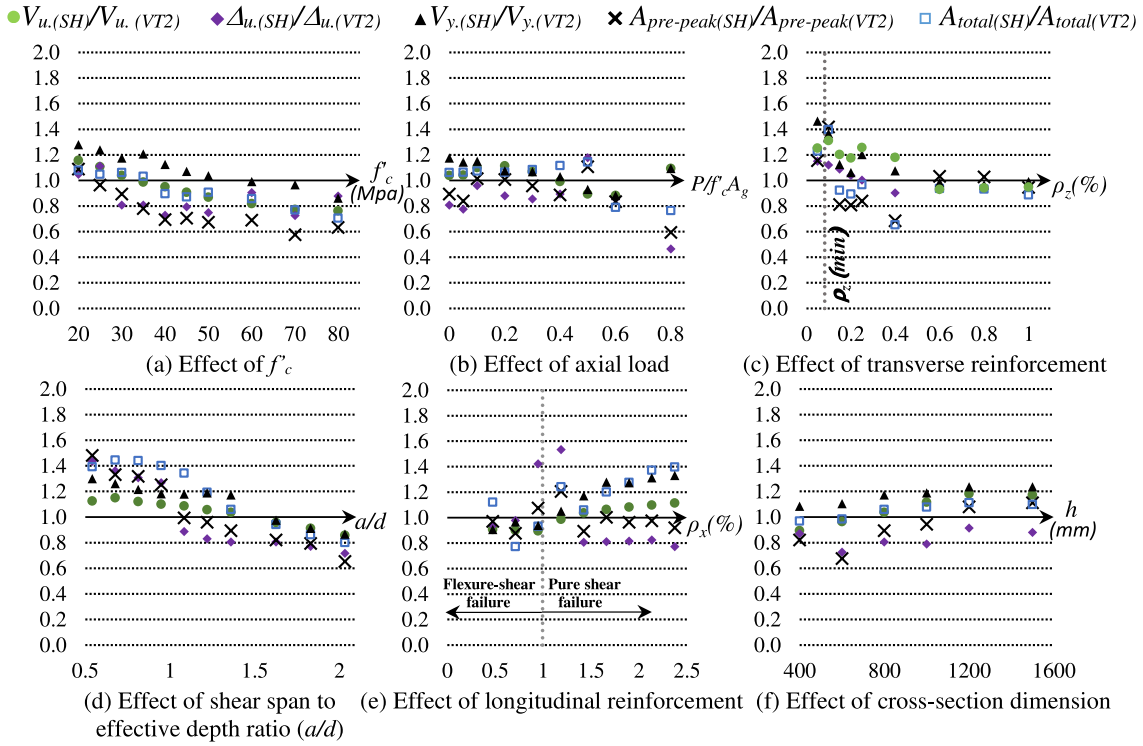

Figure 5-6 Performance of the proposed shear hinge (SH) model for RC deep members with various design parameters (1 mm = 0.0394 in.; 1 kN = 0.225 kip)

The average and coefficient of variation (CV) of the response parameter ratios for all 49 members considered in the parametric study are provided in Table 5-3. It can be seen that the average values for all the five response parameters were between 0.94 and 1.11 and the CV values were within a reasonable range, which showed good accuracy and consistency in the predictions of the proposed model. The CV of the strength-related parameters (V_u and V_y) was lower than that for the rest of the response parameters (Δ_u, $A_{pre\text{-}peak}$, A_{total}) which was expected since the prediction of displacement in RC members is typically more challenging than strength.

Table 5-3 Summary of the response parameter ratios for 49 deep RC members

Response parameter ratio	Average	%CV
$V_{u.(SH)}/V_{u.\ (VT2)}$	1.01	10.9
$\Delta_{u.(SH)}/\Delta_{u.(VT2)}$	0.94	23.9
$V_{y.(SH)}/V_{y.(VT2)}$	1.11	12.4
$A_{pre\text{-}peak\ (SH)}/A_{pre\text{-}peak\ (VT2)}$	0.94	22.2
$A_{total(SH)}/A_{total(VT2)}$	1.08	18.5

5.5 Application study at system-level

A multi-storey RC coupled shear wall was considered to assess the performance and effectiveness of the proposed shear hinge model for analysis of structures at the system-level. The frame consisted of two RC shear walls connected by coupling beams along the height as shown in Figure 5-7. The material and geometrical properties of the coupling beams were the same as the "CBF1" specimen that was tested experimentally by Fisher (2016), and also described in Section 5.3 of this thesis. The same wall properties used by Fisher (2016) in his experimental program were also used in this study for all storeys. An analytical model was constructed in the OpenSees program in which the walls were modeled using the *Multiple-Vertical-Line-Element-Model (MVLEM)* elements and the coupling beams were modeled using the *ForceBeamColumn* elements with fiber sections. The wall and coupling beam elements were connected through rigid links. The proposed shear hinge was incorporated into the OpenSees model using *ZeroLength* elements added to the ends of coupling beams enabling the model to capture nonlinear shear effects. The structure was subjected to a constant gravity load of $0.1f'_cA_g$ imposed to each shear wall and a monotonically increasing lateral displacement applied at the roof level, as shown in Figure 5-7.

The analysis results are shown in Figure 5-7. According to this figure, the load-deflection response of the OpenSees model with the proposed shear hinges was in good agreement with the VecTor2 analysis results. It can be seen that removing the shear hinges from the OpenSees model led to significant overestimation of the peak strength and underestimation of the ductility which was the result of computing incorrect failure mode and neglecting shear deformations. A shear failure mode in the coupling beams occurred when the proposed shear hinge model was considered in the analysis which was consistent with the failure mode computed by VecTor2. Whereas axial-flexural failure of the shear walls governed the behavior when the shear hinges were not included in the OpenSees model. Moreover, by comparing the results of OpenSees models with and without the shear hinges, it can be seen that shear deformations of the coupling beams account for a considerable portion of the total lateral deformation of the structure. This shows the importance of considering shear deformations in deep members and their effect on the response of the entire structure as a system. Also, considering the shear strength and deformation at the peak point for the coupling beams based on the model of Pan and Li (2013) resulted in a peak strength close to VecTor2, but the ductility was underestimated. This issue was previously observed in the analysis of the "CBF1" specimen in the Verification section at the component-level where the model of Pan and Li underestimated the deflection compared to the experiment. This was attributed to using an oversimplified equation that unlike the proposed model does not consider the effect of longitudinal and principal compressive strains on the shear deformation.

In terms of computational efficiency, the analysis time required by the OpenSees model with the proposed shear hinges was 21 seconds which was almost 0.1% of that for the

VecTor2 FE software which took 349 minutes (~21000 seconds) to analyze the structure. As the structure becomes larger and more complex, the improvement in the computational performance will be even more pronounced. Modeling the entire structural system with multiple shear walls in different directions would not be even possible with most detailed FE analysis tools. Thus, macro-modeling methods such as the one developed in this study would be highly effective for the system-level performance assessment and design of structures.

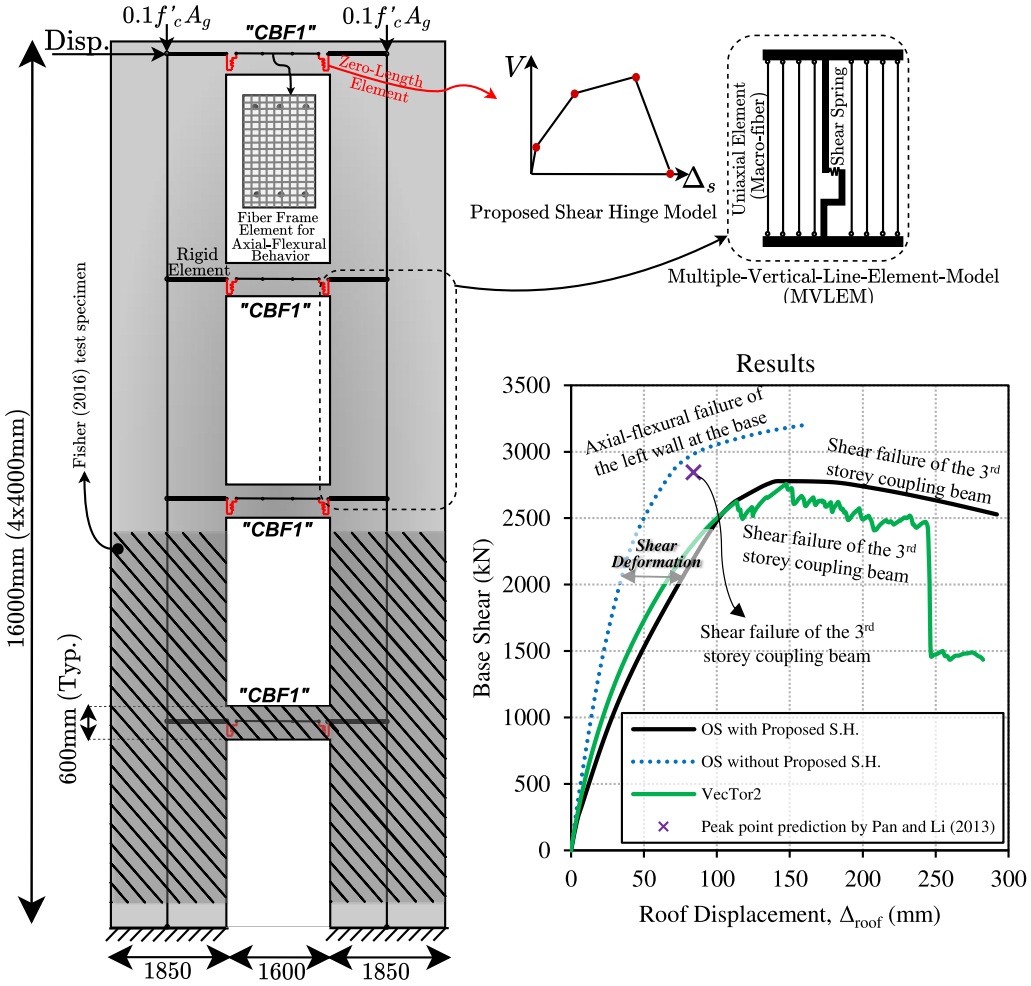

Figure 5-7 OpenSees model (left) and the base shear versus lateral roof displacement response (right) of the RC coupled wall (1 mm = 0.0394 in.; 1 kN = 0.225 kip)

5.6 Summary and conclusions

This chapter presented a new shear hinge model for calculating the nonlinear shear response of RC deep members using the lumped plasticity approach. The model considers the effect of beam action and arch action separately based on the MCFT theory and the deformation compatibility condition. Compared to other beam-arch action models that are mostly limited to the calculation of the peak shear strength, the proposed model provides the complete shear force-displacement response of deep members which is essential for accurate safety assessment and full performance evaluation of shear-critical structures. The proposed model is also computationally efficient and does not require any iteration or having substantial modeling experience unlike other analysis approaches such as strut-and-tie and FE methods. Development of the model based on the MCFT theory enables it to consider important second-order material effects such as compression softening, tension stiffening, and aggregate interlock mechanism.

The proposed model was verified against experimental results of 12 deep shear-critical specimens. The results of the model agreed well with the experiments and FE analysis method. The importance of considering the arch action for determining the shear response of deep members with *a/d* ratios less than 2 was also demonstrated. Through a comprehensive parametric study, it was shown that the proposed model can accurately calculate the shear response of RC deep members with various design parameters. The accuracy of the model was relatively lower for members with high concrete compressive strength or an extremely high axial load ratio. Lastly, the proposed model was used for analysis of a multi-storey coupled shear wall structure. The model was able to provide the same level of accuracy as the FE method but with much less computational effort

demonstrating the effectiveness of the model for analysis of large structural systems. It was shown that consideration of nonlinear shear effects in deep members will not only affect the strength and ductility of the member but also can have a significant influence on the response of the entire structure.

The presented shear hinge model for RC deep members along with the previously developed models for slender beams and columns described in Chapters 3 and 4, enable accounting for nonlinear shear effects in macro-modeling of almost any type of structural system that contains shear-critical members in a practical and efficient manner.

5.7 Notation

$A_{pre\text{-}peak}$= area under the pre-peak portion of the response

A_{sl}= area of tensile longitudinal reinforcement

A_{st}= area of transverse reinforcement

A_{total}= total area under the load-deflection response

a= shear span

b= member width

c= concrete clear cover

C= summation of the forces acting on the compression side of the cross-section

c_a= inclined strut width

d= effective depth

d_v= effective shear depth, taken as the greater of $0.9d$ or $0.72h$

E_s= modulus of elasticity of steel

f'_c= cylindrical compressive strength of concrete

f_{c1}= principal tensile stress in concrete

f_{c2}=principal compressive stress in concrete

f_{sx} and f_{sz}=average stress in longitudinal and transverse reinforcements

f'_t= modulus of rupture of concrete

f_x and f_z= stress applied to element in x and z directions

f_{yl}= yield strength of longitudinal reinforcement

f_{yt}= yield strength of transverse reinforcement

G= initial shear modulus of concrete

h= member height

K= shear stiffness

L= member length

n= ratio of the modulus of elasticity of steel to concrete

P= axial compressive load (negative sign for compression)

s= spacing of transverse reinforcement

s_z= crack spacing parameter, as defined in CSA A23.3

s_{ze}= equivalent crack spacing that allows for influence of aggregate size

T= summation of the forces acting on the tension side of the cross-section

V_c= shear resistance provided by concrete

V_s= shear resistance provided by transverse reinforcement

V= shear force

v= shear stress

v_c= shear stress in concrete

v_{ci}= shear stress on crack surfaces

X= distance from extreme compression fiber to neutral axis

β= contribution factor accounting for strength of cracked concrete

ε_0= strain in concrete at f'_c

ε_1= principal tensile strain in concrete

ε_2= principal compressive strain in concrete

ε_x= longitudinal strain

ε_z= transverse strain

γ= shear strain

θ= angle between crack inclination and x-axis

ρ_x and ρ_z= longitudinal and transverse reinforcement ratios

φ= strut inclination with respect to the longitudinal axis of the member

Subscripts “u”, “f”, “y”, and “cr” are related to each of the four key points in the model. Also, subscripts “a” and “b” are used for parameters used in arch action, and beam action mechanisms, respectively. For example, K_{ya} represents the shear stiffness of the cross-section at the yielding point due to the arch action.

Chapter 6: Summary and Conclusions

This study presented a series of new plastic hinge models, developed based on the Modified Compression Field Theory (MCFT) (Vecchio and Collins, 1986), for nonlinear analysis of shear-critical RC structures applicable to both slender and deep members. This is the first time that the MCFT theory was extended to the lumped plasticity analysis approach which enabled eliminating the limitations of existing shear hinge models by capturing advanced mechanisms such as interactions between sectional forces, effects of nonlinear stress and strain distributions through the section, and second-order material effects in RC structures in a concentrated manner.

The proposed shear hinge models were verified against a total of 36 experimental tests of shear-critical RC slender beams, columns and deep members, and their application range was evaluated through extensive parametric studies conducted on a total of 97 case studies. Moreover, the shear hinge models were implemented into the OpenSees analysis software to demonstrate the effectiveness of the proposed lumped plasticity modeling approach for the system-level performance assessment of two multi-storey frames and a coupled shear wall structure. Based on the analysis results obtained at the component- and system-level and the ability of the plastic hinges in capturing nonlinearity effects due to shear, it is expected that the proposed lumped plasticity modeling approach enhances the safety assessment of existing structures and contributes to the design of high-performance complex structural systems.

The main advantages of the proposed shear hinge models can be summarized as follows:

- Unlike the existing models which mainly focused on predicting the shear strength, the proposed models provide the complete shear force-deformation response of RC members which is essential for computing and understanding the behavior of shear-critical structures.
- From the comprehensive verification studies conducted in this thesis, it can be concluded that the proposed models can calculate the nonlinear response of shear-critical members with better accuracy compared to other existing plastic hinge models. The analysis results also confirmed that the accuracy of the lumped plasticity analysis method is directly related to the ability of plastic hinges to capture nonlinearity effects. Therefore, special care must be taken in choosing and defining plastic hinges when using the lumped plasticity analysis approach.
- The proposed shear hinges are computationally efficient since they do not require any iterations and can be easily implemented in any analysis tool using simple spring elements. As it was demonstrated in the system-level studies, using the proposed shear hinges can substantially reduce the analysis time compared to the distributed plasticity and finite element methods, while providing almost the same level of accuracy in predicting the shear behavior.
- The proposed shear hinge models were developed based on a rational theory and fundamental equations of equilibrium and compatibility in conjunction with well-recognized constitutive material models enabling them to be used for shear-critical RC structures with a wide range of design parameters, as shown in the extensive parametric studies conducted in this research.

- The original MCFT formulation is complicated and requires a trial-and-error procedure. The closed-form equations proposed in this study enable direct calculation of the shear force and shear deformation of RC members at key points of the shear response providing a simple calculation method for engineers to evaluate the shear response of RC members based on the principles of the MCFT theory.

Chapter 7: Recommendations for Future Research

The following recommendations for future research and improvements on the proposed shear hinge models are suggested:

- The proposed models were developed for RC members subjected to monotonic loading. Work is needed to extend the application of models to members subjected to cyclic and reversed cyclic loading conditions.
- The shear plastic hinge length in this study was considered using a simple approach as described in Chapters 3 to 5. This parameter directly influences the calculation of shear deformation and consequently the shear response of RC members. Work is needed to evaluate the effect of various design parameters on the shear plastic hinge length and propose a refined equation or method to better estimate this parameter.
- It was tried to develop the shear hinge models in the simplest possible form. However, computing the shear response still requires using a large number of closed-form equations and considerable effort, especially if hand calculation is used. Although using a spreadsheet can significantly facilitate calculation of the model parameters, one can propose a more simplified version of the models by eliminating unnecessary parameters that do not have considerable effect on the accuracy or neglecting some key points in the shear response for special cases. An example of this simplification was carried out on the beam shear hinge model in a recently published conference paper (Tabkhi and Sadeghian, 2021c).
- The effect of dowel action was neglected in the formulation of the proposed shear hinge models. The influence of this mechanism on the shear force and the shear deformation at different stages of the structural response needs to be investigated,

especially for lightly reinforced concrete members. The proposed equations can then be modified accordingly to account for the dowel action to improve the accuracy of the models.

- Another potential future research area can be extending the model to members with complex reinforcement detailing (e.g., coupled beams with diagonal reinforcements).
- Using the procedure described in this study and based on the MCFT method, a new plastic hinge model can be developed to account for torsional behavior of RC members in a concentrated manner.

References

ACI Committee 318. (2019). *Building Code Requirements for Structural Concrete (ACI 318-19) and Commentary (ACI 318R-19)*. American Concrete Institute.

ASCE/SEI 41-17. (2017). *Seismic Evaluation and Retrofit of Existing Buildings*. American Society of Civil Engineers.

Barney, G. B., Shiu, K. N., Rabbat, B. G., Fiorato, A. E., Russell, H. G., & Corley, W. G. (1980). Behavior of Coupling Beams Under Load Reversals. *Portland Cement Association, Research and Development Bulletin RD068.01B*.

Bentz, E., C. & Collins, M. P. (2001). Response-2000, Membrane-2000, Triax-2000, and Shell-2000 User Manual. Retrieved from http://www.ecf.utoronto.ca/~bentz/manual2/final.pdf.

Bentz, E. C., & Collins, M. P. (2006). Development of the 2004 Canadian Standards Association (CSA) A23.3 Shear Provisions for Reinforced Concrete. *Canadian Journal of Civil Engineering*, 33(5), 521-534.

Bentz, E. C., Vecchio, F. J., & Collins, M. P. (2006). Simplified Modified Compression Field Theory for Calculating Shear Strength of Reinforced Concrete Elements. *ACI Structural Journal*, 103(4), 614-624.

Bristowe, S. (2000). *Seismic Response of Normal and High-strength Concrete Members.* PhD thesis, McGill University, Montreal.

Calvi, G. M., Magenes, G., & Pampanin, S. (2002). Experimental Test on a Three Storey RC Frame Designed for Gravity Only. *12th European Conference on Earthquake Engineering*, London, UK.

Canadian Commission on Building and Fire Codes. (1995). *National Building Code of Canada: 1995*. National Research Council of Canada.

Červenka, V., Jendele, L., & Červenka, J. (2020). *ATENA Program Documentation – Part 1 - Theory*. Červenka Consulting, Prague, Czech Republic.

Cladera, A. (2002). *Shear Design of Reinforced High-Strength Concrete Beams*. PhD thesis, Universitat Politècnica De Catalunya, Barcelona, Spain.

Collins, M. P., Quach, P. T., & Bentz, E. C. (2020). Shear Behavior of Thick Slabs. *ACI Structural Journal*, 117(4), 115-126.

CSA Committee A23.3. (1994). *Design of Concrete Structures (CSA A23.3-94)*. Canadian Standards Association.

CSA Committee A23.3. (2004). *Design of Concrete Structures (CSA A23.3-04)*. Canadian Standards Association.

CSA Committee A23.3. (2019). *Design of Concrete Structures (CSA A23.3-19)*. Canadian Standards Association.

Duong, K. V., Sheikh, S. A., & Vecchio, F. J. (2007). Seismic Behavior of Shear-Critical Reinforced Concrete Frame: Experimental Investigation. *ACI Structural Journal*, 104(3), 304-313.

Elwood, K. J. (2004). Modelling Failures in Existing Reinforced Concrete Columns. *Canadian Journal of Civil Engineering*, 31(5), 846-859. https://doi.org/10.1139/l04-040

Elwood, K. J., & Moehle, J. P. (2005). Axial Capacity Model for Shear-Damaged Columns. *ACI Structural Journal*, 102(4), 578-587.

Elwood, K. J., Matamoros, A. B., Wallace, J. W., Lehman, D. E., Heintz, J. A., Mitchell, A. D., Moore, M. A., Valley, M. T., Lowes, L. N., Comartin, C. D., & Moehle, J. P. (2007). Update to ASCE/SEI 41 Concrete Provisions. *Earthquake Spectra*, 23(3), 493–523.

Esfandiari, A., & Adebar, P. (2009). Shear Strength Evaluation of Concrete Bridge Girders. *ACI Structural Journal*, 106(4), 416-426.

Fisher, A. W. (2016). *Shear Performance of Heavily Reinforced High-Strength Concrete Coupling Beams.* Master's thesis, University of Toronto, Toronto.

Frosch, R. J. (2000). Behavior of Large-Scale Reinforced Concrete Beams with Minimum Shear Reinforcement. *ACI Structural Journal*, 97(6), 814-820.

Galano, L., & Vignoli, A. (2000). Seismic Behavior of Short Coupling Beams with Different Reinforcement Layouts. *ACI Structural Journal*, 97(6), 876-885.

Guner, S. (2008). *Performance Assessment of Shear-Critical Reinforced Concrete Plane Frames*. PhD thesis, University of Toronto, Toronto, ON, Canada.

Guner, S., & Vecchio, F. J. (2008). User's Manual of VecTor5. Retrieved from http://www.vectoranalysisgroup.com/software.html.

Hayashi, H., Marui, T., Taniguchi, N., & Kayano, S. (2000). Restoration of Hanshin Expressway after Kobe/Awaji Earthquake – Challenge of 623 Days Before Opening. *Cement and Concrete Composites*, 22(1), 29-38. https://doi.org/10.1016/S0958-9465(99)00046-3

Hognestad, E. (1951). *Study of Combined Bending and Axial Load in Reinforced Concrete Members*. University of Illinois Engineering Experiment Station, 399.

Ikeda, A. (1968). *Report of the Training Institute for Engineering Teachers*. Yokohama National University, Japan.

Imai, H., & Yamamoto, Y. (1986). A Study on Causes of Earthquake Damage of Izumi High School Due to Miyagi-Ken-Oki Earthquake in 1978. *Transactions of the Japan Concrete Institute*, 8, 405-418.

Ismail, K. S., Guadagnini, M., & Pilakoutas, K. (2018). Strut-and-Tie Modeling of Reinforced Concrete Deep Beams. *Journal of Structural Engineering*, 144(2). https://doi.org/10.1061/(ASCE)ST.1943-541X.0001974

Johnson, P. M., & Commission d'enquête sur le viaduc de la Concorde (Québec) (2007). *Report of the Commission of Inquiry into the Collapse of a Portion of the De La Concorde Overpass*. Commission d'enquête sur le viaduc de la Concorde Québec.

Kassem, C., Farghaly, A. S., & Benmokrane, B. (2011). Evaluation of Flexural Behavior and Serviceability Performance of Concrete Beams Reinforced with FRP Bars. *Journal of Composites for Construction*, 15(5), 682-695. https://doi.org/10.1061/(ASCE)CC.1943-5614.0000216

Kim, D., Kim, W., & White, R. N. (1999). Arch Action in Reinforced Concrete Beams—A Rational Prediction of Shear Strength. *ACI Structural Journal*, 96(4), 586-593.

Kim, W., & Jeong, J. (2011). Decoupling of Arch Action in Shear-Critical Reinforced Concrete Beams. *ACI Structural Journal*, 108(4). 395-404. https://doi.org/10.14359/51682979

Kokusho S., Reported by Hirosawa M. (1973). *A List of Past Experimental Results of Reinforced Concrete Columns*. Tsukuba, Japan: Building Research Institute, 2.

LeBorgne, M. R., & Ghannoum, W. M. (2014). Analytical element for simulating lateral strength degradation in reinforced concrete columns and other frame members. *Journal of Structural Engineering*, 140(7).

Leondardt, F. (1965). Reducing the Shear Reinforcement in Reinforced Concrete Beams and Slabs. *Magazine of Concrete Research*, 17(53), 187-198. https://doi.org/10.1680/macr.1965.17.53.187

Lim, E., Hwang, S., Cheng, C., & Lin, P. (2016). Cyclic Tests of Reinforced Concrete Coupling Beam with Intermediate Span-Depth Ratio. *ACI Structural Journal*, 113(3), 515-524.

Lynn, A. C. (2001). *Seismic Evaluation of Existing Reinforced Concrete Building Columns*. PhD thesis, University of California, Berkeley.

Mazzoni S., McKenna F., Scott M. H., & Fenves G. L. (2006). *OpenSees Command Language Manual*. Pacific Earthquake Engineering Research (PEER) Center.

Mohr, D. S. (2007). *Nonlinear Analysis and Performance Based Design Methods for Reinforced Concrete Coupled Shear Walls*. Master's Thesis, University of Washington.

Nabilah, A. B., Koh, C. G., Safiee, N. A., & Nasir, N. A. M. (2020). Analysis of Conventionally Reinforced Coupling Beams Using Non-Linear Strut-and-Tie Model. *Structures and Buildings*, 173(6). https://doi.org/10.1680/jstbu.18.00095

Nguyen, P. T. (2013). *A Study of Shear Behavior on Reinforced Concrete Deep Beams*. PhD Thesis, The University of Texas at Austin.

Pan, Z., & Li, B. (2013). Truss-Arch Model for Shear Strength of Shear-Critical Reinforced Concrete Columns. *Journal of Structural Engineering*, 139(4). https://doi.org/10.1061/(ASCE)ST.1943-541X.0000677

Park, R., & Paulay, T. (1975). *Reinforced Concrete Structures*. John Wiley and Sons.

Park, Y., & Ang. A. (1985). Mechanistic Seismic Damage Model for Reinforced Concrete. *Journal of Structural Engineering*, 111(4), 722-739. https://doi.org/10.1061/(ASCE)0733-9445(1985)111:4(722)

Pincheira, J. A., Dotiwala, F. S., & D'Souza, J. T. (1999). Seismic Analysis of Older Reinforced Concrete Columns. *Earthquake Spectra*, 15(2). 245–72.

Podgorniak-Stanik, B. A. (1998). *The Influence of Concrete Strength, Distribution of Longitudinal Reinforcement, Amount of Transverse Reinforcement and Member Size on Shear Strength of Reinforced Concrete Members*. MASc Thesis, University of Toronto, Toronto, ON, Canada.

Sadeghian, V., & Vecchio, F. (2018). The Modified Compression-Field Theory: Then and Now. *ACI Symposium Publication*, 328.

Sae-Long, W., Limkatanyu S., Prachasaree, W., Horpibulsuk, S., & Panedpojaman, P. (2019). Nonlinear Frame Element with Shear–Flexure Interaction for Seismic Analysis of Non-Ductile Reinforced Concrete Columns. *International Journal of Concrete Structures and Materials*, 13(8). https://doi.org/10.1186/s40069-019-0343-2

Salgado, R. A., & Guner, S. (2018). A Comparative Study on Nonlinear Models for Performance-Based Earthquake Engineering. *Engineering Structures*, 172, 382-391.

Sherwood, E. (2008). *One-Way Shear Behaviour of Large, Lightly-Reinforced Concrete Beams and Slabs*. PhD thesis, University of Toronto, Toronto, ON, Canada.

Tabkhi, A. R., & Sadeghian, V. (2021a). A Shear Hinge Model for Analysis of Reinforced Concrete Beams. *ACI Structural Journal*. 118(6), 279-290. http://dx.doi.org/10.14359/51733001

Tabkhi, A. R., & Sadeghian, V. (2021b). A Shear Hinge Model for Analysis of Reinforced Concrete Columns. *ACI Structural Journal* (Accepted for publication).

Tabkhi, A. R., & Sadeghian, V. (2021c). A Lumped Plasticity Model for Performance Assessment of Shear-Critical Reinforced Concrete Beams. *fib Symposium*, Lisbon, Portugal.

Tamai, S., Shima, H., Izumo, J., & Okamura, H. (1988). Average Stress-Strain Relationship in Post Yield Range of Steel Bar in Concrete. *Concrete Library of JSCE*, 11. 117-129.

Tran, C. T. N. (2010). *Experimental and Analytical Studies on the Seismic Behavior of Reinforced Concrete Columns with Light Transverse Reinforcement*. PhD thesis, Nanyang Technological University, Singapore.

Tran, C. T. N., & Li, B. (2015). Experimental Studies on the Backbone Curves of Reinforced Concrete Columns with Light Transverse Reinforcement. *Journal of Performance of Constructed Facilities*, 29(5). https://doi.org/10.1061/(ASCE)CF.1943-5509.0000626.

Umehara, H., & Jirsa, J.O. (1982). *Shear Strength and Deterioration of Short Reinforced Concrete Columns Under Cyclic Deformations*. PMFSEL Report No. 82-3, Department of Civil Engineering, University of Texas at Austin, Austin, Texas.

Vecchio, F. J., & Collins, M. P. (1986). The Modified Compression-Field Theory for Reinforced Concrete Elements Subjected to Shear. *ACI Journal*, 83(22), 219-231.

Wong, P. S., Vecchio, F. J., & Trommels, H. (2013). *VecTor2 and FormWorks User's Manual, 2nd Edition*. Department of Civil Engineering, University of Toronto, Canada.

Yoshimura, M., & Yamanaka, N. (2000). Ultimate Limit State of RC Columns. *Second U.S.- Japan Workshop on Performance-Based Earthquake Engineering Methodology for Reinforced Concrete Structures*. Sapporo, Japan, PEER Center, 313-326.

Zimos, D. K., Papanikolaou, V. K., Kappos, A. J., & Mergos, P. E. (2020). Shear-Critical Reinforced Concrete Columns under Increasing Axial Load. *ACI Structural Journal*, 117(5), 29-39.

Appendices

Appendix A

Equations for factors of the beam model (Chapter 3)

$k_1 = \frac{750(1+\alpha)}{A_{sl}E_s}$	$k_2 = 0.4\sqrt{f_c'}bd_v\frac{1300}{1000+s_{ze}}\ \ (SI)$ $\left(k_2 = 4.8\sqrt{f_c'}bd_v\frac{51}{39+s_{ze}}\ \ (Imperial)\right)$	$k_3 = 1.73\xi$	$k_4 = 1 + 0.2\xi k_1$
$k_5 = \frac{\frac{h}{2}-X_u}{d-X_u}$	$k_6 = \begin{cases} 1.0 & ; \ \frac{\rho_z f_{yt}}{f_c'} \geq 0.1 \\ \left(\frac{\rho_z f_{yt}}{0.1 f_c'}\right)^{0.2} & ; \ 0 < \frac{\rho_z f_{yt}}{f_c'} < 0.1 \\ 0.88 + \frac{s_{ze}}{2500} \leq 1.3 \ \ (SI) \ \ \left(0.88 + \frac{s_{ze}}{98} \leq 1.3 \ \ (Imperial)\right); \ \frac{\rho_z f_{yt}}{f_c'} = 0 \ (without\ stirrups) \end{cases}$		
$k_7 = 440 - \frac{206}{\left[1+\left(\frac{s_{ze}}{450}\right)^5\right]^{18}}\ \ (SI)$ $\left(k_7 = 440 - \frac{206}{\left[1+\left(\frac{s_{ze}}{17.7}\right)^5\right]^{18}}\ \ (Imperial)\right)$			$k_9 = \frac{h}{d-X_u}$
$k_{10} = (\rho_z f_{yt} + f_{c1y})b.d_v$	$k_8 = \mu\varepsilon_0 - 1 + \sqrt{(\mu\varepsilon_0 - 1)^2 + 4\mu\varepsilon_{xu}\frac{\delta}{\delta+1} + 0.8\frac{f_{c2u}}{f_c'}}$		
$k_{11} = \frac{400-\theta_u}{360}$	$k_{12} = \frac{45-\theta_u}{36.V_u}$	$k_{13} = \frac{h}{d-X_y}$	$k_{14} = \frac{h}{d-X_p}$
$k_{15} = \frac{A_{st}f_{yt}d_v}{s}$	$\alpha = \frac{M_f}{V_f d_v} \geq 1.0$; $\delta = \sqrt{1+\tan^2(2\theta_u)}$	$\xi = \frac{\frac{A_{st}f_{yt}d_v}{s}}{\left(\frac{\rho_z f_{yt}}{0.1 f_c'}\right)^{0.23}}$	$\mu = 85\frac{\delta+1}{\delta-1}\frac{f_{c2u}}{f_c'}$
$X_y = \frac{\varepsilon_{xy.top}}{\varepsilon_{xy.top}+\varepsilon_{xy.bot.}}d$	$X_p = \frac{\varepsilon_{xp.top}}{\varepsilon_{xp.top}+\varepsilon_{xp.bot.}}d$	$s_{ze} = \begin{cases} \frac{35s_z}{15+a_g} \geq 0.85s_z \ ; \ with\ stirrups \\ 300mm \quad ; without\ stirrups \end{cases}\ \ (SI)$ $\left(s_{ze} = \begin{cases} \frac{1.38s_z}{0.59+a_g} \geq 0.85s_z \ ; \ with\ stirrups \\ 11.81in. \quad ; without\ stirrups \end{cases}\ \ (Imperial)\right)$	

Appendix B

Equations for factors of the column model (Chapter 4)

$k_1 = \frac{750(1+\alpha)}{A_{sl}E_s}$	$k'_1 = \frac{375P}{A_{sl}E_s}$	$k_2 = 0.4\sqrt{f_c'}bd_v\frac{1300}{1000+s_{ze}}\quad (SI)$ $\left(k_2 = 4.8\sqrt{f_c'}bd_v\frac{51}{39+s_{ze}}\quad (Imperial)\right)$		
$k_3 = (1.73 - 0.2k'_1)\xi$	$k_4 = 1 + 0.2\xi k_1$	$k_5 = \frac{\frac{h}{2} - X_u}{d - X_u}$	$k'_7 = A_{s.Comp.}\varepsilon_{x.Ten.}E_s$	
$k_6 = \begin{cases} 1.0 & ; \quad \frac{\rho_z f_{yt}}{f_c'} \geq 0.1 \\ \left(\frac{\rho_z f_{yt}}{0.1 f_c'}\right)^{0.2} & ; \quad 0 < \frac{\rho_z f_{yt}}{f_c'} < 0.1 \end{cases}$		$k_9 = \frac{h}{d - X_u} \leq \frac{h}{h-d}$		
$k_{10} = (\rho_z f_{yt} + f_{c1y})b.d_v$	$k_8 = \mu\varepsilon_0 - 1 + \sqrt{(\mu\varepsilon_0 - 1)^2 + 4\mu\varepsilon_{xu}\frac{\delta}{\delta+1} + 0.8\frac{f_{c2u}}{f_c'}}$			
$k_{11} = \frac{400 - \theta_u}{360}$	$k_{12} = \frac{45 - \theta_u}{36.V_u}$	$k_{13} = \frac{h}{d - X_y} \leq 1.2k_9$		
$k_{15} = \frac{A_{st}f_{yt}d_v}{s}$	$\alpha = \frac{M_f}{V_f d_v} \geq 1.0$	$\delta = \sqrt{1 + \tan^2(2\theta_u)}$	$\xi = \frac{\frac{A_{st}f_{yt}d_v}{s}}{\left(\frac{\rho_z f_{yt}}{0.1 f_c'}\right)^{0.23}}$	$\mu = 85\frac{\delta+1}{\delta-1}\frac{f_{c2u}}{f_c'}$
$X_y = \frac{\varepsilon_{xy.top}}{\varepsilon_{xy.top} + \varepsilon_{xy.bot.}}d$	$s_{ze} = \frac{35s_z}{15 + a_g} \geq 0.85s_z \quad (SI)$ $\left(s_{ze} = \frac{1.38s_z}{0.59 + a_g} \geq 0.85s_z \quad (Imperial)\right)$			
$X_u = \begin{cases} \frac{\sqrt{\frac{k'^2_7\varepsilon_0^2}{4} + k'_7\varepsilon_0\left[bd'f'_c\varepsilon_{xu.Ten.} + \frac{C\varepsilon_0}{2}\right] + C\varepsilon_0\left[bdf'_c\varepsilon_{xu.Ten.} + \frac{C\varepsilon_0}{2}\right]} - \frac{k'_7 + C}{2}}{bf'_c\varepsilon_{xu.Ten.}} & ; \quad Advanced\ Equation \\ \frac{\sqrt{C\varepsilon_0\left[bdf'_c\varepsilon_{xu.Ten.} + \frac{C\varepsilon_0}{2}\right]} - \frac{C}{2}}{bf'_c\varepsilon_{xu.Ten.}} & ; \quad Simplified\ Equation \end{cases}$				

Appendix C

Equations for factors of the deep members' model (Chapter 5)

$k_1 = \frac{750(1+\alpha)}{A_{sl}E_s}$	$k'_1 = \frac{375P}{A_{sl}E_s}$	$k_2 = 0.4\sqrt{f'_c}bd_v\frac{1300}{1000+s_{ze}}\ \ (SI)$ $\left(k_2 = 4.8\sqrt{f'_c}bd_v\frac{51}{39+s_{ze}}\ \ (Imperial)\right)$		
$k_3 = (1.73 - 0.2k'_1)\xi$	$k_4 = 1 + 0.2\xi k_1$	$k_5 = \frac{\frac{h}{2} - X_u}{d - X_u}$	$k'_7 = A_{s.Comp.}\varepsilon_{x.Ten.}E_s$	
$k_6 = \begin{cases} 1.0 & ; \ \frac{\rho_z f_{yt}}{f_c'} \geq 0.1 \\ \left(\frac{\rho_z f_{yt}}{0.1 f_c'}\right)^{0.2} & ; \ 0 < \frac{\rho_z f_{yt}}{f_c'} < 0.1 \end{cases}$		$k_9 = \frac{h}{d - X_u} \leq \frac{h}{h-d}$		
$k_{10} = (\rho_z f_{yt} + f_{c1y})b.d_v$	$k_8 = \mu\varepsilon_0 - 1 + \sqrt{(\mu\varepsilon_0 - 1)^2 + 4\mu\varepsilon_{xu}\frac{\delta}{\delta+1} + 0.8\frac{f_{c2u}}{f'_c}}$			
$k_{11} = \frac{400 - \theta_u}{360}$	$k_{12} = \frac{45 - \theta_u}{36.V_{ub}}$	$k_{13} = \frac{h}{d - X_y} \leq 1.2k_9$		
$k_{15} = \frac{A_{st}f_{yt}d_v}{s}$	$\alpha = \frac{M_f}{V_f d_v} \geq 1.0$	$\delta = \sqrt{1 + \tan^2(2\theta_u)}$	$\xi = \frac{\frac{A_{st}f_{yt}d_v}{s}}{\left(\frac{\rho_z f_{yt}}{0.1 f_c'}\right)^{0.23}}$	$\mu = 85\frac{\delta+1}{\delta-1}\frac{f_{c2u}}{f'_c}$
$X_y = \frac{\varepsilon_{xy.top}}{\varepsilon_{xy.top} + \varepsilon_{xy.bot.}}d$	$s_{ze} = \frac{35s_z}{15 + a_g} \geq 0.85s_z \ \ (SI)$ $\left(s_{ze} = \frac{1.38s_z}{0.59 + a_g} \geq 0.85s_z \ \ (Imperial)\right)$			
$X_u = \begin{cases} \frac{\sqrt{\frac{k'^2_7\varepsilon_0^2}{4} + k'_7\varepsilon_0\left[bd'f'_c\varepsilon_{xu.Ten.} + \frac{C\varepsilon_0}{2}\right] + C\varepsilon_0\left[bdf'_c\varepsilon_{xu.Ten.} + \frac{C\varepsilon_0}{2}\right]} - \frac{k'_7 + C}{2}}{bf'_c\varepsilon_{xu.Ten.}} & ; \ Advanced\ Equation \\ \frac{\sqrt{C\varepsilon_0\left[bdf'_c\varepsilon_{xu.Ten.} + \frac{C\varepsilon_0}{2}\right]} - \frac{C}{2}}{bf'_c\varepsilon_{xu.Ten.}} & ; \ Simplified\ Equation \end{cases}$				
$C = T - P = \min\{(1+\alpha)V_{ub} + 0.5P\ , A_{sl}f_{yl}\} - P$	$\varepsilon_{xu.Ten.} = \frac{k_1V_{ub} + k'_1}{750}$			
$f_{c2u.Ten.} = v_u(tan\theta_{u.Ten.} + cot\theta_{u.Ten.})$	$f_{c2u.Comp.} = v_u(tan\theta_{u.Comp.} + cot\theta_{u.Comp.})$			
$\theta_{u.Ten.} = \frac{\theta_u}{1 - \frac{2X_u}{3h}}$	$\theta_{u.Comp.} = \frac{\theta_{u.Ten.}}{3}$			
$f_{c2u} = \frac{f_{c2u.Comp.}X_u + f_{c2u.Ten.}(h - X_u)}{h}$	$f_{c1y} = (0.2 + 0.3\frac{X_u}{h})f'_t$			
$\varepsilon_{xy.Ten.} = \frac{k_1V_y + k'_1}{750}$	$\varepsilon_{xy.Comp.} = \frac{k_1V_u + k'_1}{750}.\frac{X_u}{d - X_u}$			